FRACTAL GEOMETRY OF WOOD INTERNAL SURFACES IN THE HYGROSCOPIC RANGE

by

Bingye Hao

B. Eng., Beijing Forestry University, 1988
M. Eng., Beijing Forestry University, 1991

A THESIS SUBMITTED IN PARTIAL FULFILMENT OF
THE REQUIREMENTS FOR THE DEGREE OF

DOCTOR OF PHILOSOPHY

In

THE FACULTY OF GRADUATE STUDIES

Department of Wood Science

We accept this thesis as conforming
to the required standard

THE UNIVERSITY OF BRITISH COLUMBIA

May 2001

In presenting this thesis in partial fulfilment of the requirements for an advanced degree at the University of British Columbia, I agree that the Library shall make it freely available for reference and study. I further agree that permission for extensive copying of this thesis for scholarly purposes may be granted by the head of my department or by his or her representatives. It is understood that copying or publication of this thesis for financial gain shall not be allowed without my written permission.

Department of Wood Science

The University of British Columbia
Vancouver, Canada

Date Oct. 9 '01

ABSTRACT

The study was aimed at exploring the geometry of the internal surfaces of wood cell walls and/or the sorbed water molecules in the hygroscopic range by using fractal theories for Douglas-fir (*Pseudotsuga menziesii (Mirb.) Frano*) (heartwood and sapwood) and western red cedar (*Thuja plicata Donn.*) heartwood (unextracted and extracted).

The study was divided into experimental and modelling parts. The experimental studies included two main targets: (1) development of sorption isotherms by using wafer-shaped specimens and (2) examination of the moisture content of the altered volumes of the cubic-shaped specimens for Douglas-fir heartwood and unextracted red cedar at a relative vapor pressure of about 0.92. The theoretical studies included: (1) development of two new sorption equations, (2) their evaluation and comparison with the classic BET (using the data from the wafer-shaped specimens), and (3) examination of the mass fractal phenomenon for bound water (using the data from the cubic-shaped specimens).

Failure of the classic BET theory to predict moisture sorption of wood at the higher sorption regions (relative vapor pressure, $h > 0.5$) can be attributed to the existence of the geometrically rough surface with a fractal dimension (D) value from about 2.3 to 2.7. The surface geometry with D values of this range is far from being implied as a flat surface ($D = 2$).

Modification of the classic BET theory based on the notation of a fractal surface was successful for the moisture sorption of wood. A modified BET equation was suggested for vapor sorption in wood to account for the state/geometry dynamics of the sorbed water molecules/internal surfaces of the cell walls. In terms of the D values of 24 cases (four types of wood, three temperature levels, and two sorption conditions), the internal surfaces of the cell

walls had variable D values between 0.4 to 0.96 of h values. The D values were less than 2, about 2.0, and tending towards 2.7. The corresponding moisture content for these three D values ranged from 0 to about 12%, 12% to 18%, and 18% to the fiber saturation point, respectively. Such D value dynamics indicated that the internal surfaces underwent a cumulative change with an increase in moisture content.

A brand new sorption theory with an appropriate equation was brought into the family of sorption theories. Its derivation considered both molecular layering and non-layering (clustering) of sorption states. Its success showed that the state dynamics of the sorbed water molecules were stepwise instead of smooth and 3 or 4 steps (states) were identified.

The moisture content of various sizes of specimens at about 0.92 relative vapor pressure did not indicate a consistently increasing or decreasing trend. For the resultant moisture content of about 16%, the weight of the adsorbed water and specimens' dimensions were measured to investigate the fractal dimension of the adsorbed water in both studied species of dimensions between 10 mm and 40 mm. The results indicated that D_m value for the water was slightly below 3. These measurements did not conclusively exhibit that the water in wood was fractal at this moisture content and this specimen sizes range.

In addition, unextracted western red cedar showed the lower hygroscopicity due to its high extractives content. Hysteresis was pronounced in the four types of wood in this study. Hygroscopicity decreased with an increase in temperature. No great difference in moisture content was found between the sapwood and heartwood in Douglas-fir. Extracted western red cedar and Douglas-fir showed no major difference in hygroscopicity.

Table of Contents

Abstract ii

Table of Contents iv

List of Tables vii

List of Figures viii

Abbreviations xii

Acknowledgements xiii

Chapter 1 1

1.1 Introduction 1

1.2 Objectives 5

Chapter 2 Literature Review 6

2.1 Surface or layering theories 8

2.1.1 The BET theory 8

2.1.2 BET modification with the capillary theory 9

2.1.3 The Dent theory 10

2.1.4 The new-type BET theories 11

2.1.5 The L-L theory 13

2.2 Clustering theory 15

2.3 Fractal fundamentals and their applications 17

2.3.1 Fractal geometry 16

2.3.2 Fractal dimensions 18

2.3.3 Approaches to determine fractal dimension at the molecular

domain 24

2.4 Percolation theory 28

2.5 Past researches on wood by using fractal theories 30

2.6 Summary 34

Chapter 3 Methodology 35

3.1 Materials 35

3.2 Specimens preparation 36

3.2.1 wafer type 37

3.2.2 cubic type 38

3.3 Sorption isotherms development 39

3.4 *EMC* measurements of the cubic specimens 41

Chapter 4 Modelling 42

4.1 Modification of the classic BET equation 42

4.1.1 theoretical model 42

4.1.2 mathematical model 45

4.2 Determination of the D value from mass fractal 47

4.3 New sorption equation 48

4.4 Optimization of the resulted equations 53

Chapter 5 Results and Discussion 54

5.1 Data collections 54

5.2 Prediction of M_m and c values 63

5.3 Fitness of the classic BET equation to the sorption data 68

5.4 dM/dh plots 71

5.5 Fitness of the FBET to the sorption data 75

5.6 Grouping 79

5.7 Fitness of the F-P to the sorption data 80

5.8 Physical implications of the FBET and F-P equations 82

5.9 Species, sorption history, temperature, and extractives 87

5.9.1 Species and locations within the same species 87

5.9.2 Sorption history (adsorption and desorption) 88

5.9.3 Temperature 88

5.9.4 Extractives 90

5.10 Examination of mass fractal phenomenon within the cell walls 116

5.10.1 Moisture content of the different volume of cubic specimens 116

5.10.2 D_m calculation 117

5.10.3 The difference between D and D_m values in this study 121

Chapter 6 Conclusion and future research Recommendations 123

6.1 Conclusions 123

6.2 Future research suggestion 124

Literature Cited 126

Appendix A 133

Appendix B 140

Appendix C 144

Appendix D 153

List of Tables

Table 1: Specific gravity of Douglas-fir and western red cedar 36

Table 2: The experimental sorption data for unextracted western red cedar 55

Table 3: The experimental sorption data for extracted western red cedar 56

Table 4: The experimental sorption data for Douglas-fir sapwood 57

Table 5: The experimental sorption data for Douglas-fir heartwood 58

Table 6: Moisture content for the cubic-shaped specimens of unextracted western red cedar 59

Table 7: Moisture content for the cubic-shaped specimens of Douglas-fir heartwood 59

Table 8: The estimated parameter values of M_m and c in the classic BET 69

Table 9: Parameter n estimation from the classic BET 70

Table 10: The estimated D values at the different sorption points from the FBET equation, Eq. (4.5). 77

Table 11: The critical h_c values obtained from Eq. (4.5) 81

Table 12: Fractal-Polynomial coefficient (k_i) estimations 83

List of Figures

Fig. 2.1: Layer or surface models as predicted by a) Langmuir, monolayer, b) BET multilayer, and c) rearranged BET multilayer model in an ascending order 8

Fig. 2.2: Comparison of the (a) BET with the (b) L-L model 14

Fig. 2.4: Illustrative profile of coastline – (a): whole, (b): part of (a), (c): part of (b) 18

Fig. 2.5: Construction of the Koch curve 18

Fig. 2.6: Construction of he disc motif 21

Fig. 2.7: A lattice model between mass and radius 21

Fig. 2.8: Surface (a), mass (b), and pore (c) fractal 23

Fig. 2.9: Principle of determination on fractal dimension by variable sizes of molecules according to the BET theory 25

Fig. 2.10: The pore definition for the fractal object 26

Fig. 2.11: Simple percolation cluster model 29

Fig. 2.12: Illustration of a percolation cluster phenomenon 30-31

Fig. 3.1: Illustration of the wafer-type specimen 38

Fig. 3.2: Illustration of the cubic-type specimen 39

Fig. 4.1: Illustration of water molecule sorption processes in wood 43

Fig. 4.2: Physical model for stacking of sorbed molecules 44

Fig. 5.1: The experimental sorption isotherms for DFS 60

Fig. 5.2: The experimental sorption isotherms for DFH 60

Fig. 5.3: The experimental sorption isotherms for E-WRC 61

Fig. 5.4: The experimental sorption isotherms for UE-WRC 61

Fig. 5.5: The moisture content of the cubic-shaped specimens with the variable sizes for UE-WRC 62

Fig. 5.6: The moisture content of the cubic-shaped specimens with the variable sizes for DFH 63

Figs. 5.7: Linear relationship in UE WRC 64

Figs. 5.8: Linear relationship in E WRC 65

Figs. 5.9: Linear relationship in DFS 66

Figs. 5.10: Linear relationship in DFH 67

Fig. 5.11: The values of *dM/dh* for DFS 72

Fig. 5.12: The values of *dM/dh* for DFH 72

Fig. 5.13: The values of *dM/dh* for E-WRC 73

Fig. 5.14: The values of *dM/dh* for UE-WRC 73

Fig. 5.15: The calculated desorption isotherms (a) and their residue patterns (b) for UE-WRC at 30°C 92

Fig. 5.16: The calculated adsorption isotherms (a) and their residue patterns (b) for UE-WRC at 30°C 93

Fig. 5.17: The calculated desorption isotherms (a) and their residue patterns (b) for UE-WRC at 40°C 94

Fig. 5.18: The calculated adsorption isotherms (a) and their residue patterns (b) for UE-WRC at 40°C 95

Fig. 5.19: The calculated desorption isotherms (a) and their residue patterns (b) for UE-WRC at 50°C 96

Fig. 5.20: The calculated adsorption isotherms (a) and their residue patterns (b) for UE-WRC at 50°C 97

Fig. 5.21: The calculated desorption isotherms (a) and their residue patterns (b) for E-WRC at 30°C 98

Fig. 5.22: The calculated adsorption isotherms (a) and their residue patterns (b) for E-WRC at 30°C 99

Fig. 5.23: The calculated desorption isotherms (a) and their residue patterns (b) for E-WRC at 40°C 100

Fig. 5.24: The calculated adsorption isotherms (a) and their residue patterns (b) for E-WRC at 40°C 101

Fig. 5.25: The calculated desorption isotherms (a) and their residue patterns (b) for E-WRC at 50°C 102

Fig. 5.26: The calculated adsorption isotherms (a) and their residue patterns (b) for E-WRC at 50°C 103

Fig. 5.27: The calculated desorption isotherms (a) and their residue patterns (b) for DFS at 30°C 104

Fig. 5.28: The calculated adsorption isotherms (a) and their residue patterns (b) for DFS at 30°C 105

Fig. 5.29: The calculated desorption isotherms (a) and their residue patterns (b) for DFS at 40°C 106

Fig. 5.30: The calculated adsorption isotherms (a) and their residue patterns (b) for DFS at 40°C 107

Fig. 5.31: The calculated desorption isotherms (a) and their residue patterns (b) for DFS at 50°C 108

Fig. 5.32: The calculated adsorption isotherms (a) and their residue patterns (b) for DFS at 50°C 109

Fig. 5.33: The calculated desorption isotherms (a) and their residue patterns (b) for DFH at 30°C 110

Fig. 5.34: The calculated adsorption isotherms (a) and their residue patterns (b) for DFH at 30°C 111

Fig. 5.35: The calculated desorption isotherms (a) and their residue patterns (b) for DFH at 40°C 112

Fig. 5.36: The calculated adsorption isotherms (a) and their residue patterns (b) for DFH at 40°C 113

Fig. 5.37: The calculated desorption isotherms (a) and their residue patterns (b) for DFH at 50°C 114

Fig. 5.38: The calculated adsorption isotherms (a) and their residue patterns (b) for DFH at 50°C 115

Fig. 5.39: Relationship of the amount of sorbed water and its size scale for UE-WRC 118-119

Fig. 5.40: Relationship of the amount of sorbed water and its size scale for DFH 120-121

Abbreviations

DFS	Douglas-fir sapwood
DFH	Douglas-fir heartwood
UE-WRC	unextracted western red cedar (heartwood)
E-WRC	extracted western red cedar (heartwood)
h	relative vapor pressure
h_c	the critical h value
BET	the classic BET theory
FBET	the fractal-based BET equation
F-P	the fractal-polynomial sorption equation
M_{fsp}	moisture content at fiber saturation point (FSP)
M_w	mass of sorbed water (bound water) within wood
M_{wt}	molecular weight of water
M	moisture content percentage, oven-dry basis
m	moisture content in fraction, over-dry basis
D	the fractal dimension
M_{emc}	equilibrium moisture content
res	residue
MSE	mean square of errors
n_{max}	the maximum number layers of sorbed water molecules
n	the number layers of the sorbed water molecules
c	constant related to the heat of adsorption
M_m	the monolayer sorption capacity

Acknowledgements

My sincere thanks goes to Dr. Stavros Avramidis, my supervisor, for his academic and research guidance and support throughout my graduate studies at UBC.

I am grateful to Dr. Ian D. Hartley for his valuable discussion and suggestion over my research program.

Also, a lot of thanks go to Dr. Simon Ellis, Dr. David J. Barrett, and Dr. S. G. Hatzikirriakos for their suggestive help during this study.

Thanks go to Dr. Harry Joe for his great help with his expert statistics consultation and to Dr. Alex MacKay for his many suggestions related to wood-water sorption thermodynamics.

Finally, I am indebted to my family for their support and encouragement over more than four years at UBC, and especially, to my wife. Some new ideas about this research were also stimulated by my beautiful daughter and handsome son.

Chapter 1

1.1 Introduction

The natural world consists of objects with different shapes and forms, from simple ones to complex ones. Not too long ago, it was widely and thoroughly recognized that many natural structures or objects possess a certain kind of geometric complexity which exhibits self-similar properties upon changes of length scales (Mandelbrot 1977; Russ 1994). The degree of complexity of such structures can be measured by a parameter D, commonly called "the fractal dimension" (Mandelbrot 1977; Avnir *et al.* 1983; Feder 1988; Russ 1994).

Fractals occupy a borderline between Euclidean geometry (point, line, circle) and complete randomness (Russ 1994); the properties of a fractal object is that its parts or components are similar to the whole in some way. It is hard to provide an unambiguous definition of fractals (Feder 1988), but its main characteristic is the existence of a non-integer dimension D that stands for the space-filling ability and indicates the degree of deviations of rough curves from lines or rough surfaces from flat surfaces. The larger the D, the rougher the surfaces or curves. The D is a quantitative link between irregularity and dimension (Avnir *et al.* 1983; Avnir and Pfeifer 1983; Pfeifer and Avnir 1983; Pfeifer *et al.* 1984; Neimark 1990).

Concepts of fractals have been applied to a vast range of different structures to study their geometric complexity which is defined as the D value, such as, landscapes (Burrough 1981), mountain topology, cloud profiles (Russ 1994), fracture surfaces (Cahn 1989), surface structure of coke (Siauw and Fairbridge 1987), surface fractal dimensions of some industrial minerals from gas adsorption isotherms, active carbons (Jaroniec *et al.* 1993), and corrosion surfaces (Sapoval 1989), just to name few. Moreover, since the first exploration of the fractal surface properties of

solids at molecular scales (Avnir and Pfeifer 1983; Avnir *et al.* 1983), the concepts of fractal geometry have frequently and successfully been used to treat sorption processes, investigate the complex nature of sorption and the distribution of the active sites (Fripiat *et al.* 1986; Pfeifer 1986; Neimark 1990). These investigations have shown that any research associated with surfaces is incomplete without consideration of their geometry.

Wood is a hygroscopic, heterogeneous (energetic and geometric) porous medium with a very large amount of internal surface within its cell walls that contains a large number of sorption sites (hydroxyl groups). These sites can exchange water molecules with the environment and reach a dynamic equilibrium under a given temperature and humidity (Stamm 1964; Skaar 1988). This dynamic relationship between the amount of water molecules adsorbed in wood and those in the air can be graphically represented by a "sigmoid" curve (Type II) which is called a sorption isotherm (Siau 1984). The presence of such a "sigmoid" relationship and the hysteresis (irreversibility) phenomenon indicates the multimolecular nature of sorption and the presence of large forces of interaction between wood and water molecules and in some cases even between sorption sites (Stamm 1964; Atkins 1970; Adamson 1990).

Normally, the internal surface area of wood is more than 200 m^2/g-wood (Stamm 1964) and will increase with an increase in moisture content (M) because of its swelling characteristics. It is not unreasonable therefore to believe that the underlying surfaces could have enough folds for sorption in a 3-dimensional wood block beyond a certain M in the hygroscopic range (oven-dry M to Fiber Saturation Point, M_{fsp}). In other words, the underlying surface could be very rough, thus resulting in a large surface area at the molecular level within the limited volume of wood.

In addition, if further internal wood surface is created by the adsorbed water molecules, and its shape and roughness are determined by the geometry of the adsorbed water molecules, then the internal surfaces of wood should be irregular. This is because sorption sites have variable sorption energies and each individual sorption site may thus adsorb a different number of water molecules.

Studies on the clustering phenomenon of the adsorbed water molecules in wood have provided more knowledge about wood sorption behavior (Hartley *et al.* 1992; Hartley and Avramidis 1993; Hartley 1994). Cluster formation makes the sorption processes in wood more complicated because the spatial organization of the sorbed water molecules is determined not only by the number and energy of the sorption sites, but also by the cluster formation level of the sorbed water molecules. According to the percolation theory, the larger cluster size mostly possesses fractal characteristics (mass fractal) (Deutscher *et al.* 1983; Russ 1994).

Apparently, the complexity of sorption processes in wood results from sorbed water molecules as well as the wood itself. Ideally, a numerical model should be able to use a single parameter to describe such complexity. Today, such an opportunity is offered by the fractal theory which has been used to describe complex and chaotic geometries or phenomena in other fields, but has had very little application on wood.

Hatzikiriakos and Avramidis (1994) were the first to determine the D value of the internal wood surfaces by three mathematical equations using sorption isotherms developed by Kelsey (1957). It was concluded that the complexity of the internal cell wall surfaces was far from being described as two dimensional at the relative vapor pressure (h) range of 0.25 to 0.85. Because they did not focus on the derivation of theoretical sorption models based on fractal theories, but just tried to apply these equations, the results could not clearly explain the effects of sorption

conditions (adsorption and desorption) and temperature on the calculated D values. Also, at $h < 0.25$ and $h > 0.85$, the results disagreed between methods. Therefore, it is evident that a systematic and comprehensive study on the fractality of wood is necessary.

This novel research project addresses the geometry of the internal wood surfaces and of the sorbed water within cell walls based on theoretical and mathematical derivations of fractal-related sorption models. A geometric parameter is introduced that provides a better understanding of the mechanisms of vapor sorption in wood. The gained knowledge could help with the rigorous derivation of reliable numerical models that will be capable of predicting transport processes in wood. This is because the actual physical structure of wood and the spatial distribution of the sorbed water molecules are being taken into account.

1.2 Objectives

The long term objective of this research effort is to introduce a new wood geometrical parameter that is capable of dealing with the complexities of sorption and diffusion as transfer processes on one hand and the structural complexities of wood on the other hand in a simple way.

The major objectives are: (1) to study the geometry of the underlying internal wood surfaces within the cell walls, (2) to study the distribution of the adsorbed water molecules within the cell walls at high relative vapor pressure, and (3) to develop a new sorption equation which is mainly dependent on the geometry of the internal wood surfaces.

In addressing objective (1), the classic BET theory was modified from assuming flat internal wood surfaces to rough or fractal ones. The modified equation was tested by implementing four different experimental sets of wood sorption data. After validation, the modified equation was used to develop the plots of D against moisture content of relative vapor pressure.

In addressing objective (2), a series of cubic specimens with different sizes for two species were used to create sorption data and to test the fractal phenomenon of the sorbed water molecules.

From the results of objective (1), it was evident that D was a dominant parameter to determine the sorption isotherms. Therefore, it was possible to develop a D-dependent new sorption model for wood as stipulated in objective (3).

Chapter 2

Literature Review

Moisture content continually changes during wood kiln drying and during subsequent use in service. This leads to changes of nearly all of physical and mechanical properties of wood within its hygroscopic range. During service use, the changes of moisture content in wood may be sporadic, cyclic, or both. Therefore, it is important for designers to be able to predict moisture content during drying and to forecast the dimensional behavior of both solid wood and wood composites under the influence of a changing ambient environment.

In addition, since wood is a complex, hygroscopic, and porous biopolymer, variations of its structure could exist between the different species and types (i.e., sapwood and heartwood) of wood. The direct quantitative evaluation of these variations, such as, the internal surface structures of the cell walls, has been proven to be difficult. As a result, sorption isotherms or models are used as an indirect tool to characterize structural properties of the cell walls as well as to predict equilibrium moisture content (M_{emc}) under variable ambient conditions. The complexity of the water sorption phenomenon in wood leads to 20 sorption mechanisms and 20 correspondent mathematical equations which were critically reviewed by Venkateswaran (1970). Skaar (1972, 1988) detailed current sorption models which are frequently used in wood. Generally, these models can be classified based upon their derivation process into surface or layering theory ones which are represented by Brunauer, Emmett, and Teller (BET) (Brunauer *et al.* 1938), and solution theory ones which are represented by Hailwood and Horrobin (HH) (Hailwood and Horrobin 1946). In addition, thermodynamic theories (Henderson 1952; Zuritz *et al.* (ZSMH) 1979) are frequently used for some food materials and have been used to predict

sorption isotherms for wood (Avramidis 1989). Spatial distribution theory (Malmquist 1958, 1959, and 1995; Skaar 1972) is the only one derived from geometric considerations, instead of thermodynamic ones. It has been proven that this theory cannot fit sorption data of wood well.

Simpson (1973, 1980) and Siau (1995) found that a polynomial sorption isotherm model (a fifth-degree polynomial with six parameters) provided a better fit to experimental sorption data than any of the theoretical, classical models. However, no theoretical basis has been offered to justify implications of model parameters yet. The theoretic validation of this model could bring new knowledge into this area.

Hartley and Avramidis (1993) applied the Zimm-Lundberg cluster analysis (Zimm and Lundberg 1959) and developed a sorption cluster isotherm for wood which provided insights into the sorption process without predicting the isotherm based on discussion of cluster theory as presented by Hartley *et al.* (1992). The successfulness of cluster analysis further validated the fact that the sorption complications are not only due to sorption sites complexity (geometric and energetic), but also due to state dynamics of the sorbed water molecules.

Because of the energetic and geometric complexity of the wood polymeric structure, the above theories are, by necessity, idealistic. Also, they might have partially explored the realness of wood. However, these theories did provide a glimpse into the particulars of sorption mechanisms. Probably, the truth lies somewhere in between. The HH theory is expected to be used extensively to predict sorption isotherms of wood because of its simple models and the good fit to sorption data. Both Henderson and ZSMH equations were evaluated by Avramidis (1989). The significance of these two equations is that they combine the M, h, and temperature (T) into one equation thus making them convenient to predict the effect of T and h on M. However, the HH, Henderson, and ZSMH theories fail to predict the heat of adsorption and to

provide wood structural information. Therefore, these models are considered of low importance to be detailed in this study compared to surface models. Surface theories have been linked to fractal theory which in turn have been proven a powerful tool that can deal with complex sorption phenomenon.

2.1 Surface or layering theories

2.1.1 The BET theory

According to the BET theory, wood is considered to have a very large internal surface within the cell walls with a large number of sorption sites (mainly hydroxyl groups) on it. The theory is based on a "multiple layer" concept which is an extension of the Langmuir (1918) treatment of a monolayer. Fig. (3.1) shows a schematic view of the formation of layers during sorption according to Langmuir and BET theories.

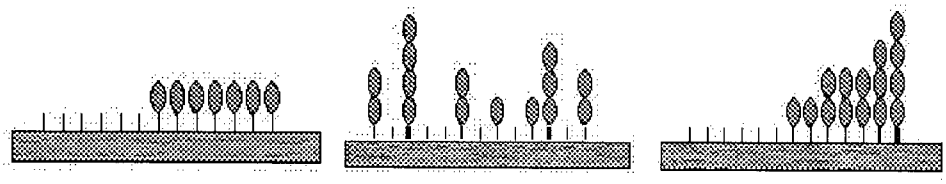

(a) (b) (c)

Fig. 2.1: Layer or surface models as predicted by a) Langmuir, monolayer model, b) BET multilayer model, and c) Rearranged BET multilayer model in an ascending order

The BET theory proposed a monolayer tightly bound to the hydroxyl groups and secondary layers (layer two and higher) that were considered to thermodynamically behave the same as the liquid water, but quite differently from the monolayer molecules. If the number of layers of the sorbed water molecules is considered to become infinity when wood becomes saturated, the BET equation is obtained:

$$\frac{M}{M_m} = \frac{ch}{(1-h+ch)(1-h)} \tag{2.1}$$

where M is moisture content in percentage, M_m is moisture content in percentage, corresponding to the capacity of the monolayer, h is the relative vapor pressure, and c is the constant related to the heat of adsorption.

Eq. (2.1) results in a "sigmoid" shape isotherm. Brunauer *et al.* (1938) refined Eq. (2.1) to consider a finite number of layers, n:

$$M = \left[\frac{M_m ch}{1-h}\right]\left[\frac{1-(n+1)h^n + nh^{n+1}}{1+(c-1)h-ch^{n+1}}\right] \tag{2.2}$$

where M and M_m are moisture content (%) at a given relative vapor pressure h and a full monolayer capacity, respectively, n is the number of layers of sorbed molecules, and c is the constant. If $n = 1$, Eq. (2.2) reduces to the Langmuir model as,

$$M = \frac{M_m ch}{1+ch} \tag{2.2a}$$

. If $n = \infty$, it becomes Eq. (2.1).

The significance of this theory is that it contains parameter M_m and c which are theoretically important parameters to some wood properties.

2.1.2 BET modification with capillary theory

At high h values, Eq. (2.2) tends to underestimate the predicted M. Simpson (1973, 1980) considered this fact to be due to capillary condensation, so he added a term to account for capillary condensation where water vapor will condense in small capillaries according to the Kelvin equation:

$$r = \frac{2SM_{wt}}{\rho RT \ln(1/h)} \tag{2.3}$$

where r is the radius of capillary (cm), S is the surface tension of liquid (dyne/cm), M_{wt} is the molecular weight of the liquid (18 g mole^{-1}), ρ is density of liquid (g cm^{-3}), R is the gas constant ($8.31*10^7$ erg.mole^{-1}-K^{-1}), T is the absolute temperature (°K), and h is the relative vapor pressure.

Eq. (2.3) predicts that the humidity at which capillary condensation occurs decreases with decreasing capillary radius. Using Eq. (2.3) as a basis, a model for capillary condensed water (M_c,%) can be derived:

$$M_c = \frac{V}{W_d} = \left[\frac{\pi\psi}{W_d}\right]\left[\frac{2SM_{wt}}{RT \ln(1/h)}\right]^2 \tag{2.4}$$

where W_d is the oven-dry weight of wood (g), ψ is the length of capillary (cm), ψ/W_d is considered as one parameter and denotes the total length of capillaries per unit weight of wood (cm/g).

The capillary modified BET equation is just a summation of Eq. (2.2) and Eq. (2.4) as,

$$M = \left[\frac{\pi\psi}{W_d}\right]\left[\frac{2SM_{wt}}{RT \ln(1/h)}\right]^2 + \left[\frac{M_m ch}{1-h}\right]\left[\frac{1-(n+1)h^n + nh^{n+1}}{1+(c-1)h-ch^{n+1}}\right] \tag{2.4a}$$

where units for all variables are same in Eqs. (2.2) and (2.4).

2.1.3 The Dent theory

Dent (1977) modified the BET model in order to consider the secondary layers (second and higher layers) to be thermodynamically the same, but different from liquid water as well as from the molecules of the first layer. That was achieved by introducing the term b_l defined as the ratio of the partition function of the primary molecules to that of the external condensed liquid in the

saturated vapor, and b_2 defined as a constant which relates the partition function of the secondary sorbed molecules to that of an external condensed liquid in equilibrium with the saturated vapor. In the BET theory, it was assumed that this constant was equal to unity because the energies of the secondary molecules were the same to liquid water energies. According to this theory, the Dent equation is obtained:

$$\frac{M}{M_m} = \frac{b_1 h}{(1-b_2 h)(1-b_2 h+b_1 h)} \tag{2.5}$$

where M and M_m are moisture content (%) at a given relative vapor pressure h and at a full monolayer capacity, respectively; b_1 is a constant defined as the ratio of the partition function of the primary sorbed molecules to that of the external condensed liquid in the saturated vapor, and b_2 is defined as a constant which relates the partition function of the secondary sorbed molecules to that of an external condensed liquid in equilibrium with the saturated vapor.

This equation can give a better fit to sorption data than the BET equation, but it still has some distinct deviations at relative vapor pressures above 0.90.

2.1.4 New-type BET theories

Based on the hypothesis that the heat of adsorption beyond the first layer either changes, or remains constant and by taking as limit the heat of evaporation-condensation, a group of BET-type multilayer models was derived and then applied to predict sorption isotherms for 74 experimental food isotherms (Aguerre *et al.* 1989a, 1989b). It was shown that such models predicted lower and higher values than the BET model in the case of the heat adsorption being increased (Case 1) and in the case of the heat of adsorption being decreased (Case 2) with the

number of layers, respectively. For the case of the heat of adsorption remaining constant (Case 3), it was identical to the Dent model. These three models are:

Case 1:

$$\frac{M}{M_m} = \frac{ch}{(1-h)(1-c\ln(1-h))} \tag{2.6}$$

Case 2:

$$\frac{M}{M_m} = \frac{ch(1+h)}{(1-h)((1-h)^2+ch)} \tag{2.7}$$

Case 3:

$$\frac{M}{M_m} = \frac{ch}{(1-c_1h)(1+(c-c_1)h)} \tag{2.8}$$

where M and M_m are moisture content (%) at a given relative vapor pressure h and at a full monolayer capacity, respectively; c_1 and c are identical to b_2 and b_1 in Eq. (2.5), respectively.

The BET theory based on infinite layers of adsorbed water molecules fits the experimental data well up to relative vapor pressure of 0.4. The BET theory based on a finite number of layers improves previous one when it comes to wood because wood is a finite swelling material. However, the finite layer BET equation will not always converge to result in a good fit. In addition, when the relative vapor pressure is between 0.40 and 0.95, the BET equation overestimates the moisture content, while it underestimates it at values over 0.95. As a result, the following questions arise: (a) why would a theory based on the assumption of adsorption on uniform surface fit experimental data which refer to adsorption on a non-uniform surface? and, (b) what information as to the nature of the surface can be deduced from the experimental isotherm when it does not agree with the BET theory over any vapor range? It is possible that the information lies in such deviations between the experimental and calculated values. Such

deviations have already resulted in some modifications based on thermodynamic considerations, such as Simpson's capillary modification (Simpson 1973, 1980), Aguerre's modifications (Aguerre *et al.* 1989a, 1989b), and Dent's modification (Dent 1977), with the latter one appearing as the most suitable to be applied to wood. Simpson's modification overestimates the components of water in capillary condensation and does not provide a good fit of the experimental data. The first and second cases of Aguerre's modifications are not suitable to sorption of wood. The third case is identical to the Dent theory and better matches the observed isotherms because it realizes that water in secondary layers is not the same as liquid water. It seems that the thermodynamic properties of the secondary layers tends to be same in the case of wood.

2.1.5 The L-L theory

A significant modification of the BET model was worked out by Le and Ly (1992), commonly referred to as the LL model. The development of the LL model closely follows that of the BET equation. However, the LL model has different assumptions. The BET model assumes that the adsorption site area, S_i, is covered by i layers of molecules, Fig. (2.2a), whereas the LL model assumes that S_i is the area occupied by the i-th layer of the adsorbed molecules, Fig. (2.2b). With this model, condensation and evaporation are assumed to occur anywhere in the layer at the vacant sites, and are not just restricted to the exposed surface.

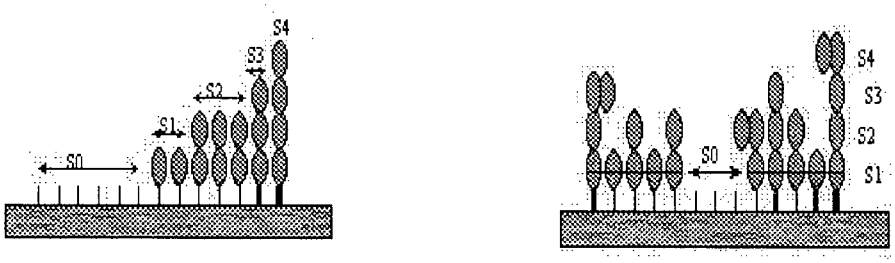

(a) (b)

Fig. 2.2: Comparison of the (a) BET with the (b) LL model

Also, the LL theory assumes that the underlying surface is energetic dual-surface to account for the energetic heterogeneity of wood, namely, the fraction of the sorption sites that contain up to n layers is α and the rest of the sites has up to $p > n$ layers. Based on these assumptions, the following model was developed:

$$\frac{M}{M_m} = \frac{ch\alpha\sum_{i=0}^{n-1} h^i + ch(1-\alpha)\sum_{i=0}^{p-1} h^i}{1+ch} \tag{2.9}$$

where M and M_m are moisture content (%) at a given relative vapor pressure h and at a full monolayer capacity, respectively; c is a constant related to the heat of adsorption, α *is* the fraction of the sorption sites that contain up to n number of layers of sorbed molecules, and the rest of the sites has up to $p > n$ layers. Eq. (2.9) can be reduced to the following:

$$\frac{M}{M_m} = \frac{ch}{1+ch}\frac{1-\alpha h^n-(1-\alpha)h^p}{1-h} \tag{2.10}$$

where all variables and their units are same in Eq. (2.9)

Even if the mathematical treatment is limited, the significance of the LL theory is that it took a non-homogeneous property of the material into account, namely, existence of dual surfaces from the sorption energy point of view. In addition, the LL model came up with a new

organization and treatment of the sorbed molecules. The fitness to sorption data is thus better than the BET.

2.2 Clustering theory

Most of the currently used sorption models for wood are based on idealistic considerations, i.e., no interactions between water molecules. The clustering theory is such a theory that considers interactions between the sorbed molecules for a non-idealistic system. In the case of the wood-water system, the interaction between the sorbed water molecules may result in cluster formation. A cluster may be a structure of one, two, three, or n number of molecules. Recently, insights into describing the isotherm in terms of water molecular clustering within cell walls have been presented in Hartley *et al.* (1992). Hartley and Avramidis (1993) analyzed wood sorption isotherms by implementing the clustering theory and the number of water molecules in a cluster was calculated by the following equation according to Zimm and Lundberg (1959):

$$c_1 G_{11} = (1-\phi)\frac{\partial \ln \phi}{\partial \ln h} \qquad (2.11)$$

where $c_1 G_{11} + 1$ is the number of the water molecules in a cluster. The term ϕ is the volume fraction of water (the volume fraction of water in the swollen cell walls) and h is the relative vapor pressure. The volume fraction of water can be calculated by using the following equation (Spalt 1957),

$$\phi = \frac{m_{wet}\rho_0}{\rho_{bw}} \frac{1}{1+\frac{m_{wet}\rho_0}{\rho_{bw}}} \qquad (2.12)$$

where ϕ volume fraction of water in the swollen cell walls, m_{wet} is the wet basis moisture content fraction in fraction, ρ_o is the density of the cell wall substance taken as 1.46g cm^{-3} (Stamm 1964;

Siau 1984) and ρ_{bw} is the density of the adsorbed water (g cm^{-3}) at the corresponding dry basis moisture content (Siau 1984).

The key to Eq. (2.11) use is to transform a dry basis moisture content into a wet basis according to Eq. (2.12) and to plot the $ln\phi$ - lnh curve. Clustering of water molecules begins to form at approximately 10% moisture content for adsorption and begins to break up at approximately 20% moisture content. The isotherm can be divided into three regions for describing the adsorption process and at least two regions for describing the desorption process. Such regions showed that water molecules in wood had different behaviors during adsorption and desorption as well as throughout the hygroscopic range. In the first region ($0 < M < 8\%$), the dominant mechanism was chemical sorption between the available sites and water molecules. Region II ($8 < M < 21\%$) was considered as an organization region with a small size of clusters and Region III ($21\% < M < M_{fsp}$) has physiosorption as the dominant mechanism (a big size of clusters) according to Hartley and Avramidis (1993). Although Hartley and Avramidis based their analysis on published sorption data (Kelsey 1957) for klinki pine, these two points (8% and 21%) have also occurred throughout the study by Hartley and Avramidis (1994) for spruce and hemlock. The h value at the transition point from one region to another was called the critical relative vapor pressure point (h_c). At about these three critical vapor pressures, the water monolayer, the water clusters, and the fiber saturation point manifested themselves, respectively. It was indicated that the critical points may have occurred at different places in the sorption isotherm, however, they were present in the sorption data.

2.3 Fractal fundamentals and applications

2.3.1 Fractal geometry

In the natural world, many objects have fractal features. For example, tree leaves, snow flakes, cloud profiles, mountains and the earth, surfaces of depositions, corrosions, and most porous materials (rocks), just to name a few, have fractal properties. The common property for these objects is that they have complex profiles that cannot be described by the classic Euclidean geometry. Fractal geometry is a generalization of the Euclidean geometry which helps scientists to address problems involving a very complex geometry with a simple power law.

Mandebrot (1977) first presented the fractal concept by studying the profile of the English coastline - "How long is the English coastline?" This seems a simple question. Probably, the total length can be calculated from the map or it can be measured by a ruler along the real coastline. However, if the length is measured by a ruler, the total length will be a function of the length of the ruler. The total length eventually approaches infinity at very small scales where distances around individual crevices of rocks and pebbles are considered. In this case, what is important is the irregularity or roughness of the coastline, instead of the actual length. In addition, another important feature of the coastline is that the profile of the part is always similar to its global profile. Fig. (2.4) schematically describes such properties of the coastline

From the above schematic picture of the coastline, the magnified sections reveal repetitive levels of details regardless of the scale chosen. This property of fractal shapes is called self-similarity, or independence of scales (Mandelbrot 1977, 1982; Feder 1988; Russ 1994).

(a) (b) (c)

Fig. 2.4: Illustrative profile of coastline – (a): whole, (b): part of (a), (c): part of (b)

2.3.2 Fractal dimensions

The classic Euclidean geometry describes a single point, a line, a plane, and a cube as 0, 1, 2, and 3 dimension, respectively. However, fractal geometry deals with any dimension between 0 and 3 (inclusive). Mostly, it is a non-integer dimension. Following are two typical examples of how fractal objects are formed in order to illustrate how to calculate the fractal dimension for a given fractal object by using classic Euclidean objects.

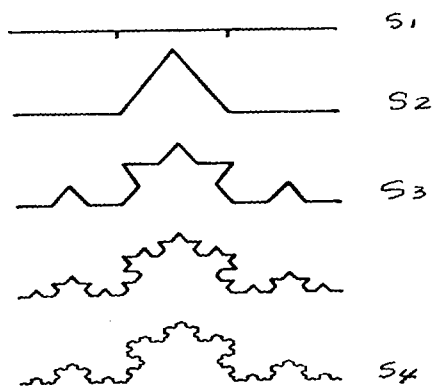

Fig. 2.5: Construction of the Koch curve

Example 1: The construction of the Koch curve which is a non-integer fractal dimension consists of the following steps. The construction begins with a straight line (S1) which is

partitioned into three equal sections. Then the middle third is replaced by an equilateral triangle while its base is removed (S2). By repeating exactly the same procedure on each of the resulting line segments, the complex curve is created (S3). If the procedure is repeated two more times, then a curve is obtained (S4). The same procedure can be repeated until the length of each segment is close to infinity. The fractal dimension can be calculated by the scaling down ratio r (= 1/3) and the self-similar parts or the increasing factor $N(r)$ (= 4) of each scaling down procedure on each of line segments which are produced by the last procedure. The fractal dimension D for the Koch curve is equal to -log(4)/log(1/3) = 1.2619. It is implied that the Koch's curve is an object between a straight line and a plane, but close to a line (Mandelbrot 1977; Pfeifer and Avnir 1983). The general formula for calculating the fractal dimension is

$$D = -\lim_{r \to 0} \frac{\log N(r)}{\log r}$$

or

$$N(r) \propto r^{-D} \qquad (2.13)$$

It shows that the self-similar parts are a function of the scaling down ratio. Eq. (2.13) can also be used to calculate dimensions of the Euclidean geometry for a line, a plane, or a cube. If there exists a unit square and the minimum number of balls of radius r that can be centered at suitable points of the square so that each point of the square lies inside at least one ball is $N(r)$, then $N(r)$ is a function of r, expressed as $(r^2)^{-1}$ when r is close to zero. If the same is done for a unit cube, then $N(r)$ is a function of r as $[(4 / 3) r^3]^{-1}$. The exponent 2 for the unit square and exponent 3 for the unit cube reflect dimensions of the square and cube, respectively. If some object with dimension $2 < D < 3$ is filled with such balls, then $N(r)$ is defined as r^{-D}. The fractal dimension for such a subset is thus D.

Example 2: the self-similar parts are also a function of the scaling up ratio with exponent is D, instead of $-D$. One of such fractal objects is illustrated in Fig. (2.6). This fractal is embedded within two-dimensional space ($d = 2$) and its construction is based on the following replications. In stage 0 of construction, the object is one solid disc with area equal to one. In stage 1, the disc in stage 0 is replaced by 5 other ones with the same size as in stage 0 and they are organized as in stage 1. In stage 2, the motif of stage 1 is replicated five times and these five replications are organized as in stage 2. This rule (replication and organization) can be repeated to infinity. The fractal dimension for such a fractal object at a certain stage k can be derived from self-similar parts $N(r)$ and scaling up ratio r. At stage k, $N(r)$ is equal to 5 and r is equal to 3. Therefore, the D is equal to ln5/ln 3 = 1.46.

It is necessary to note that the fractal dimension for this object can also be calculated by the total number of discs $N(k)$ and diameter $r(k)$ of the motif at stage k. At stage k, $N(k)$ is 5^k, the diameter is 3^k. $N(k)$ ($= 5^k = 3^{k\ln5/\ln3} = r(k)^{\ln5/\ln3}$) is equal to $r(k)^D$. The diameter $r(k)$ is the diameter of the circle which is centered at the center of the motif. The relation of $N(k)$ to $r(k)$ is well known as the mass-radius relation for a fractal object (Russ 1994). Practically, the fractal dimension for a fractal object is frequently based on this mass-radius relation. Fig. (2.7) is used to define a site-radius relation based on a lattice model. The site here can be replaced by any quantity of interest such as surface, mass, or pore.

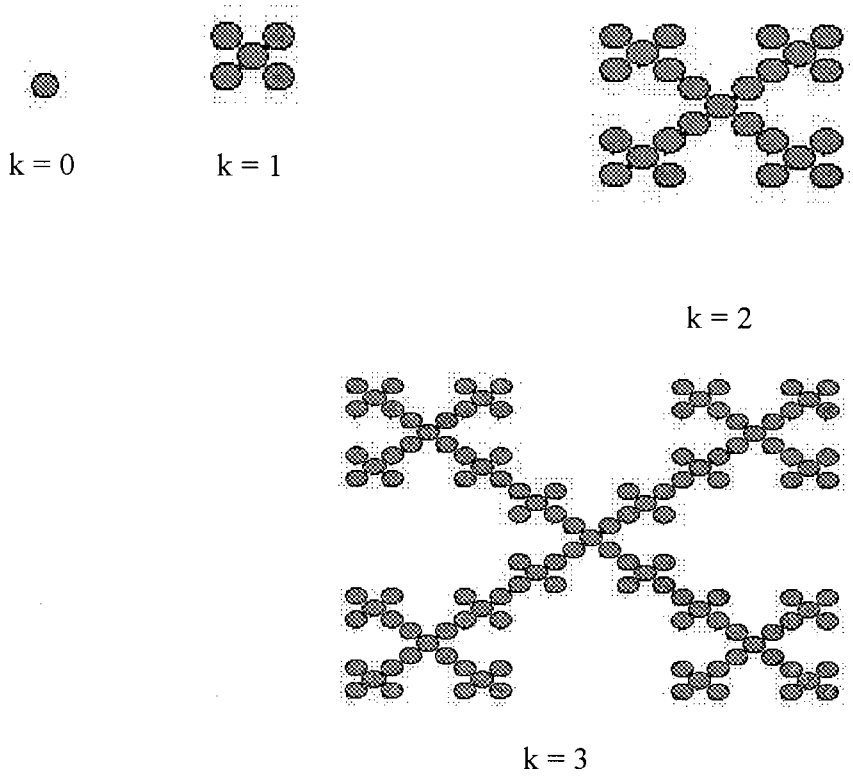

Figs. 2.6: Construction of disc motif

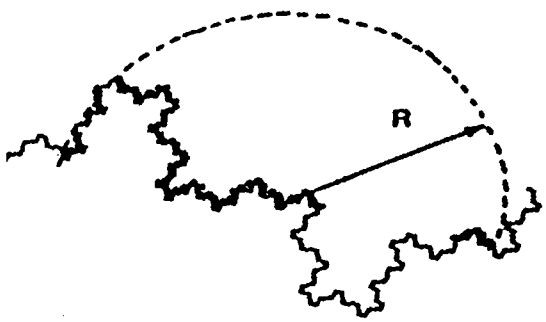

Fig. 2.7: A lattice model between mass and radius

The lattice sites are used to count increasingly distant neighbors. To make things easy to be understood, it is assumed that the disorder or roughness exists at all length scales (no inner/outer

cutoff of the fractal regime), and the distance between the nearest neighboring sites is one, then the quantity of interest (all sites on the surface, or part of sites which are randomly and uniformly distributed occupied sites) is the number of sites located within distance R from a given site. If M_{sites} (r) is called quantity of interest in a sphere of radius R and grows as follows (Vanselow and Howe 1988)

$$M_{site}(R) \propto R^{D} \tag{2.14}$$

If D is equal to 1, it indicates that the quantity increases with R linearly. If D is equal to 2, it indicates that the quantity increases by coating a flat surface. If D equals to 3, the mass increases with R in volume. If D is less than one, it indicates that the sites are discrete and result in dust. If D is any non-integer between 0 and 3, it is evident that the surface or system has fractal properties.

According to the distribution of mass in space, the system can be classified either as a mass, a surface, or a pore fractal. Specifically, if a solid has internal surfaces (interface between solid and pore) and part of its surface is occupied by the other solid object with certain mass and with uniform distribution along the surface, the system is called a mass fractal (Fig. (2.8b)). If each of the possible sites on the underlying surface is occupied or the occupied sites with the unoccupied

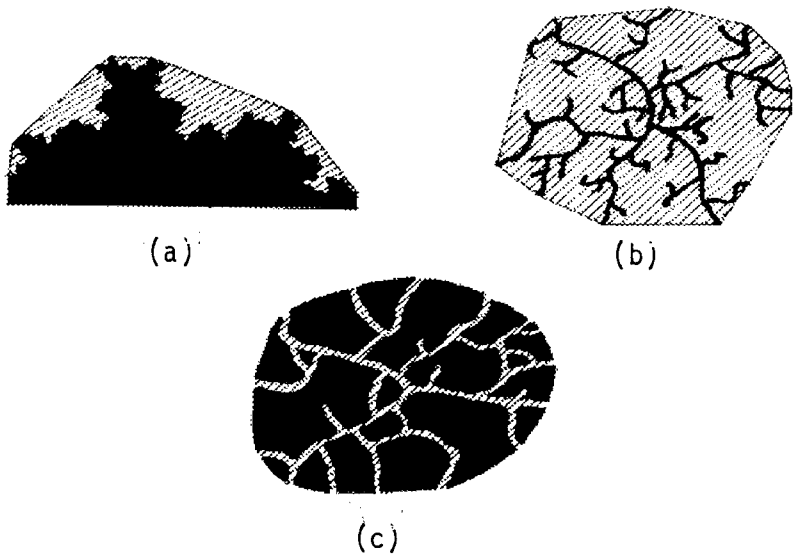

Fig. 2.8: Surface (a), mass (b), and pore (c) fractal

sites are considered together, the system is called a surface fractal (Fig.(2.8a)). If pore volume and surface scale are alike, it is then called a pore fractal (Fig. (2.8c)) (Avnir and Jaroniec 1989; Russ 1994).

In terms of the general definition of fractals (Fig. (2.7), and Eq. (2.14)), if the occupied sites are referred to as mass sites, if the occupied sites with adjacent empty sites are referred to as surface sites, and if the empty sites in the convex hull of the occupied sites are called the pore fractal, then Eq. (2.14) can be changed to the following three subset equations for mass, surface, and pore fractals, respectively,

$$M_{mass}(R) \propto R^{D_{mass}} \tag{2.15a}$$

$$M_{surface}(R) \propto R^{D_{surface}} \tag{2.15b}$$

$$M_{pore}(R) \propto R^{D_{pore}} \tag{2.15c}$$

These three sub-fractal systems frequently exist in the natural world and have successfully been applied to deal with some complex processes involved in complex geometry.

Since the first applications of the fractal surface at molecular scales, the experimental investigations have covered a wide variety of materials with well defined fractal dimension which is proven to be a key factor in controlling physical and chemical processes (Avnir *et al.* 1983). In recent years, the concept of fractal geometry has frequently and successfully been used to treat adsorption processes. This approach is helpful in investigating the nature of adsorption complexes and the distribution of active sites (Pfeifer 1986; Fripiat *et al.* 1986; Kutarov and Kats 1993).

2.3.3 Approaches to determine fractal dimension at the molecular domain

In general, the fractal objects could appear in two cases: One is that the adsorbate is adsorbed on a fractal surface of the adsorbent and just tightly follows such a surface (surface fractal), and the other is that the adsorbate does not always follow the surface. As the process progresses, the adsorbate itself could pack up (cluster) together or grow up on the surface because of the interaction among the sorbed molecules. In this situation, the sorbed molecules will be distributed in space with a certain geometry (mass fractal).

For the former case, Pfeifer and Avnir (1983) have proposed three methods to evaluate the roughness or irregularity of the underlying surfaces. These are

(a) Formation of monolayers by using different adsorbates of similar shape on the underlying surface.

(b) Formation of monolayers with one certain adsorbate on adsorbent particles with altered sizes and a similar shape.

(c) Determination of the pore-size distribution of the underlying surfaces.

In a typical adsorption experiment, the surface area of a solid is determined by the amount of the adsorbate corresponding to the monolayer formation. The coverage or capacity of the monolayer is a function of the radius of the adsorbate. The fractal information is contained in such a function. The principles are shown in Fig.(2.9) according to the BET theory. The fractal dimension D of such surface can be calculated based on Eq.(2.13). This is the basic idea in case (a) above. This method for determining the fractal dimension is easy to be understood. However, it is difficult to choose a suitable series of molecules with different cross-sectional areas, but the same shape.

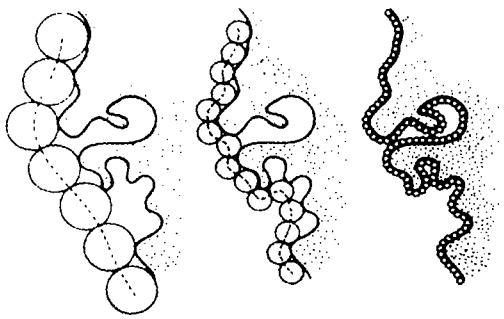

Fig. 2.9: Principle of determination on fractal dimension by variable size of molecules according to the BET theory

The principle behind case (b) is similar to the mass-radius mechanism. The fractal dimension would be demonstrated when larger and larger specimens are probed with a single molecule. This possibility is important because it frees the determination of the D value from the need to find a suitable series of the adsorbates. However, the shape of the surfaces is difficult to be the same at different particle sizes.

The principle behind case (c) is that the inaccessibility of the rough surface to molecules of

a given size is related to the volume of pores. The volume of a pore with radius r is defined as the volume around the surface that is inaccessible to spheres of radius r (Fig. (2.10)).

Case (c) is applicable to the situations in which the pore distribution is wide. In the case of wood, the pore distribution within cell walls is narrow and the pore diameter is microscopically small. Therefore, this method may not work well on wood. Case (b) would also not work in the case of vapor sorption in wood because wood is a swelling material.

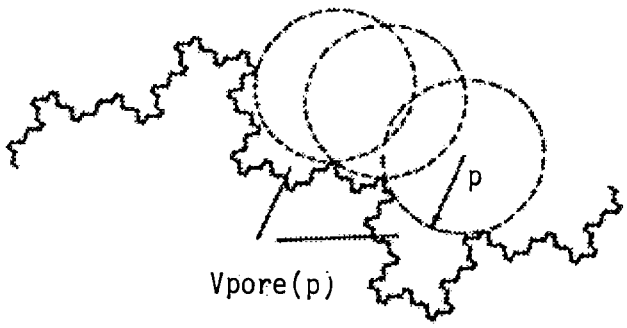

Fig. 2.10: The pore definition for the fractal object

These three cases have extensively been used to determine the D value of complex materials based on adsorption data for different areas. Avnir *et al.* (1983) applied cases (a) and (b) to adsorption data of seven porous materials (graphite, dume silica, faujasite, crushed glass, charcoals, and silical gel) and determined D based on Eq. (2.13). The D value varied from 2 to almost 3 (for smooth and very irregular surfaces), respectively. Siauw and Fairbridge (1987) applied cases (b) and (c) to determine D of oil samd coke by using specimens with different particle sizes based on sorption data of nitrogen and carbon dioxide. These two methods

produced identical D (= 2.48) values. Eltekova *et al.* (1993) applied several adsorbents on carbon black and calculated the apparent surface area based on the BET theory. The calculated D values were 2.8, 2.6, 2.5, and 2.0 for four different oxidization periods, respectively. Case (c) is normally based on mercury intrusion data for porous material where the pore size distribution can be determined, and thus D can be derived (Zhang and Li 1995). Nagai and Yano (1990) applied cases (a), (b), and (c) to study the fractal structure of deformed potato starch. The results between methods were quite different.

For some polar, porous, and hygroscopic materials, the adsorption is not just limited to one layer, but there does exist a multilayer formation phenomenon. Sometimes, the monolayer and multilayer develop simultaneously. In this case, the above three methods cease to function. Several methods that deal with the multilayer adsorption on rough surfaces have been introduced in the past (Pfeifer *et al.* 1989a; Aguerre *et al.* 1996; Pfeifer *et al.* 1989b; Cole and Holter 1986; Lefebvre *et al.* 1992; Fripiat *et al.* 1986; Neimark 1990; Kutarov and Kats 1993; and Avnir and Jaroniec 1989).

One approach to determine D of rough surfaces is based on sorption isotherms originating from the BET and FHH (Frenkel, Halsey, and Hill in Steele 1974) theories. The main difference between FHH and BET is that in the former, a complete adsorption film can be formed and the shape of the film is identical to that of the surface on which the film is adsorbed. The surface-adsorbate interaction is a so called long range one, that is, such all interaction will control all layers in the film. As a result, the surfaces based on the FHH theory will produce much higher heat of adsorption than surfaces that are based on based on the BET theory. By contrast, the BET theory is short range, namely, the interaction between adsorbate and surface controls just the first layer or first several layers (Avnir and Jaroniec 1989; Pfeifer and Cole 1990). In addition,

it will be difficult for adsorbates to form a complete film on the surface. Therefore, the BET theory is somehow suitable for mass fractals while the FHH theory is suitable for surface fractals. Determination of D by the BET and FHH theories is based on their framework of changing their original flat surfaces to rough ones. Because the FHH theory has lower chances of application at the relatively high humidities in real processes, especially for wood, this theory is of less importance than the BET.

Conversion of the classic BET theory that is suitable for smooth surfaces into a fractal-based BET one that is supposed to be more suitable for rough surfaces is mainly based on two methods: molecular and topological approaches (Fripiat *et al.* 1986; Pfeifer 1988).

According to the molecular approach, if a fractal surface such as the Koch curve (Fig. (2.5)) is covered by a number of i layers of the molecules, the D value of the resulting surface at the i-th layer (D_i) is less than that at the (i-1)-th layer (D_{i-1}).

According to the topological approach and the pore fractal theory, a fractal surface could also be defined by porous characteristics and thus, the adsorption on the fractal surface becomes the adsorption on the pores of various sizes. For a single pore of radius ρ, there holds the BET isotherm. This approach is not applicable to the wood cell wall case because the distribution of pore sizes within cell walls is very narrow and the pore sizes are very small.

2.4 Percolation theory

One theory which links a cluster with its geometry is the percolation cluster theory. Such links are provided by the fractal theory (Staufer and Aharony 1992; Russ 1994). For example, a small part of a large two-dimensional array of squares is shown in Fig. (2.11a). Physically, such an array is called a square lattice. A certain fraction of squares is filled with a big dot in the center

while the other squares are left empty, Fig. (2.11b). A cluster is defined as a group of neighboring squares occupied by these big dots. These clusters are encircled in Fig. (2.11c). It is noted that the neighboring squares are referred to as squares that they have one side in common and they are not only touching at one

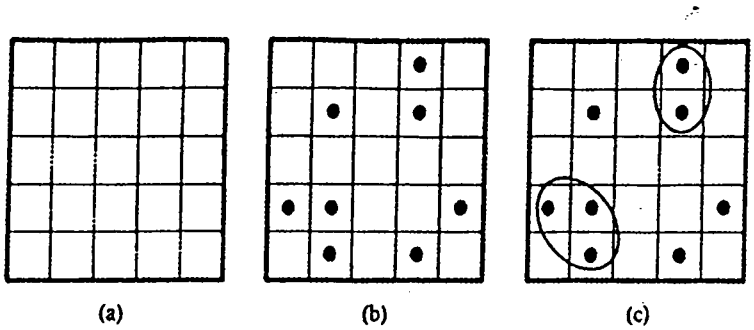

Fig. 2.11: A simple percolation cluster model

corner. Percolation theory just deals with the number and properties of these clusters, such as their size, their distribution, and the geometry of each cluster based on the assumption that occupation of squares is random and independent of the occupation status of its neighbors (Deutscher *et al.* 1983). If p is the probability by which a square is being occupied by a big dot, then the number of the occupied squares will be N × p, where N is the total number of squares of a large array of squares. The empty squares are (1 - p) × N. The cluster size increases with the probability p by which one square is occupied. When p is up to a particular value, one cluster size will grow dramatically. Such p is then defined as threshold concentration or critical concentration, p_c. This particular phenomenon of percolation near the concentration p_c is called the critical phenomenon. Figs.(3.12a, 3.12b, and 3.12c) are examples of percolation on a 60 × 50 square lattice for three different p's as indicated. Occupied squares are shown as "*", empty

squares are ignored. The threshold concentration is 0.5928 (Staufer and Aharony 1992). When p is equal 0.5, there are two clusters within the lattice, Fig. (2.12a). When p is equal to 0.6 (larger than p_C = 0.5928), the largest cluster extends the lattice from left to right and from top to bottom, Fig. (2.12b). At p equal to 0.7, the cluster almost spreads out to the whole lattice, Fig. (2.12c). The percolation theory deals with a number of these clustering critical phenomena that have to do with cluster geometry according to mass fractal theory within one cluster.

2.5 Past research on wood by using fractal theories

Because fractal geometry deals with quantitatively complexity with a single parameter, it could be a powerful tool to study geometric heterogeneity of wood. Currently, only three papers have been published by Hatzikiriakos and Avramidis (1994), Redinz and Guimaraes (1996), Fan *et al.* (1999) in the past. The former one studied the D value of wood internal

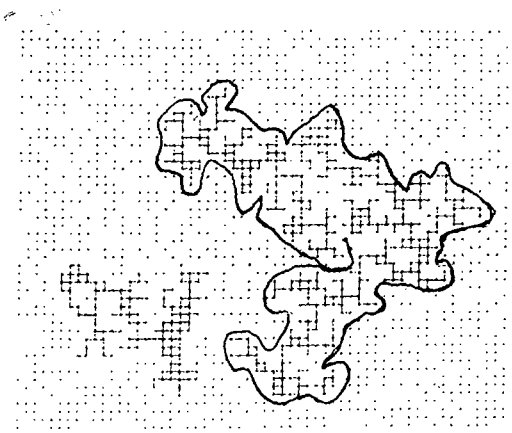

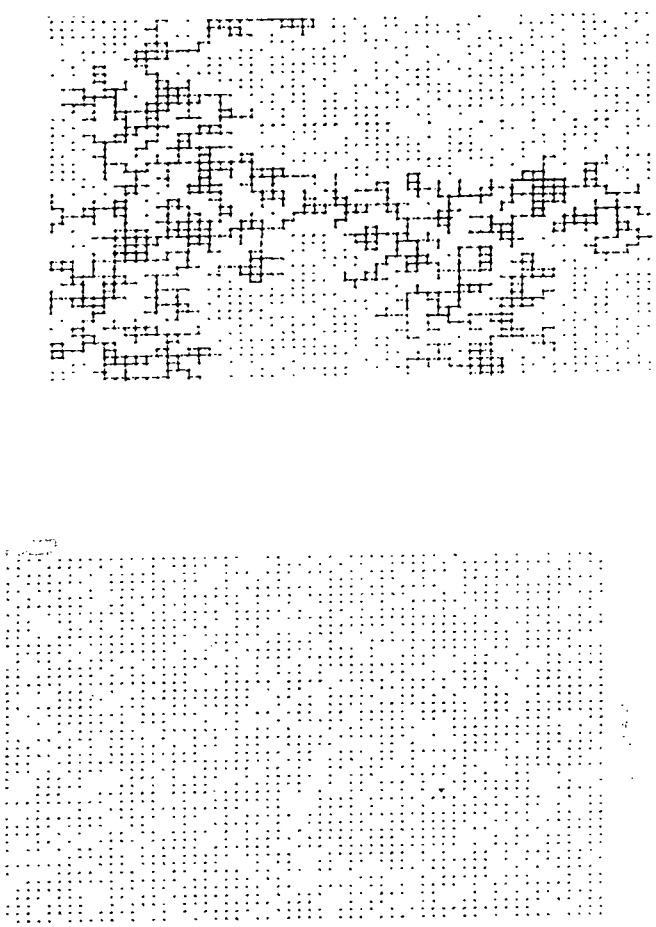

Fig. 2.12: Illustration of a percolation cluster phenomenon

surfaces of the cell walls by using sorption data from Kelsey's (1957) study. It was indicated that the complexity of internal cell wall surfaces was far from being described

as two dimensional. The latter one used the same methods as in the former one and studied the D values of five British Columbian softwood species. The results further indicated the complexity of the sorption processes in wood. The study done by Redinz and Guimaraes (1996) calculated the D value of pore spaces of wood by water absorption for four Brazilian wood species. It was also indicated that the complexity of the pore space (cell cavities) was not three-dimensional, but between 2.5 and 3.

Studies on the D value of wood surfaces in Hatzikiriakos and Avramidis (1994) and Fan *et al.* (1999) used theories as described in (Kutarov and Kats 1993). The first was based on extending the FHH theory to polymolecular adsorption on fractal surfaces, Eq. (2.16). The second, so called thermodynamic approach, was based on the adsorption-film surfaces and was effectively applied to determine the D value for the surface from sorption isotherms, Eq. (2.17). The third approach was based on the modified BET multilayer sorption equation, Eq.(2.18). The respective equations are,

$$D = 3 + \frac{d[\ln M(h)]}{d[\ln(-\ln h)]} \tag{2.16}$$

$$D = 2 + \frac{d\left[\ln\left(\int_m^{m_{max}} (-\ln h)dM\right)\right]}{d[\ln(-\ln h)]} \tag{2.17}$$

$$M = M_m \frac{ch(1-h^n)(1+h^n)^{\frac{1}{3}}}{(1-h)(1-h+ch)} \tag{2.18}$$

where M and M_m are moisture content at a given relative vapor pressure h and at a full monolayer capacity, respectively; c is a constant related to the heat of adsorption, and n is the number of layers of sorbed molecules.

Physically, n should be a positive integer. However, analysis of sorption data usually shows that n is not a integer. Kutarov and Kats (1993) assumed that the fractional part of n in Eq. (2.18) reflects the fractal nature of sorption and stated as:

$$D = 2 + n_{fs} \tag{2.19}$$

where n_{fs} is the fractional part of n.

Based on Eqs. (2.16), (2.17), (2.18), and (2.19), the calculated D values were between 2.4 and 2.805 at h between 0.25 and 0.85, dependent on the equation which was applied.

Results from Eq. (2.16) agreed with those from Eq.(2.18), but disagreed with those from Eq. (2.17). It seemed that Eqs. (2.16) and (2.18) could be applied to determine the fractal dimension of wood surfaces. However, this conclusion should be critically treated because in Eq. (2.18), the parameter n of the BET theory is always adjusted for the best fit to the experimental data.

In addition, Eqs. (2.16) and (2.17) provided totally different D values outside the hygroscopic range of 0.25 to 0.85. It pointed out that at least one of these two methods Eqs.(2.16) and (2.17), could not be suitable for wood. To resolve these issues, determination of the true D value along the hygroscopic range seems paramount.

Redinz and Guimaraes (1997) used a simple experimental procedure of the pressured water absorption to show the fractal nature of the pore space (mainly cell lumens) in wood based on the mass fractal (mass-radius relation) mechanism. The mass (water which is absorbed in a cubic shape specimen of wood) is a function of the length of the cubic shape sample edge,

$$M(L) \propto L^{D} \tag{2.20}$$

where D is the fractal dimension of the pore space (mainly void space) of wood, and L is the length of the edge of the cubic shape specimens (mm), and M(L) is weight of absorbed water in cube with edge length of L, (g).

Based on Eq. (2.20), the calculated D values ranged from 2.46 to 2.92 among four species and four pressure levels. Such D values show that the distribution of the void volume in space is not volume-filling (three-dimensional), but a kind of filling between two-dimensional and three-dimensional. It also put forward the D value as a new relevant parameter to characterize the porosity of the wood.

2.6 Summary

Geometrically, complex objects can quantitatively be characterized by using a D value. Wood vapor sorption process is a complicated phenomenon that takes place in a very complex environment, namely, the cell walls. Within cell walls, the geometry is unambiguous, and because of the swelling properties of wood, their geometry could be changing with the relative vapor pressure. Under different temperature levels, the sorption energy distribution between sorption sites is variable. Also, the sorbed water molecules could have a chance to form a cluster. Such geometric and energetic complexities in addition to the dynamic states of the sorbed water demand that the wood vapor sorption process requires a new approach to somehow account for them all together. Fractal geometry could be a solution.

0Eqs. (2.16), (2.17), (2.18), and (2.19) were able to determine the D values from sorption data. The calculated D values may not reflect the geometry of the cell walls because the derivations of these three equations were based on the thick sorption films located at the top of the underlying surfaces. Water molecules could not form an entire film on the internal surfaces of the cell walls.

Since wood is a swelling material, the geometry of its internal cell walls could be changing with h. A new equation or approach is therefore needed to be able to reflect such multi-geometry/fractal phenomenon.

Chapter 3

Methodology

This research project was divided into two experimental phases. The first produced sorption isotherms to validate the new sorption models which are presented in Chapter 4. The second was focused on measuring the equilibrium moisture content for different specimen sizes that could be used in calculating the D value. For each phase, air temperatures of 30, 40, and 50°C were used.

3.1 Materials

The two species used for this study were Douglas-fir (*Pseudotsuga menziesii* (Mirb.) Franco) and Western red cedar (*Thuja plicata* Donn). They were saved for RF/V (radio frequency/vacuum dryer) experimentation and wrapped in thick black plastic to minimize the loss of water. The moisture content was 85% sapwood, 43% heartwood for Douglas-fir and 51% heartwood for Western red cedar. Each species was further separated into two types, namely, Douglas-fir sapwood (DFS), Douglas-fir heartwood (DFH), and also extracted Western red cedar heartwood (E-WRC) and unextracted Western red cedar heartwood (UE-WRC). The specific gravities of these two species are listed in Table 1.

The main reason for the choice of these two species in this study was their distinct difference in specific gravity and extractive content which are potential factors for affecting their sorption ability (Kolin and Janezic 1996) and which in turn, could affect the geometry of the wood internal cell wall surfaces. Wood with higher extractives content showed in many

cases significantly reduced hygroscopicity than woods with lower extractives content (Stamm 1964, 1971; Spalt 1958; Wangaard and Granados

Table 1: Specific gravity of Douglas-fir and Western red cedar (Jessome 1977)

Species	**Oven-dried specific gravity**	**Green specific gravity**
Douglas-fir	0.51	0.45
Western red cedar	0.34	0.31

1967). This results from the deposition of extractives within the cell walls allowing less space in the wood for water sorption. The low hygroscopicity may also result from the fact that the extractives could cover a number of active sorption sites.

Three temperature levels, namely, 30, 40, and 50°C, were chosen to evaluate temperature effects on the D value of the internal cell wall surfaces. The M value decreases with an increase in temperature by 0.1% per °C on the average (Skaar 1972) and this change could be related to the change of geometry of the internal surfaces of the cell walls.

3.2 Specimens preparation

Two shapes of specimens were used. One was wafers with a uniform size, and the other was cubes with various sizes. For each shape, the number of replicates was ten which theoretically, might not sound large enough for accuracy. However, equilibrium moisture content measurements are very time-consuming and sensitive method which is greatly affected by the number of specimens and the particular experimental set-up. The use of conditioning chambers, as in this study, considerably limited the maximum number of replications. The wafers were

used for developing experimental sorption isotherms, and the cubes for investigating moisture content levels of different sizes.

3.2.1 Wafer type

Wafer-type wood specimens (30mm × 20mm × 2mm in thickness) (Fig. 3.1) were used in phase 1 of this study. Their thickness direction was aligned with the tree's tangential direction. To decrease anatomic variation, the specimens were made by cutting a bar of 20mm × 20 mm × 200 mm in length along the longitudinal direction to make sure the straight and parallel annual rings. Specimens were then made by slicing (2mm in thickness) the resulting bar radially and longitudinally with a circular saw. Each specimen contained 7~10 straight annual rings that were parallel to each other and parallel to the side edges. The specimens were free of visual defects and had smooth surfaces. Low thickness was used to facilitate the rapid establishment of equilibrium. In addition, the utilization of such thin specimens made the rapid removal of extractives possible without adversely affecting the wood substance. For western red cedar, one set of specimens was extracted. Ten best specimens were selected out of 30 specimens for each type of wood based on visual evaluation (no defects).

The solvent used to remove the extractives from Western red cedar was methanol. It was chosen because it can remove both volatile and involatile extractives. Twenty wafer-type specimens were extracted in a soxhlet apparatus with methanol for about 12 hours. The extraction continued until the solution surrounding the samples in the apparatus was visibly free of color from dissolved extractives. This was followed by distilled water extraction for 4 hours. The extracted samples were then washed several times with hot distilled water. After these three steps, the initial extractives content of western red cedar was 9.5%, calculated by dividing the

oven-dried weight of the specimen into the weight of extractives which was calculated by a subtraction of the pre-extracted and post-extracted specimen weights. The extractive-free specimens were wrapped in wet cloth to avoid of pre-drying before the experimental determination of sorption isotherms.

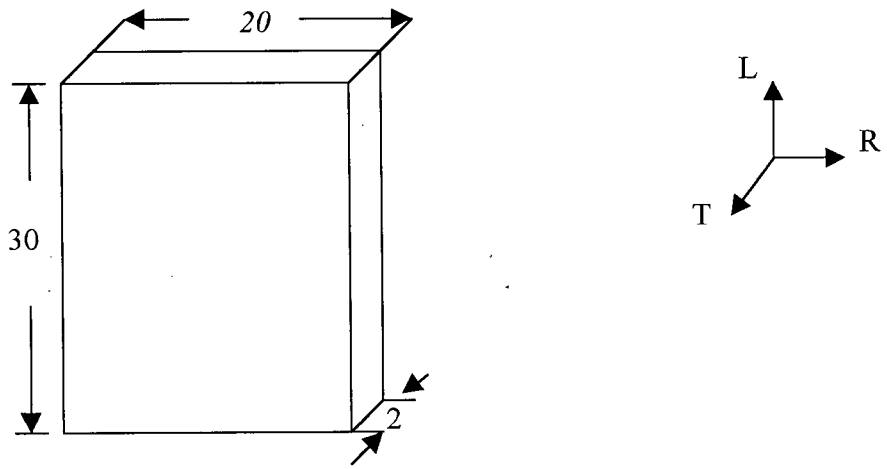

Fig. 3.1: Schematic of the wafer-type specimen (unit: mm)

3.2.2 Cubic type

Douglas-fir heartwood and unextracted Western red cedar heartwood materials were used to make cubic type specimens with variable sizes (Fig. 3.2). The way these specimens were prepared was similar to the one used for wafer-type specimens. To minimize the anatomic variations, 50mm× 50mm × 300mm in length bars were initially made (close to each other) and then all cubes were cut from them with a circular saw. The specimens were as close to each other as possible. The edge length of the cubic specimens was about 10, 15, 20, 25, 30, 35, and 40 mm with the direction of the grain parallel to the edge. For each size, the ten best specimens

were selected out of 20 specimens considering smooth surfaces, straight grains, checks, and lack of corners.

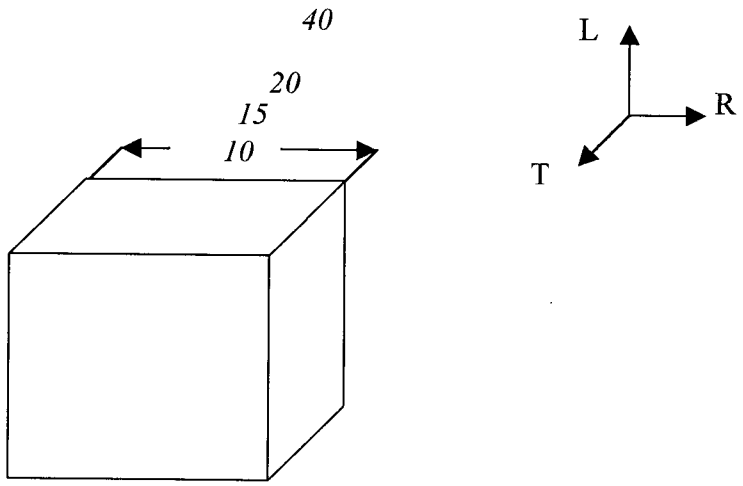

Fig. 3.2: Schematic of the cubic-type specimen (unit: mm)

3.3 Sorption isotherms development

The tests were carried out in the two conditioning chambers (Parameter Generation and Control , models 4 - PC and 9 - SS) located in the UBC Wood Physics Lab. Each chamber created a stable climate with an accuracy of ±1% in relative humidity and ±1°C in air temperature. The calculation of the *h* value was based on direct dry-bulb and wet-bulb readings from the chamber. An accurate calculation of the saturation vapor pressure within approximately 1% between 0°C and 160°C was obtained from Kirchoff's equation (Siau 1995).

$$p_o = \exp(53.421 - \frac{6516.3}{T} - 4.125 \ln T) \qquad (3.1)$$

where p_o is the saturation vapor pressure, (Pa), and T is absolute temperature, (°K). The determination of the partial vapor pressure was obtained from equation (Siau 1995) as:

$$p = P_{ow} - \frac{(P_{atm} - P_{ow})(C - C_w)}{1546 - 1.44C_w} \qquad (3.2)$$

where p is the partial vapor pressure, (P_a), P_{ow} is the saturated vapor pressure at the wet-bulb temperature, (P_a), C is the dry-bulb temperature, (°C), C_w is the wet-bulb temperature, (°C), and P_{atm} is the atmosphere pressure, (P_a). The determination of the h value was obtained from its definition as:

$$h = \frac{p}{p_o} \qquad (3.3)$$

Each specimen was placed in a weighing bottle. The procedure of sorption measurement followed a stepwise mode. For each temperature, the measurement was started with desorption, then the humidity of the chamber was decreased by decreasing the water temperature. The relative vapor pressure was produced in each chamber ranged throughout this study from about 0.96 to 0.06. The lowest h value of 0.06 was created by a saturated solution of LiCl that was contained in a desiccator. The specimens were placed above the solution and the solution temperature was controlled by the conditioning chamber. A magnetic stirrer was used to eliminate the formation of a water film on the surface of the solution.

After equilibrium at the lowest humidity, the specimens were transferred to a vacuum oven until constant weight was reached to determine their oven-dried weight. Because some Western red cedar specimens were not extracted, the oven temperature was set at about 45°C to minimize removal of volatile extractives. The specimens remained in the oven for one week and

were then removed in order to initiate the adsorption process. The weight of the weighing bottle and specimen was measured by using a digital balance with a precision of 0.0001g.

3.4 *EMC* measurements of the cubic specimens

The sorption of the cubic type specimens at a h (> 0.92) was carried out in the same conditioning chambers as the wafer-type specimens at 30, 40, and 50°C. The choice of h = 0.92 was based on the water molecule clustering consideration. When the weight of the specimens measured by an electrical balance with a precision of 0.0001g in three consecutive times changed less than 0.0005g for 24 hours, they were assumed to be at equilibrium. Because of the difficulty of a complete removal of extractives from a thick specimen, no extraction was performed.

Chapter 4

Modeling

4.1 Modification of the classic BET equation with fractal theory (FBET)

4.1.1 Theoretical model

By contrast with non-swelling materials, wood cell walls may not exhibit a large internal surface area when M is close to zero. This area, however, would increase with an increase in moisture content because wood is a swelling material. At low relative humidity, the sorption sites may be scattered and thus, cannot form a complete "surface". At a certain point or range of h, such a surface could be formed and the sorbed water molecules may afterwards follow this trend (monolayer in the classic BET theory). However, beyond a certain h value, the adsorbed water molecules may no longer trail the formed surfaces. Instead, they might cluster over the surface. The geometry of such clusters will determine the geometry of the cell wall internal surfaces. In short, the sorption of water molecules makes the internal cell wall surfaces ever-rough and ever-irregular. It should be pointed out here that the geometry of the surface in fractal theory may be a point or many points or a curve, namely, it may be any object with a D value between 0 and 3.

The internal surfaces of the cell walls could be ever-roughened with an increase in M because of water molecular clustering above a certain h level as well as because of the high energetic distribution among sorption sites. Fig. (4.1) shows the sorption process from a low to a high h based on the above analysis. At a low h, the sorbed water molecules break internal wood bonds and create gaps between wood substrates, Fig. (4.1a). As h increases, the interfaces (wood internal surfaces) between water molecules

a)

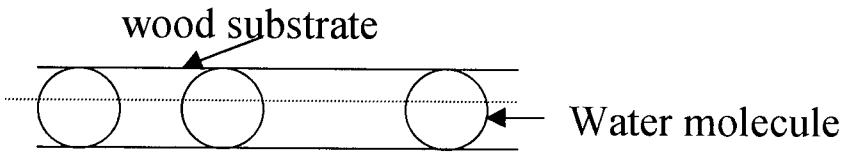

b)

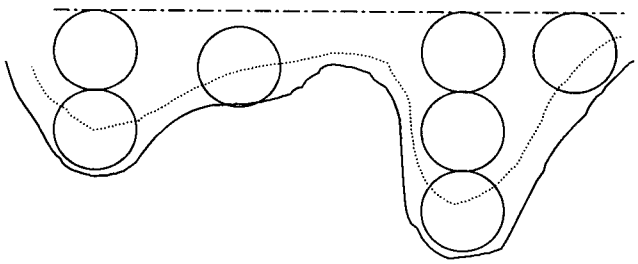

c)

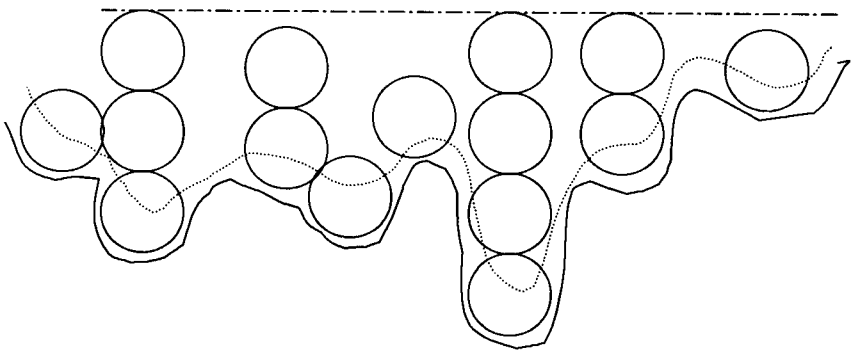

Fig. 4.1: Illustration of water molecule sorption processes in wood

(***Note***: solid line is wood surface, dash line shows molecules which touch the wood surface directly, and dot-dash line implies the base line where the molecules start. Either side of dot-dash line could have sorbed molecules.)

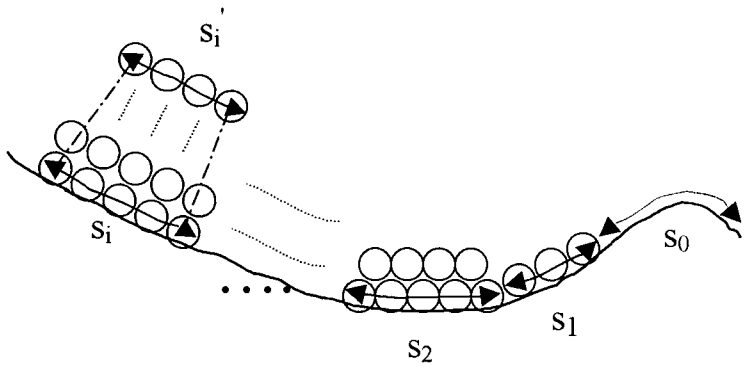

Fig. 4.2: Physical model for stacking of sorbed water molecules

(*Note*: S_i is the bottom area occupied by a molecule stack with i layers and S_i' is the top area of the molecule stack.)

and wood substrate get larger, Figs. (4.1b and 4.1c), the gaps get wider and wood swells. The interfaces get rougher because of the upcoming water molecules that depress the wood substrate down or up at different degrees from point to point. The first layer is marked by a dash line. All its immediate neighboring molecules form the second layers. A part of the surface from Fig. (4.1c) was enlarged and then the molecules were rearranged by moving same height water molecules together as a stack. Fig. (4.2) shows the simplified model for the part of Fig. (4.1c) to facilitate the development of the mathematical model. Basically, Fig. (4.2) is the same to the one used in the classic BET model, except that a non-flat surface has being considered. In an *i*-layer stack, the number of the molecules on its bottom layer is represented by s_i and the number of the

molecules on its top layer is represented by s_i'. On a rough surface, s_i and s_i' is related together by the degree of roughness of this surface, namely, its D value (Pfeifer, *et al.* 1989a).

All water molecules within the cell walls can be simplified as a series of water molecule piles with 0, 1, 2, 3, ..., up to n layers. The total number of sorbed water molecules in wood can then be obtained by adding up all molecules in all these stacks. The number of water molecules in the first layer, namely, the ones directly touching the wood substrate, can also be accounted for by adding up all bottom layer molecules from each stack. The fractal based BET model can thus be derived from the above two summations.

4.1.2 Mathematical model

In fractal surfaces, unlike the classic BET model, the number of water molecules on each layer of the same stack is different because of the non-flat surface. In a stack, the difference of the number of the sorbed molecules between two consecutive layers, Fig. (4.2), over a rough/fractal surface is related to its D value and defined by coefficient f_i (Pfeifer *et al.* 1989a)

$$f_i = i^{2-D} \tag{4.1}$$

where i is the i-th layer from the bottom layer. The implication of Eq. (4.1) is that the number of sorbed water molecules become fewer and fewer as we move further away from the substrate because the available room for additional molecular sorption decreases.

The derivation of the fractal BET model has followed the framework of the classic BET (Brunaner *et al.* 1938; Skaar 1972), but has also taken the decreasing factor f_i into account on each layer of the stack. The following is a guideline of derivation. The detail is in Appendix A. The total number of the water molecules (N_n) for a stack with n layers can be obtained by using

Eq. (4.1) as:

$$N_n = p_n \sum_{i=1}^{n} i^{2-D} \tag{4.2}$$

where p_n is the number of the water molecules of the first layer in the stack and n is the number of layers in the stack.

The total number of the water molecules (V) for all j possible stacks is then obtained as,

$$V = \sum_{i=1}^{j} N_i = \sum_{i=1}^{j} p_i \sum_{m=1}^{i} m^{2-D} = \sum_{i=1}^{n} \left(cx^i s_0 i^{D-2} \sum_{m=1}^{i} m^{2-D} \right) \tag{4.3}$$

The amount of the entire potential space for all water molecules on all first layers of the stacks can be expressed as:

$$V_m = \sum_{i=0}^{j} s_i = s_0 + \sum_{i=1}^{j} cx^i s_0 i^{D-2} \tag{4.4}$$

Therefore, the derived mathematical model has the following form when the right-hand side of Eq. (4.3) is divided by the right-hand side of Eq. (4.4) and *h, n_{max}, M, M_m are in place of* x, j, V, and V_m, respectively.

$$M = \frac{M_m c \sum_{n=1}^{n_{max}} \left(h^n n^{D-2} \sum_{i=1}^{n} i^{2-D} \right)}{1 + c \sum_{n=1}^{n_{max}} \left(h^n n^{D-2} \right)} \tag{4.5}$$

where M and M_m are moisture content (%) at a given relative vapor pressure h and at a full monolayer capacity, n is the number of layers, n_{max} is the maximum possible number of layers of the adsorbed water molecules in wood, and c is a constant related to the heat of adsorption.

Eq. (4.5) is called FBET equation and used to obtain the D value from very low to very

high relative vapor pressures.

4.2 Determination of *D* value from mass fractal

An alternative way to calculate D is by determining the mass distribution in an Euclidean dimension of the space (d_{top}) in which the fractal is being embedded. The D value is between 0 and d_{top}. This approach totally ignores the internal characteristics of the space in which the fractal exists. The key to mass fractal is that fractals are related to their volume with respect to their linear size. This is visually illustrated in Fig. (2.7). In terms of the principle of mass fractal, the amount of the sorbed water molecules in a cubic block would be a function of the linear size of the cube, namely, the length of the edge of the cube as:

$$M_w \propto L^D \tag{4.6}$$

where M_w is the amount of the adsorbed water molecules (g), and L is the length of the edge of the cubic shape specimen (mm).

A series of specimen with different edge lengths was used. A plot of $\ln(M_w)$ vs.$\ln(L)$ was created to assess if the relationship between them was linear. A linear relationship shows that the sorbed water molecules within the internal cell walls have fractal properties. The D value can then be obtained from the slope of the plot. A t-test is used to test the significant level of the difference between the calculated slope of D value and hypothesized value of 3. Test hypothesis is,

H_0: estimate of slope = 3; H_1: estimate of slope < 3 at $p < 0.05$

t - test is conducted by

$$t = \frac{(parameter\_estimate) - (parameter\_value\_hypothesized)}{s} \qquad (4.6.1)$$

where s is the standard error of estimate.

4.3 New sorption equation

Based on Eq. (4.5) and results from Hao and Avramidis (2001), the calculated D value from Kelsey's (1957) sorption isotherm data was not constant from about h = 0.40 to 0.96. Instead, the D value increased with an increase in h value beyond 0.4. Generally, the D values for each sorption isotherm could be grouped into 2 or 3 regions. This observation showed that a multi-fractal condition was present within the cell walls with respect to the sorbed water molecules. In terms of fractal property, a perfect fractal object can simply be represented by a single D value. In the case of wood, the sorption process/state is dynamic. Therefore, there could be more than one D values associated with. The second part of the new equation can be obtained by using multi-fractal terms as,

$$M_{fractal} = \sum k_i h^{D_i} \qquad (4.7a)$$

where $M_{fractal}$ is moisture content (%) for fractal part, h is the relative vapor pressure, D_i is one of multi-fractal dimension values, and k_i is the corresponding constant to D_i.

The number of D_is depends on the results from FBET (section 5.3.1) with an assumption that D value is stepwise and the number of steps is finite for wood vapor sorption between h = 0.4 to h = 0.97.

The D value could not be calculated when h is less than about 0.4. This is probably because at such low relative humidities, the wood internal surfaces may not have formed a

continuous surface yet. Instead, the "surfaces" are just composed of the discrete sorption sites, from sparse ones to dense ones as h increases to an upper limit of 0.4. These sites are either impossible or very challenging to be described by a fractal concept.

The classic BET's good fitness to wood sorption data below h = 0.5 has extensively been used to estimate its two useful parameter values, M_m and c, and to also estimate the potential sorption area (Stamm 1964).

Two approaches can be followed to achieve this estimation: one is curve-fitting for parameters M_m and c from Eq. (2.2) and the other is based on consideration of linear regression on experimental sorption data (Stamm 1964; Skaar 1972). For the former, the results will have only statistical meaning because the obtained parameter values result from the best curve fitness to sorption data. For the latter, the approach turns out to be more accurate because the experimental sorption data at low sorption regions (below h = 0.5) pose a significantly linear relationship, Eq. (4.7b), between the two variables. Beyond about 0.5 of h, multilayer sorption is dominant. These two variables are obtained from a rearrangment of Eq. (2.1) which is obtained from a consideration of an infinite layer number of sorbed molecules,

$$\frac{h}{M(1-h)} = \frac{1}{M_m c} + \frac{c-1}{M_m c} h \qquad (4.7b)$$

where M and M_m are moisture content (%) at a given relative vapor pressure h and at a full monolayer capacity, respectively, and c is a constant related to the heat of adsorption. Linear relationship between $h/(M(1\text{-}h))$ and h is evident for wood moisture sorption at low sorption regions with a slope of $(c\text{-}1)/(M_m c)$ and an intercept of $1/(M_m c)$. The values of M_m and c can in turn be calculated from the slope and intercept if the theoretical relationship predicted by Eq.

(5.2) is obeyed. The validation of this approach to estimate the parameter M_m and c values is the following,

$$y_i = \frac{1}{M_m c} + \frac{c-1}{M_m c} x_i + \varepsilon_i = \alpha + \beta \cdot x_i + \varepsilon_i \qquad (4.7c)$$

where the data (h_i, M_i) are transformed to (x_i, y_i) and $x_i = h_i$, $y_i = h_i/(M_i(1-h_i))$,

Theoretically, the linear relationship is valid only for $h < 0.6$ in the case of moisture sorption in wood (Stamm 1964, Skarr 1972). The assumption here is that the ε_i are independent and identically distributed normal random variables.

If considering estimation of M_m and c through least squares by minimizing

$$\sum_i (y_i - \frac{1}{M_m c} - \frac{c-1}{M_m c} \cdot x_i)^2 \qquad (4.7d)$$

then this is equivalent to finding α and β by minimizing

$$\sum_i (y_i - \alpha - \beta \cdot x_i)^2 \qquad (4.7e)$$

and then solving

$$\alpha = \frac{1}{M_m c} \text{ and } \beta = \frac{c-1}{M_m c} \qquad (4.7f)$$

Hence, the point estimates for M_m and c are least squares estimates.

As shown above, M_m and c are least squares estimates, provided that the estimated intercept is non-zero. The variances of c and M_m could be calculated by using the variances of estimates α and β as,

$$c = \frac{\beta}{\alpha} + 1 \text{ and } M_m = \frac{1}{\alpha + \beta} \qquad (4.7g)$$

In the large sample situation, the following method can be used. For a function g of the α and β, the variance of the function is given as,

$$\text{Var}(g(\alpha, \beta)) =\sim [dg/d\alpha]^2 * \text{Var}(\alpha) + [dg/d\beta]^2 * \text{Var}(\beta) + 2\,[dg/d\alpha][dg/d\beta]\,\text{Cov}(\alpha,\beta) \quad (4.7g\text{-}1)$$

and an asymptotic confidence interval is

$$g(\alpha\text{hat}, \beta\,\text{hat}) \pm t\text{-value} * \text{sqrt}(\text{Var}(g(a, \beta)) \quad (4.7g\text{-}2)$$

where the sample estimates αhat, βhat are put into the partial derivatives of g.

However, if the sample size is small, the above method to calculate confidence intervals of c and M_m is prone to be erroneous. A confidence region for (α,β) or (c, M_m) can be obtained by inverting a sequence of hypothesis tests.

H0: $\alpha = \alpha 0$, $\beta = \beta 0$ (or $c = c0 = 1 + \beta 0/\alpha 0$, $M_m = M_m 0 = 1/(\beta 0 + \alpha 0)$)

The test statistics is

$$F_{ratio} = \frac{(SSE1 - SSE2)/2}{SSE2/(n-2)} \quad (4.7g\text{-}3)$$

where *SSE2* is the sum of squares of residuals from the least squares fit:

$$SSE2 = \sum (y_i - \alpha hat - \beta hat \cdot x_i)^2 \quad (4.7g\text{-}4)$$

and

$$SSE1 = \sum (y_i - \alpha 0 - \beta 0 \cdot x_i)^2 \quad (4.7g\text{-}5)$$

is the sum of squares of residuals with the null values for the slope and intercept.

Under H0, F_{ratio} has an F distribution with (2, n-2) degrees of freedom, and can be compared with a critical value from the F table.

The confidence region for (c, M_m) consists of the values of ($c0$, M_m0) for which the corresponding null hypothesis

H0: $\alpha = \alpha 0$, $\beta = \beta 0$ is accepted, i.e.,

$$\frac{(SSE1 - SSE2)/2}{SSE2/(n-2)} \leq critical\_value_{(2,n-2)} \qquad (4.7g\text{-}6)$$

Finally, the region of *SSE1* can be marginalized to get confidence intervals for c and M_m separately. The calculation algorithm is simply by using an iterative method to get the *SSE1* region to satisfy the above condition from both directions. The program in C is listed in Appendix B.

The implication of the linear relationship between dependent and independent variables is that M_m is a constant. Physically, it represents the amount of the sorbed water molecules when the sorption sites have, on the average, adsorbed just one water molecule. This usually occurs below a relative vapor pressure of about 0.5. This point is considered to be the completion point of monolayer sorption. The other constant c in Eq. (4.7b) is a function of sorption energy.

By using the classic BET equation with n equal to one in Eq.(2.2), the monolayer part of sorption can be obtained as,

$$M_{non-fractal} = k\frac{M_m ch}{1+ch} \qquad (4.7h)$$

By adding the fractal part (Eq. (4.7a)) and non-fractal part (Eq.(4.7h)) together, a new sorption equation refered to as F-P equation, can be stated as,

$$M = k\frac{M_m ch}{1+ch} + \sum k_i h^{D_i} \qquad (4.8)$$

where, k and k_i are constants for the monolayer term and multi-fractal terms, and D_i is fractal

dimension for one of multi-fractal terms.

Fundamentally, Eq. (4.7a) is identical to the polynomial equation reported by Simpson (1973, 1980) who indicated that a fifth-degree polynomial with six parameters in terms of M and h gave a better fit to sorption data than any of the theoretical classic models. However, no theoretical basis was given, but it took advantage of the ease of mathematical manipulation.

From the point of fractal theory, the polynomial model from Siau (1995) and Simpson (1973, 1980) can be explained by using mass fractals with the exception of non-integer power. If each power of the supposed polynomial equation is no longer an integer, the total number of the terms should be at most five, including both non-fractal and fractal parts.

The value of D_i for one fractal of multi-fractal terms is obtained from the results of the FBET regression with a assumption that the D value increases in h in a locative or stepwise manner. The value of D_i can be calculated by taking an average of D values in one locality or in one step.

4.4 Optimization of the proposed equations

By using curvilinear and linear fit regression techniques with MathCad and Microsoft Excel programs, Eqs. (4.5, 4.6, and 4.8) were fitted to the sorption data and the values of the parameters were predicted. The residue plots were drawn to obtain the goodness of fit of the proposed equations.

Chapter 5

Results and Discussion

5.1 Data collections

Data were collected from four wood species (UE-WRC, E-WRC, DFS, and DFH) and two types of specimens (wafer-shaped and cube-shaped) over 17 months, namely, from December 1988 to May 2000. For each testing point, the wafer-shaped specimens remained in the chamber from about 7 days until equilibrium depending on temperature and relative humidity levels that were used. Normally, lower temperature or higher humidity would need a longer time for the specimens to reach equilibrium. The weights were continuously monitored.

The cube-shaped specimens remained in the chamber for longer times in order to achieve equalized moisture content due to their larger sizes. Normally, it took about one month to achieve equilibrium and one more month was used to equalize the moisture content for specimen sizes. The weights and dimensions were measured after two months of conditioning at h values near 0.92 at 30, 40, and 50°C.

The moisture contents for the wafer-type specimens are listed in Tables 2, 3, 4, and 5 and for the cube-type are listed in Tables 6 and 7. The former is also illustrated in Figs. 5.1 to 5.4 and the latter in Figs. 5.5 and 5.6. There were 10 replications for both the wafer types and cubic types and the listed numbers are all averages coupled with specimen standard deviations.

Table 2: The experimental sorption data for UE-WRC

30°C			40°C			50°C		
h	*M*	*st. dev.*	*h*	*M*	*st. dev.*	*h*	*M*	*st. dev.*
desorption								
0.91	18.05	0.34	0.94	17.11	0.15	0.98	18.30	0.33
0.85	15.94	0.27	0.86	13.76	0.27	0.91	13.83	0.25
0.76	12.65	0.22	0.77	11.50	0.15	0.80	10.65	0.20
0.64	10.46	0.18	0.66	9.32	0.15	0.70	8.42	0.16
0.55	9.05	0.17	0.52	7.52	0.15	0.65	7.53	0.22
0.50	8.20	0.20	0.44	6.44	0.17	0.53	5.96	0.18
0.43	7.24	0.15	0.37	5.33	0.09	0.30	3.79	0.16
0.40	6.97	0.14	0.31	4.98	0.15	0.26	3.41	0.12
0.07	2.92	0.15	0.30	4.86	0.10	0.19	2.76	0.09
0.00	0.00	0.00	0.06	2.28	0.22	0.10	2.11	0.11
			0.00	0.00	0.00	0.06	1.56	0.08
						0.00	0.00	0.00
adsorption								
0.00	0.00	0.00	0.00	0.00	0.00	0.00	0.00	0.00
0.07	1.87	0.14	0.06	1.33	0.09	0.10	1.41	0.17
0.41	4.62	0.16	0.40	3.86	0.16	0.19	1.82	0.12
0.43	4.92	0.16	0.48	4.53	0.18	0.23	2.32	0.11
0.49	5.44	0.17	0.63	6.23	0.18	0.30	2.90	0.21
0.58	6.42	0.11	0.76	8.45	0.17	0.40	3.38	0.22
0.64	7.52	0.25	0.85	11.09	0.18	0.53	4.25	0.24
0.75	9.31	0.21	0.94	15.91	0.33	0.66	5.69	0.26
0.85	12.10	0.16				0.79	7.43	0.18
0.97	18.07	0.26				0.89	10.68	0.27
						0.97	15.39	0.37

Table 3: The experimental sorption data for E-WRC

30°C			40°C			50°C		
h	*M*	*st. dev.*	*h*	*M*	*st. dev.*	*h*	*M*	*st. dev.*
desorption								
0.91	21.53	0.28	0.94	21.59	0.73	0.97	21.55	0.28
0.85	18.25	0.35	0.86	16.76	0.42	0.91	17.55	0.27
0.76	14.85	0.24	0.77	13.49	0.52	0.82	12.94	0.12
0.64	11.56	0.22	0.66	10.84	0.50	0.70	9.81	0.23
0.55	10.14	0.19	0.52	8.15	0.45	0.65	8.68	0.16
0.50	9.17	0.15	0.44	7.29	0.34	0.53	7.14	0.11
0.43	8.15	0.38	0.37	6.20	0.33	0.30	4.43	0.22
0.40	7.63	0.33	0.31	5.81	0.40	0.26	4.11	0.18
0.07	3.79	0.12	0.30	5.70	0.41	0.19	3.56	0.14
0.00	0.00	0.00	0.06	2.99	0.13	0.10	2.61	0.18
			0.00	0.00	0.00	0.06	1.87	0.18
						0.00	0.00	0.00
adsorption								
0.00	0.00	0.00	0.00	0.00	0.00	0.00	0.00	0.00
0.07	2.48	0.13	0.06	1.82	0.11	0.06	1.20	0.22
0.41	5.42	0.25	0.40	4.59	0.23	0.10	1.76	0.11
0.43	5.78	0.21	0.48	5.34	0.19	0.19	2.44	0.12
0.49	6.43	0.24	0.63	7.32	0.31	0.23	2.89	0.14
0.58	7.66	0.23	0.76	9.55	0.24	0.30	3.21	0.08
0.64	8.84	0.21	0.85	12.88	0.25	0.40	4.03	0.10
0.75	11.42	0.24	0.94	17.37	0.37	0.53	5.04	0.14
0.85	14.68	0.27				0.66	6.84	0.15
0.97	21.12	0.30				0.74	8.02	0.11
						0.86	11.28	0.15
						0.97	18.01	0.39

Table 4: The experimental sorption data for DFS

30°C			40°C			50°C		
h	*M*	*st. dev.*	*h*	*M*	*st. dev.*	*h*	*M*	*st. dev.*
				desorption				
0.91	20.21	0.37	0.94	20.43	0.19	0.96	20.98	0.33
0.85	16.64	0.25	0.86	15.41	0.11	0.90	15.45	0.30
0.76	13.78	0.22	0.77	12.98	0.17	0.82	12.21	0.29
0.64	10.92	0.19	0.66	10.25	0.08	0.70	9.58	0.28
0.55	9.83	0.18	0.52	8.32	0.07	0.65	8.60	0.20
0.50	8.73	0.18	0.44	6.79	0.10	0.53	6.97	0.23
0.43	7.70	0.12	0.37	5.83	0.05	0.30	4.47	0.13
0.40	7.29	0.16	0.31	5.41	0.10	0.26	3.69	0.15
0.07	3.71	0.18	0.06	2.67	0.06	0.19	3.22	0.09
0.00	0.00	0.00	0.00	0.00	0.00	0.10	2.20	0.14
						0.06	1.58	0.19
						0.00	0.00	0.00
				adsorption				
0.00	0.00	0.00	0.00	0.00	0.00	0.00	0.00	0.00
0.07	2.46	0.17	0.06	1.65	0.10	0.06	1.01	0.09
0.41	5.73	0.15	0.40	4.86	0.09	0.10	1.86	0.16
0.43	6.00	0.11	0.48	5.77	0.13	0.19	2.49	0.16
0.49	6.70	0.18	0.63	7.87	0.08	0.23	2.83	0.18
0.58	7.74	0.15	0.76	10.63	0.12	0.30	3.40	0.20
0.64	9.07	0.18	0.85	13.81	0.14	0.40	4.07	0.14
0.75	11.54	0.20	0.94	18.52	0.27	0.53	5.61	0.19
0.85	14.85	0.33				0.66	7.16	0.25
0.97	22.01	0.24				0.74	8.84	0.31
						0.90	13.61	0.16
						0.98	19.29	0.32

Table 5: The experimental sorption data for DFH

30°C			40°C			50°C		
desorption								
h	*M*	*st. dev.*	*h*	*M*	*st. dev.*	*h*	*M*	*st. dev.*
0.91	20.33	0.27	0.94	20.36	0.26	0.96	18.26	0.31
0.85	17.64	0.22	0.87	15.02	0.22	0.82	12.28	0.28
0.76	14.23	0.24	0.77	12.22	0.34	0.72	9.77	0.18
0.64	10.60	0.19	0.66	9.79	0.21	0.67	8.74	0.27
0.55	9.02	0.23	0.52	7.65	0.25	0.55	7.11	0.41
0.50	8.37	0.16	0.44	6.26	0.21	0.31	4.25	0.27
0.43	7.30	0.24	0.37	5.76	0.15	0.26	3.87	0.26
0.40	6.89	0.20	0.31	5.15	0.14	0.19	3.21	0.28
0.07	3.19	0.12	0.06	2.57	0.09	0.10	2.30	0.22
0.00	0.00	0.00	0.00	0.00	0.00	0.06	1.78	0.28
						0.00	0.00	0.00
adsorption								
0.00	0.00	0.00	0.00	0.00	0.00	0.00	0.00	0.00
0.07	2.52	0.18	0.06	1.85	0.04	0.06	1.29	0.17
0.41	5.33	0.17	0.40	4.70	0.11	0.10	1.76	0.33
0.43	5.71	0.21	0.48	5.45	0.12	0.19	2.44	0.11
0.49	6.36	0.22	0.63	7.32	0.18	0.23	2.71	0.21
0.58	7.77	0.25	0.76	9.90	0.26	0.30	3.26	0.18
0.64	8.62	0.26	0.85	13.03	0.37	0.41	4.15	0.21
0.75	11.17	0.33	0.94	18.40	0.25	0.57	5.59	0.14
0.85	14.51	0.22				0.68	7.01	0.19
0.97	21.09	0.49				0.78	8.84	0.22
						0.86	11.54	0.23
						0.93	15.29	0.24
						0.98	18.74	0.20

Table 6: Moisture content for the cubic-shaped specimens of UE-WRC

	30C					40C					50C			
L	M_w	M	n_s	*st. dev.*	L	M_w	M	n_s	*st. dev.*	L	M_w	M	n_s	*st. dev.*
9.51	0.07	16.45	10	0.15	9.53	0.06	15.51	10	0.18	10.02	0.06	14.69	9	0.22
14.34	0.22	15.95	10	0.09	15.16	0.21	15.56	10	0.13	14.61	0.18	14.62	9	0.09
19.32	0.50	16.14	10	0.09	19.57	0.47	15.47	10	0.12	19.20	0.43	14.89	10	0.17
25.09	1.02	16.72	10	0.16	25.63	0.96	15.97	10	0.22	25.06	0.91	15.28	10	0.23
30.88	1.88	16.75	10	0.11	30.41	1.82	16.27	10	0.14	29.89	1.63	14.80	10	0.19
35.14	2.69	16.21	10	0.24	34.75	2.58	15.61	10	0.29	34.79	2.37	14.83	10	0.37
40.20	3.98	16.66	10	0.16	39.56	3.80	16.03	10	0.17	39.43	3.58	15.23	10	0.31
st. dev.		0.32					0.31					0.26		

Table 7: Moisture content for the cubic-shaped specimens of DFH

	30C					40C					50C			
L	M_w	M	n_s	*st. dev.*	L	M_w	M	n_s	*st. dev.*	L	M_w	M	n_s	*st. dev.*
9.01	0.10	17.51	10	0.35	9.75	0.10	16.73	10	0.40	10.09	0.10	16.66	7	0.32
14.82	0.39	17.52	10	0.40	14.63	0.37	16.77	10	0.36	14.86	0.38	16.58	9	0.38
19.35	0.78	17.67	10	0.46	20.09	0.77	17.17	10	0.19	19.72	0.70	16.24	10	0.58
25.06	1.57	17.94	10	0.26	24.98	1.47	17.02	10	0.18	25.13	1.46	16.69	10	0.30
30.63	2.89	17.67	10	0.49	30.69	2.69	16.64	10	0.48	29.69	2.65	16.44	10	0.48
35.06	3.98	17.55	10	0.25	35.06	3.77	16.78	10	0.25	35.36	3.69	16.50	10	0.29
39.89	6.43	17.55	10	0.19	40.34	6.03	16.62	10	0.17	40.08	6.10	16.48	10	0.19
st. dev.		0.15					0.20					0.15		

Note: L: the edge length in average, mm; M_w: mass of sorbed water in average (bound water), g;
n_s: the number of specimens; M: moisture content in average, %

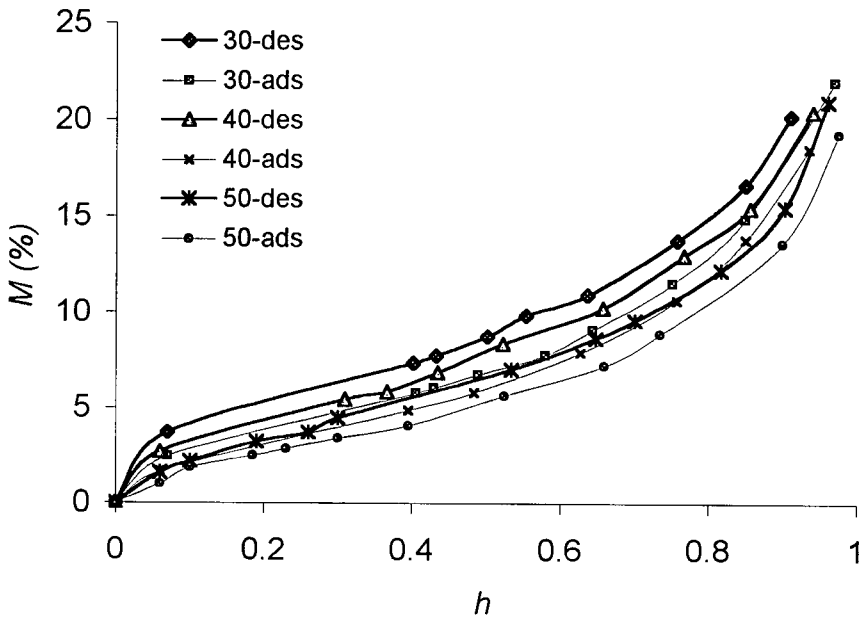

Fig. 5.1: The experimental sorption isotherms for Douglas-fir sapwood (wafer-type)

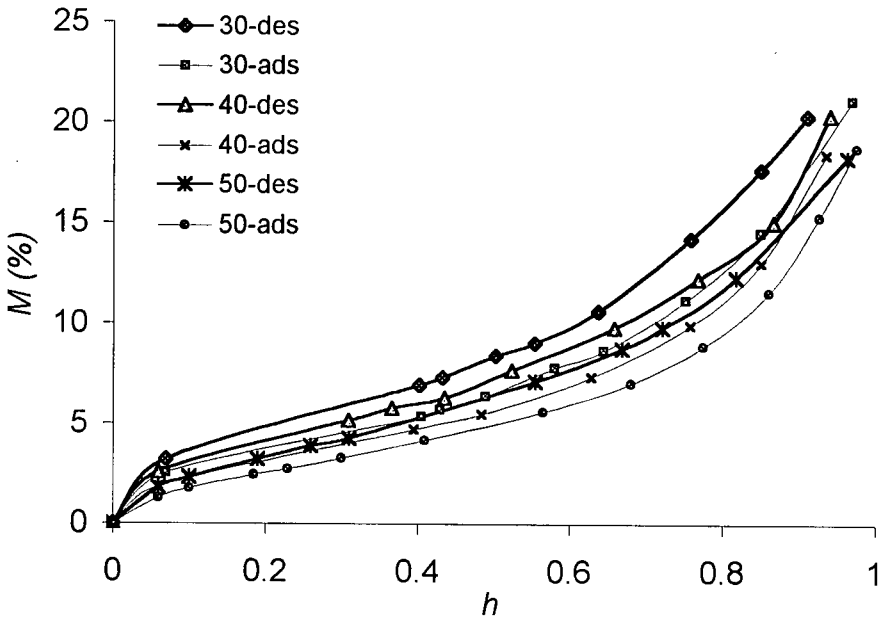

Fig. 5.2: The experimental sorption isotherms for Douglas-fir heartwood (wafer-type)

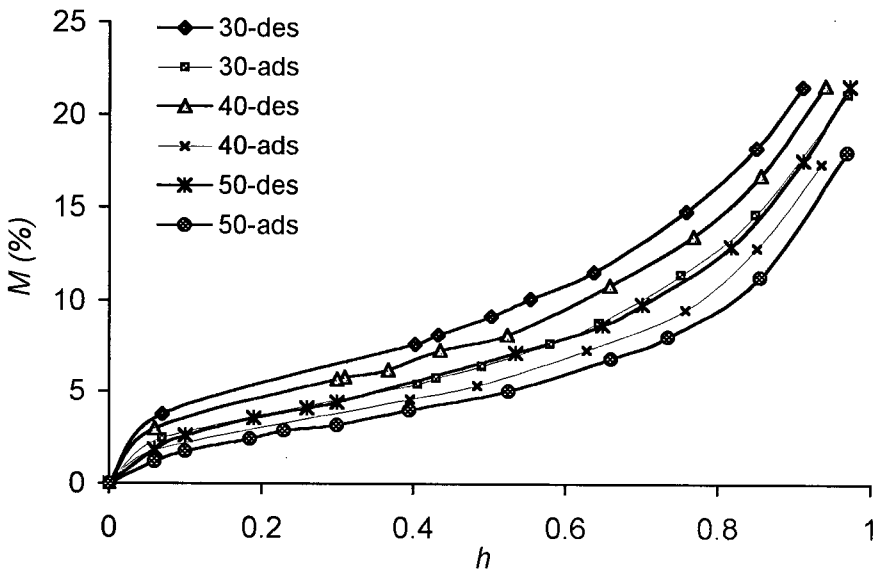

Fig.5.3: The experimental sorption isotherms for extracted western red cedar (wafer-type)

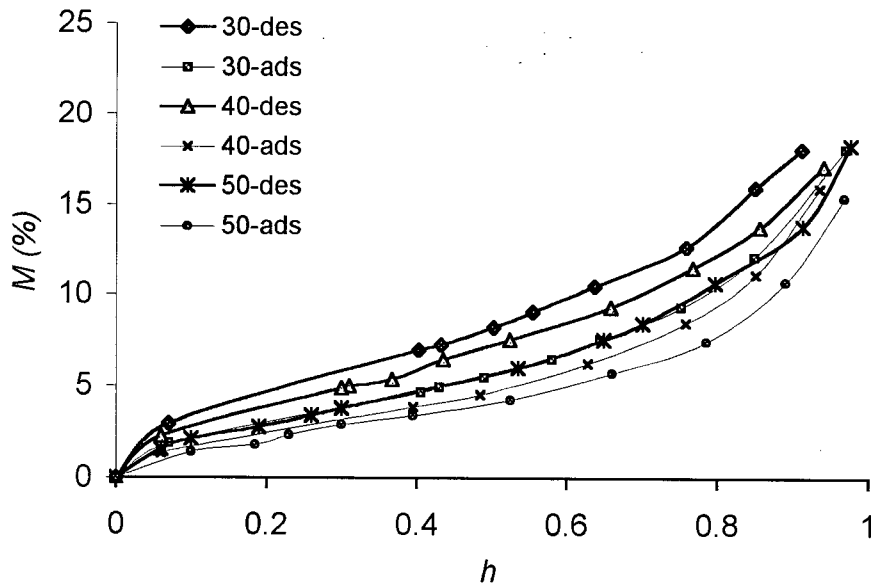

Fig. 5.4: The experimental sorption isotherms for unextracted western red cedar (wafer-type)

From Figs. 5.1 to 5.4, it can be seen that all sorption isotherms exhibited the typical sigmoid curves (Type II). The value of M decreased with an increase in temperature at the same relative humidity, and hysteresis was pronounced in all types of wood specimens at each temperature level in this study. There was no distinctive difference between DFH and DFS regarding to the M value at a corresponding h. A difference existed between UE-WRC and E-WRC of about 3% of M at the high sorption regions.

In Figs. 5.5 and 5.6, the M values with standard error bars for the cubic-shaped specimens with different sizes are plotted for the three different temperature levels. The effect of temperature on the resulting equilibrium moisture content is also apparent in both species and all cubes dimensions. Also, it is noted that Douglas-fir always reached higher M values for the same dimension, partial relative vapor pressure and temperature level.

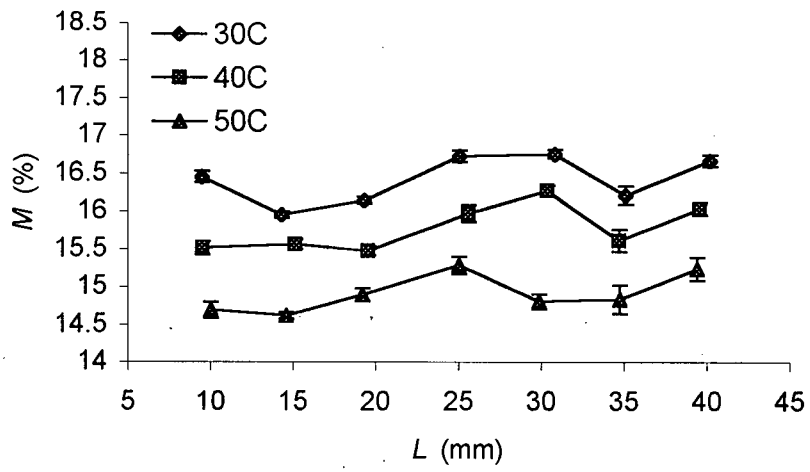

Fig. 5.5: The moisture content of the cubic-shape specimens with the variable sizes for unextracted western red cedar heartwood.

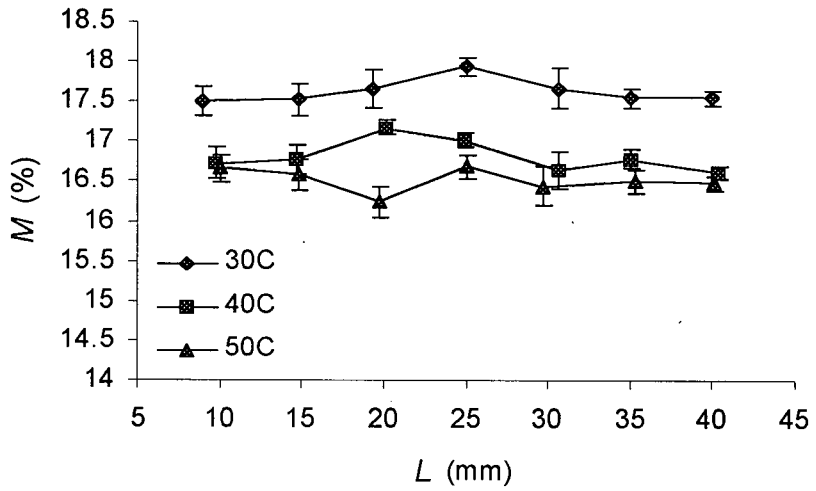

Fig. 5.6: The moisture content of the cubic-shape specimens with the variable sizes for Douglas-fir heartwood.

5.2 Prediction of M_m and c values

The plot of $h/(M(1-h))$ against h in Eq. (4.7b) fitted the experimental data below about 0.5 of h very well in all types of wood in this study (Figs. 5.7 to 5.10). The coefficients of determination were all greater than 0.97. The linear regression results, calculated M_m and c values, and their confidence intervals for only the lower points are listed in Table 8. The detailed results for confidence intervals are attached in Appendix C. Because the linear relationship was well obeyed for all wood types in this study, the obtained M_m and c values from this approach were used in all subsequent analyses. It should be noted that the linear regression was valid up to partial vapor pressure of about 0.6. Beyond that point the linearity was lost and the points were not taken into account.

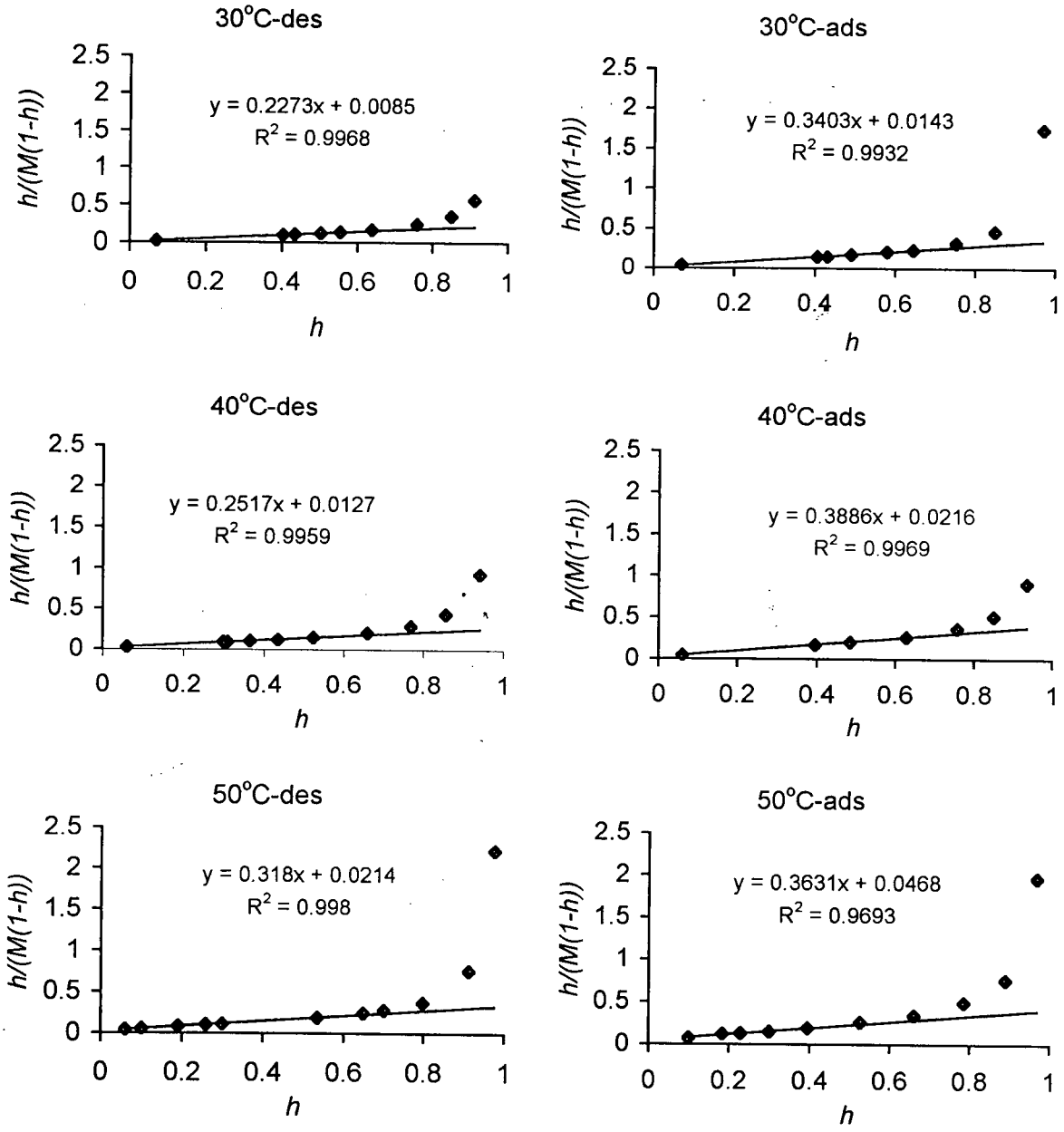

Figs. 5.7: Linear relationship in unextracted western red cedar (ads = adsorption, des = desorption)

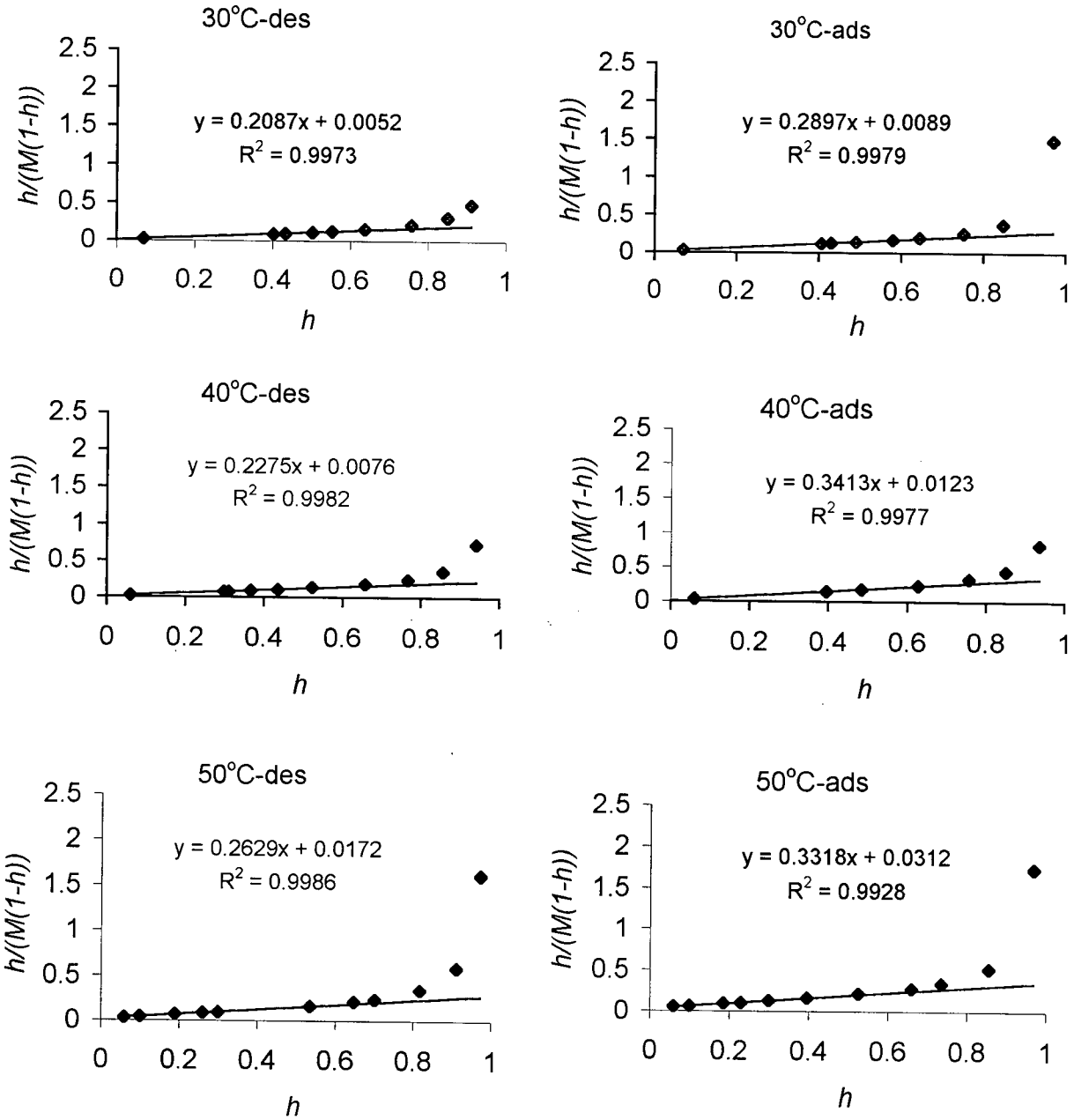

Figs. 5.8: Linear relationship in extracted western red cedar (ads = adsorption, des = desorption)

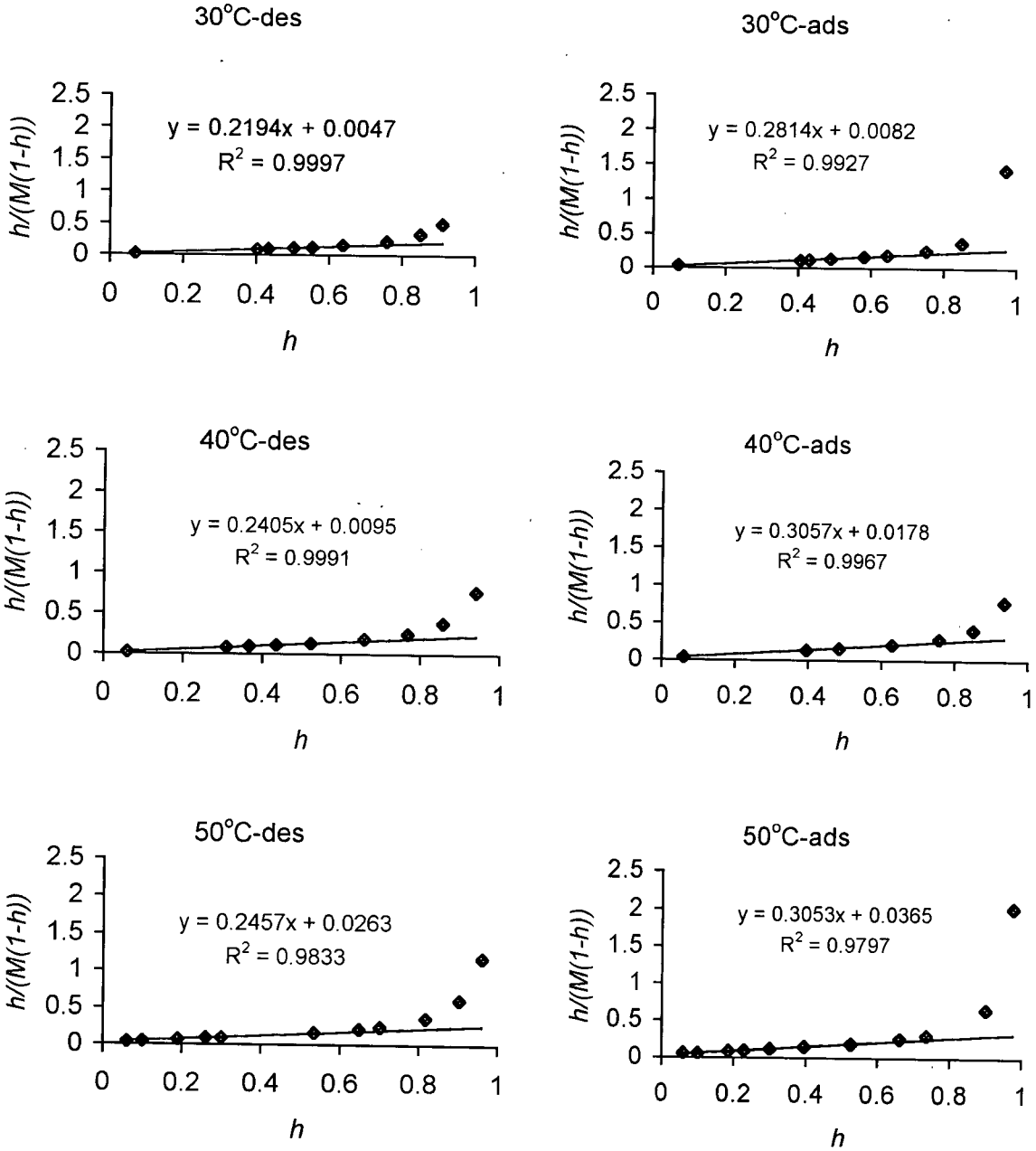

Figs. 5.9: Linear relationship in Douglas-fir sapwood (ads = adsorption, des = desorption)

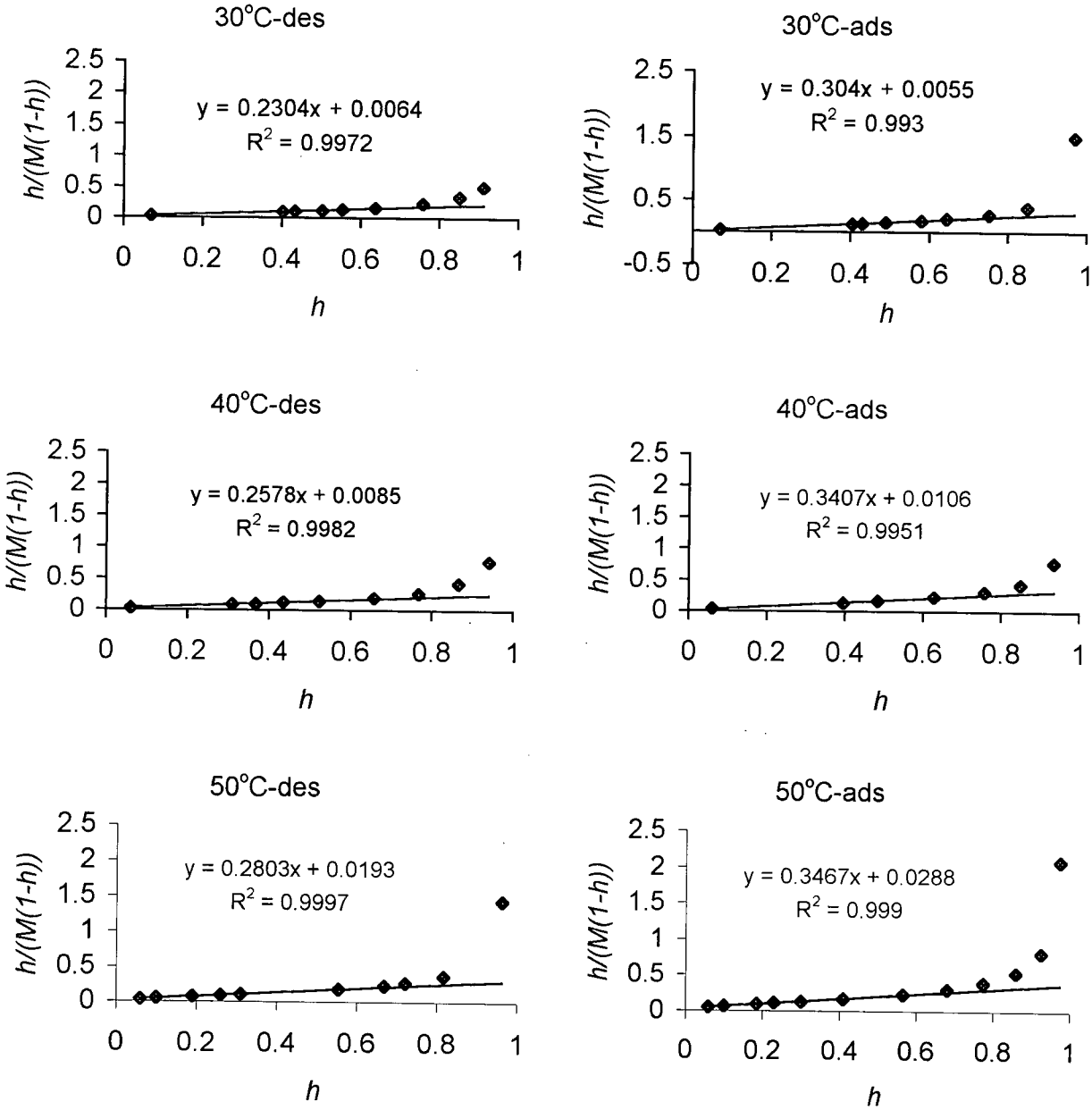

Figs. 5.10: Linear relationship in Douglas-fir heartwood (ads = adsorption, des = desorption)

The values for both M_m and c decreased with temperature for all four types of wood thus verifying that the surface area within the cell walls accessible to the water molecules decreased

with an increase in temperature. Parameter c held the same trend with temperature. The M_m and c values in desorption were greater than the ones in adsorption because of the wood hysteresis phenomenon. The difference in the c value between DFS and DFH were temperature-dependent. At 30°C, DFS's was greater than DFH's while reversed at 40 and 50°C. As to the M_m values, DFS's were greater than DFH's at the three temperature levels. It can be concluded that DFH exhibits less surface area than DFS within the cell walls. The values of M_m and c in UE-WRC were apparently lower than those in E WRC because of the high extractive content in WRC.

5.3 Fitness of the classic BET equation to the sorption data

It is well known that the classic BET equation, Eq. (2.2) with a finite number of layers of the sorbed water molecules cannot fit sorption data well at least for wood at a higher sorption region ($h > 0.5$) with a few exceptions (Simpson 1973; Hartley 1994; Hao 1997), depending on the shape of the isotherm curves. This lack of fit occurred exactly in the same way in this study. All plots of M vs. h from the BET calculations were drawn with the FBET and F-P together in Figs. 5.15 to 5.38 with a thin line. The respective regression residue pattern for each plot of M vs. h was shown in a separate figure. The residue pattern is a powerful tool along with the coefficient of determination (R^2) to indicate if a proposed equation fits the data well. If appropriate, the residue points should be uniformly, closely, and symmetrically distributed along the dependent variable-axis which in this study, is h- axis. The narrower the scattering band, the better the regression.

Table 8: Parameter values of M_m and c in the classic BET from only lower points by using Eq. (4.7b) – CI stands for confidence interval

species	temp.(°C)	intercept	slope	c	M_m	CI of c	CI of M_m
UEWRC	30-des.	0.0085	0.2273	27.6693	4.2404	11.6244 - 84.769	3.9545 - 4.4708
	30-ads.	0.0143	0.3351	24.4499	2.8620	9.7375 - 76.3123	2.6199 - 3.0287
	40-des.	0.0127	0.2528	20.9419	3.7661	12.7969 - 54.591	3.6117 - 3.8995
	40-ads.	0.0216	0.3886	18.9674	2.4376	8.2960 - 59.1789	2.2322 - 2.5914
	50-des.	0.0214	0.3180	15.8805	2.9470	11.8182 - 23.011	2.8247 - 3.0463
	50-ads.	0.0468	0.3631	8.7645	2.4396	4.1790 - 35.5201	2.0065 - 3.0195
EWRC	30-des.	0.0052	0.2070	41.1712	4.7141	1.2637 - 121.682	4.5573 - 4.8392
	30-ads.	0.0089	0.2897	33.7126	3.3494	4.8825 - 101.175	3.1887 - 3.4555
	40-des.	0.0076	0.2275	30.9935	4.2535	15.3836 - 79.219	4.0597 - 4.4235
	40-ads.	0.0123	0.3413	28.8299	2.8284	10.6654 - 89.265	2.6100 - 2.9833
	50-des.	0.0172	0.2629	16.3171	3.5709	12.8505 - 21.895	3.4118 - 3.7159
	50-ads.	0.0312	0.3318	11.6299	2.7545	7.9802 - 19.5807	2.4788 - 3.0172
DFS	30-des.	0.0047	0.2195	48.0613	4.4602	30.6395 - 89.453	4.4377 - 4.5195
	30-ads.	0.0082	0.2814	35.1742	3.4530	9.4425 - 109.777	3.1611 - 3.7207
	40-des.	0.0095	0.2405	26.3492	3.9998	15.6956 - 72.884	3.8053 - 4.1518
	40-ads.	0.0178	0.3057	18.1493	3.0910	7.9496 - 56.4285	2.8405 - 3.2824
	50-des.	0.0263	0.2457	10.3525	3.6764	5.9961 - 23.1125	3.1667 - 4.2950
	50-ads.	0.0365	0.3053	9.3729	2.9262	5.7164 - 19.8504	2.5587 - 3.3132
DFH	30-des.	0.0064	0.2304	36.7732	4.2219	3.4997 - 111.378	3.9827 - 4.4653
	30-ads.	0.0055	0.3040	56.2895	3.2312	1.7685 - 169.968	3.0574 - 3.4614
	40-des.	0.0085	0.2578	31.4639	3.7564	15.6138 - 94.975	3.5555 - 3.9483
	40-ads.	0.0106	0.3407	33.0389	2.8462	8.4101 - 104.902	2.5612 - 3.0969
	50-des.	0.0193	0.2803	15.5569	3.3380	14.0825 - 16.937	3.3325 - 3.3567
	50-ads.	0.0288	0.3467	13.0294	2.6633	11.0534 - 15.281	2.5805 - 2.7773

Table 9: Parameter n estimation from the classic BET (30d = desorption @ 30°C; 30a = adsorption @ 30°C)

species		30d	30a	40d	40a	50d	50a
DFH	n	10.080	12.580	10.188	13.480	10.330	12.92
	MSE	0.066	0.239	0.761	0.460	0.234	0.681
	R^2	0.998	0.994	0.979	0.988	0.993	0.981
DFS	n	8.841	12.110	9.630	12.380	9.960	12.05
	MSE	0.351	0.450	0.515	0.270	1.433	0.646
	R^2	0.989	0.989	0.996	0.994	0.966	0.982
UE-WRC	n	8.433	11.930	8.453	13.620	11.135	11.3
	MSE	0.164	0.371	0.213	0.383	0.465	0.891
	R^2	0.994	0.987	0.991	0.987	0.986	0.961
E-WRC	n	9.119	12.060	9.610	12.690	11.021	12.193
	MSE	0.240	0.229	0.490	0.338	0.689	0.678
	R^2	0.994	0.994	0.988	0.991	0.985	0.976

The R^2 is a quantitative index to indicate if regression is appropriate. The higher the value of R^2, the better the fit. In the case of the calculated sorption isotherms, R^2 loses such a power because the correlation coefficient between M and h was as high as at least 0.94. Actually, even though the BET failed to fit the sorption data at the high sorption region for the most cases in this study, it still produced significantly high values of R^2. Typically, this case is shown in Figs. 5.20 and 5.38. Obviously, the BET failed at the high sorption regions while it still produced R^2 values of 0.961 and 0.981, respectively. Such high R^2 values are apt to give an incorrect conclusion on suitability of the tested equation. The failure of the BET model at high humidity sorption regions was similar in all types of wood in this study. The regression results for all types of wood in this study are listed in Table 9. From this research, it can be noted that if the sorption isotherm curve was less inflectional (curvature) at the high sorption region, BET could fit the sorption data better (Figs. 5.15, 5.17, and 5.21). It failed otherwise. The reason for this is that its underlying assumption of being a flat sorption surface and the layering organization of the sorbed water may have deviated more from reality at these failed cases, thus

resulting in a worse fit. Also, it seemed that there was some link between the inflection (degree of curvature) of the sorption isotherm curves and the flat layering formation of the sorbed water molecules. Specifically, the less inflectional the sigmoid curve at high sorption regions ($h > 0.5$) was, the more the chance for the BET to fit the experimental data. In other word, the less inflection of the sorption curves meant the less deviation from the flat layering formation.

5.4 d*M*/d*h* plots

The derivative plots were obtained for experimental points from the second lowest to the second highest of each of 24 sorption isotherms. The derivative for each calculated point was obtained by (moisture content $_{\text{its immediate upper point}}$ – moisture content $_{\text{its immediate lower point}}$)/($h_{\text{its immediate upper point}}$ -$h_{\text{its immediate lower point}}$).

The degree of inflection for a sorption curve can be revealed by a plot of d*M*/d*h* vs. *h*. Physically, it means that the rate of increase in *M* per unit increase in *h*. A Type II sorption curve (sigmoid) is due to a polymolecular sorption. Since the wood vapor sorption is always a sigmoid Type II curve, the value of d*M*/d*h* is initially quite significant. It decreases with an increase in *h* (calculation of d*M*/d*h* started from the second lowest point and the decreasing trend didn't exhibit obviously) and keeps constant later on and then begins to increase steadily until *h* is near to 1.0. This feature existed in this study as seen in Figs. 5.11 to 5.14.

The fact that the BET can fit the experimental sorption isotherms with less inflection at high sorption regions can be described by the value of d*M*/d*h*. The more inflectional the sorption curve, the greater the value of d*M*/d*h*. In short, the greater the value of d*M*/d*h* at the high sorption region, the less chance for the BET to fit the sorption data. It can also be further inferred that the greater the value of d*M*/d*h*, the more the deviation from a flat layer formation.

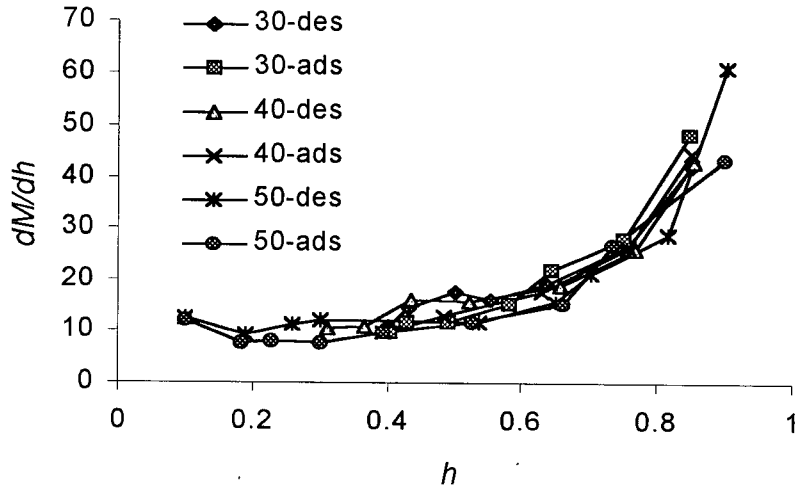

Fig. 5.11: The value of *dM/dh* for Douglas-fir sapwood (30d: 30°C, desorption and 30a: 30°C, adsorption)

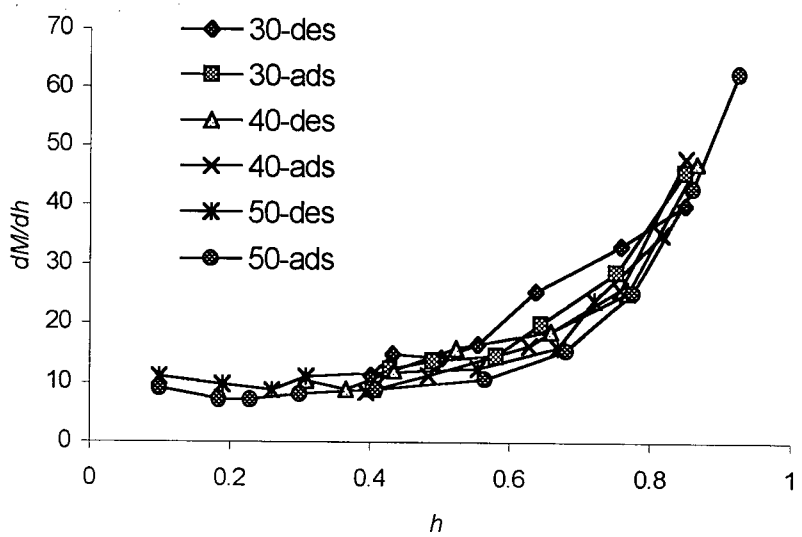

Fig.5.12: The value of *dM/dh* for Douglas-fir heartwood

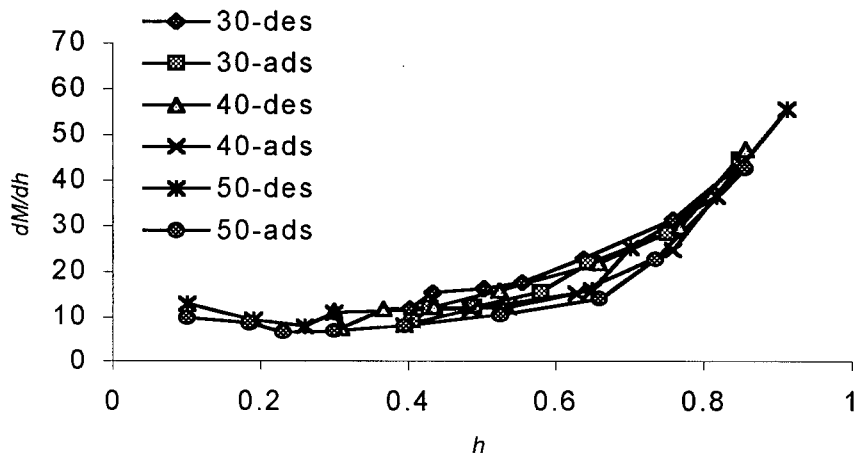

Fig.5.13: The value of *dM/dh* for extracted western red cedar

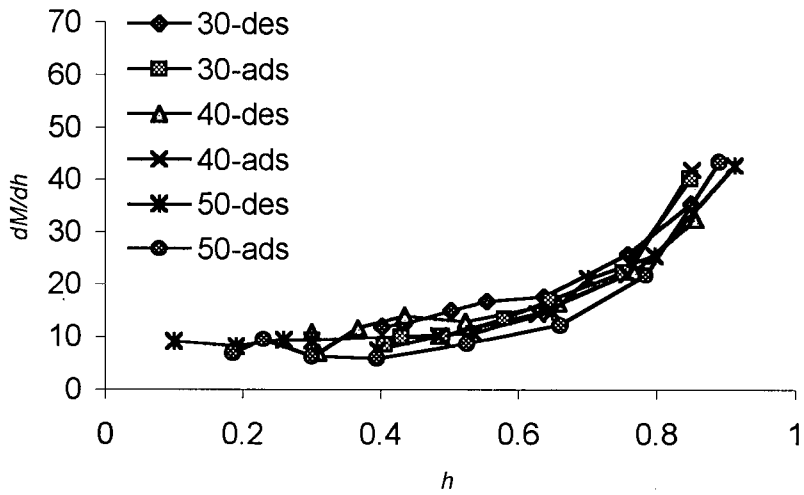

Fig. 5.14: The value of *dM/dh* for unextracted western red cedar

In order to explain such an ever-increasing value of *dM/dh* at the high sorption region, several assumptions with corresponding equations were posed in the past. These included Dent theory (Dent 1977), capillary theory (Simpson 1980), solution theory (Hailwood and Horrobin 1946), commonly referred to as the HH theory), dual surface (Le and Ly 1992), and Aguerre

theories (Aguerre 1989a, 1989b). They all considered the flat surface as the basis for derivation with the only exception of solution theory which is actually mathematically similar to the Dent theory. In common, these theories treated the bound water as different states during the sorption process. The number of the states was either two (Dent, HH, L-L theories) or three (capillary theory) or many more (Aguerre theories). The common state among these theories was the tightly bound first layer which is directly sorbed on the sorption sites. Except for the HH theory, all other theories were still based on the BET's flat surface and molecular layering formation. Therefore, their prediction of moisture content at high humidities is not very accurate.

There is increasing evidence to show that assumptions such as the underlying surface being flat and layering formation of the bound water at high h value are questionable. Also, assumptions regarding the water states during the sorption process should be critically treated. A thorough review of water interaction in cellulosic-systems, particularly wood, was presented by Hartley *et al.* (1992). They suggested that the water cluster theory was more adequate to explain the sigmoid curve of the wood isotherms according to Nuclear Magnetic Resonance (NMR) results, the classic sorption theories, and conformational analysis of cellulose crystals and amorphous cellulose. NMR has extensively been used to investigate the wood or cellulose-water systems and has been proven capable of identifying the different states of water within the material (Tait *et al.* 1972; Childs 1972; Froix, and Nelson 1975; Hsi *et al.* 1977; Goring 1978; Hartley and Avramidis 1993; Hartley *et al.* 1992; Hartley *et al.* 1994, 1996; Menon *et al.* 1987).

Researches on the geometry of the underlying surfaces by using fractals have been successful in many complicated physical phenomena, especially, sorption in porous materials. The investigations continuously indicated the existence of non-flat surfaces or rough surfaces or fractal surfaces in many natural porous materials. On the other hand, the investigations on

sorbed water molecules suggested that cluster formation by the sorbed water molecules was very likely. For either case, the failure of BET fit to the sorption data at high humidities can be expected. As a matter of fact, if the layering formation existed within the cell walls throughout the entire sorption process ($0 < h < 1$), the M value should not have been greatly increasing with an increase in h beyond 0.9. Instead, a different state of sorbed water may have been involved. The cluster theory could be the one to explain dynamics of the states geometrically.

5.5 Fitness of the FBET to the sorption data

By assuming a non-flat surface within internal cell walls that result either from its origin or most probably caused by sorbed water molecules organized with some structure, the BET model was modified from the flat surface basis to the fractal surface one. The resulting equation (Eq. 4.5, FBET) was fitted to the sorption data and the results are listed in Table 10 and drawn in Figs. 5.15 to 5.38 with a thick solid line. The residue pattern of each regression was coupled for each of 24 cases.

It is apparent that the FBET fitted the sorption data better than BET did for each of 24 cases in this study (Figs. 5.15 to 5.38). The biggest *MSE* value from the BET was 0.891 while it was 0.4277 from FBET by comparing Table 9 with Table 10. The *MSE* value was from 1 to 16 times less than that from the BET, depending on the inflection or the rate of dm/dh of the sorption isotherm curve at the high sorption region. The more the inflection, the more the improvement. The *MSE* value is preferable to R^2 to facilitate comparison because R^2 values were so significantly high that their differences between BET and FBET were not distinctive and an erroneous conclusion may thus be made. The FBET can fit well at both the low and high humidities. The significantly improved degree of fit can be seen from the residue pattern at the

high sorption region. The residue points became closer to the h-axis than those from BET at the high sorption region for each of 24 cases from Figs. 5.15 to 5.38. The distribution of the residue points was more closely uniform and symmetrical to the h-axis. This suggests that the proposed equation is appropriate from the statistical point view.

It should be noticed here that the values in Table 10 were obtained by repeatedly fitting Eq. (4.5) to the different sorption regions from h of zero up to different h values. The comparison above is made from just the first line of each case. The results for all other lines were obtained based on the assumption that each h would cause a corresponding D value; Eq. (4.5) was repeatedly fitted to the sorption data set with one fewer data point at a time until the results did not make sense or no longer related to the parameter D. All calculated D values and their corresponding h values are listed in Table 10.

Table 10: The D values at the different sorption points from Eq. (4.5)

	UE-WRC				E-WRC			
	n	*MSE*	*h*	*D*	*n*	*MSE*	*h*	*D*
30d	12	0.14	0.91	2.33	14	0.13	0.91	2.35
	10	0.12	0.85	2.22	10	0.06	0.85	2.06
	7	0.04	0.76	1.90	9	0.04	0.76	2.12
	8	0.01	0.64	2.13	7	0.03	0.64	2.12
	7	0.01	0.55	1.77	7	0.04	0.55	1.78
	6	0.01	0.50	1.51	7	0.04	0.50	1.78
					6	0.02	0.43	1.70
30a	24	0.12	0.97	2.43	15	0.21	0.97	2.29
	18	0.08	0.85	2.37	10	0.01	0.85	2.24
	12	0.03	0.75	2.18	10	0.01	0.75	2.20
	12	0.02	0.64	2.08	9	0.01	0.64	2.07
	12	0.03	0.58	2.06	7	0.00	0.58	2.01
	9	0.01	0.49	1.72	7	0.01	0.49	1.77
						0.01	0.43	1.49
40d	17	0.11	0.94	2.52	20	0.10	0.94	2.49
	12	0.04	0.86	2.39	12	0.04	0.86	2.42
	9	0.03	0.77	2.21	25	0.02	0.77	2.34
	8	0.03	0.66	2.20	7	0.01	0.66	2.32
	7	0.03	0.52	1.67	7	0.01	0.52	2.11
						0.01	0.44	1.82
40a	30	0.10	0.94	2.40	23	0.09	0.94	2.36
	20	0.06	0.85	2.32	15	0.05	0.85	2.36
	20	0.05	0.76	2.27	9	0.03	0.76	2.14
	15	0.02	0.63	2.04	9	0.01	0.63	1.98
	12	0.02	0.48	1.71	5	0.01	0.48	1.77
50d	24	0.25	0.98	2.48	30	0.06	0.97	2.56
	18	0.04	0.90	2.43	22	0.04	0.91	2.51
	20	0.03	0.80	2.40	18	0.03	0.82	2.49
	16	0.01	0.70	2.30	7	0.02	0.70	2.34
	16	0.01	0.65	2.24	7	0.03	0.65	2.35
	14	0.01	0.53	2.04	5	0.00	0.53	2.04
	10	0.02	0.30	1.61	5			
50a	55	0.02	0.97	2.68	55	0.07	0.97	2.63
	30	0.01	0.89	2.68	30	0.07	0.86	2.58
	55	0.01	0.79	2.62	25	0.08	0.74	2.51
	30	0.01	0.66	2.62	40	0.09	0.66	2.45
	18	0.01	0.53	2.68	5	0.02	0.53	2.22
	14	0.02	0.40	2.13	40	0.00	0.40	2.15
	14	0.03	0.30	2.02				
	14	0.03	0.23	1.36				

Note: 30d same as in Table 9

Table 10: The D values at the different sorption points from Eq. (4.5) (continued)

	DFS				DFH			
	n	*MSE*	*h*	*D*	*n*	*MSE*	*h*	*D*
30d	15	0.27	0.91	2.45	14	0.05	0.91	2.27
	9	0.05	0.85	2.12	9	0.06	0.85	1.91
	9	0.04	0.76	2.15	7	0.05	0.76	1.61
	7	0.03	0.64	1.85	7	0.01	0.64	1.71
	9	0.02	0.55	1.90	7	0.01	0.55	1.53
	7	0.07	0.50	1.77	7	0.01	0.50	1.48
	7	0.04	0.43	1.73				
30a	22	0.16	0.97	2.38	18	0.14	0.97	2.26
	12	0.03	0.85	2.29	15	0.07	0.85	2.16
	12	0.04	0.75	2.24	12	0.04	0.75	2.01
	12	0.04	0.64	1.95	12	0.05	0.64	1.99
	7	0.01	0.58	1.70	9	0.02	0.58	1.80
	9	0.00	0.49	1.58	7	0.05	0.49	1.71
					7	0.09	0.43	1.62
40d	22	0.27	0.94	2.52	18	0.43	0.94	2.40
	12	0.02	0.86	2.31	12	0.03	0.86	2.27
	9	0.10	0.77	2.08	9	0.01	0.77	2.28
	9	0.11	0.66	2.12	9	0.02	0.66	2.07
	7	0.07	0.52	2.05	7	0.03	0.52	1.93
	6	0.04	0.44	1.98				
	5	0.09	0.37	1.67				
40a	22	0.11	0.94	2.36	25	0.05	0.94	2.35
	20	0.10	0.85	2.34	18	0.05	0.85	2.28
	12	0.03	0.76	2.10	9	0.02	0.76	2.09
	12	0.01	0.63	1.99	9	0.02	0.63	2.00
	9	0.02	0.48	1.53	9	0.04	0.48	1.53
50d	40	0.27	0.96	2.68	20	0.05	0.96	2.46
	18	0.02	0.90	2.55	16	0.02	0.82	2.36
	16	0.02	0.82	2.55	16	0.02	0.72	2.30
	9	0.01	0.70	2.29	9	0.00	0.67	1.86
	7	0.01	0.65	2.30	9	0.00	0.55	1.83
	7	0.02	0.53	2.01	7	0.00	0.31	1.84
	7	0.02	0.30	1.83	7	0.00	0.26	1.52
					5	0.00	0.19	1.43
50a	40	0.13	0.98	2.59	40	0.05	0.98	2.54
	40	0.07	0.90	2.63	40	0.04	0.93	2.55
	20	0.23	0.74	2.48	20	0.05	0.86	2.43
	15	0.02	0.66	2.40	15	0.04	0.78	2.37
	12	0.02	0.53	2.05	15	0.04	0.68	2.36
					9	0.03	0.57	2.04
					7	0.00	0.41	1.73
					7	0.00	0.30	1.87

It can be seen that the *MSE* values became smaller when h decreased due to the fact that sorption data at a very high h value are less reliable. The D values became larger with an increase in h and the value of n increased with an increase in h as well.

5.6 Grouping

To determine finite D_i values in Eq. (4.8), the D values in Table 10 were grouped by using the following partitioning guidelines:

$\boldsymbol{D}$ <= 1.9 (between a line and a surface)

1.9 < $\boldsymbol{D}$ <= 2.2 (about a planar surface)

2.2 < $\boldsymbol{D}$ <= 2.3 (formation of a rough surface begins)

2.3 < $\boldsymbol{D}$ <= 2.5 (rougher surface)

$\boldsymbol{D}$ > 2.5 (towards a spatial filling)

These partitioning guidelines were based on fractal theories and the experimental data collected. It would have been preferable to establish the D values that defined each of the different groups prior to collecting the experimental data. Unfortunately, this approach was not used. Therefore, it is acknowledged that the experimental data collected was used in determining the criteria used to evaluate that same data and that this practice does not follow the best, normally accepted scientific experimental approach. D values in Table 10 and by no means that all 5 groups are present for each type of wood at each temperature.

By following these guidelines, three or four D value groups were identified from the low to high h values for all types of wood (Table 10) in this study. The lower bound point of each group was treated as the turning point or critical point (h_c) from one group of the D value to the

next regarding the value of h. The h_c values and their corresponding D values are listed in Table 11. The average D values for each group, namely, D_i in Eq. (4.8), are listed in Table 12. The D_i values were used to evaluate F-P model (Eq. (4.8)) and thus, inversely, validated this stepwise assumption by goodness of fit. The goodness of fit was shown by residue plots because R^2 is not sensitive (section 5.3 pages 66, 71, 77 and Figs. 5.15 – 5.38). Because of the experimental limitations, the turning points for each type of wood are just approximations.

5.7 Fitness of the F-P to the sorption data

If a sorption curve is more inflectional at high humidities, the classic BET fails to fit the sorption data well. The FBET fitted much better at both low and high humidities after the non-flat surface was taken into account. The derivation of the F-P equation, Eq. (4.8), was based on the assumption that the geometry of the internal cell wall surfaces changed with h in a stepwise manner. The D (D_i in Table 12) value for each step was obtained by calculating the average on the grouped D values from Table 10 for each type of wood at each temperature. If the state of the sorbed water changes in a stepwise manner and each state is described geometrically with a D value, then a combination of several such D values become a multi-fractal equation in addition to the monolayer component. Eq. (4.8) was just a mathematical translation of this idea. By using a linear regression technique, Eq. (4.8) was fitted to all experimental sorption isotherms in this study. The fitted results are listed in Table 5.10 and calculated sorption isotherms are presented in Figs. 5.15 to 5.38 for all twenty four cases with the classic BET and FBET equations together. The residue pattern is also given respectively. The residue points for each of the twenty four cases were more uniformly, symmetrically, and closely scattered around h-axis. It means that it fitted the sorption

data better than the FBET. It provided the best curve-fitness among three equations. This implied that the stepwise manner assumption is reasonable.

Table 11: The critical h_c values with respective to the D value (30d = desorption @ 30°C; 30a = adsorption @ 30°C)

	UE-WRC		E-WRC		DFS		DFH	
	h_c	D	h_c	D	h_c	D	h_c	D
30d	0.50	1.51	0.43	1.70	0.43	1.73	0.50	1.48
	0.64	2.13	0.64	2.12	0.76	2.15	0.85	1.91
	0.85	2.22	0.91	2.35	0.91	2.45	0.91	2.27
	0.91	2.33						
30a	0.49	1.73	0.43	1.49	0.49	1.58	0.43	1.62
	0.58	2.06	0.58	2.01	0.64	1.95	0.64	1.99
	0.85	2.37	0.75	2.20	0.75	2.24	0.97	2.26
					0.97	2.38		
40d	0.52	1.67	0.44	1.82	0.37	1.67	0.52	1.93
	0.66	2.20	0.52	2.11	0.44	1.98	0.77	2.28
	0.86	2.40	0.66	2.33	0.86	2.31	0.94	2.40
	0.94	2.52			0.94	2.52		
40a	0.48	1.71	0.48	1.77	0.48	1.53	0.48	1.53
	0.63	2.04	0.63	1.98	0.63	2.00	0.63	2.00
	0.76	2.27	0.85	2.36	0.85	2.34	0.85	2.28
	0.85	2.32					0.94	2.35
50d	0.30	1.61	0.53	2.04	0.30	1.83	0.19	1.43
	0.53	2.04	0.65	2.35	0.53	2.01	0.72	2.30
	0.65	2.24	0.91	2.51	0.65	2.30	0.82	2.36
	0.80	2.40			0.82	2.55		
50a	0.23	1.36	0.40	2.15	0.53	2.05	0.30	1.87
	0.30	2.13	0.53	2.22	0.66	2.40	0.57	2.04
	0.53	2.68	0.66	2.45	0.90	2.63	0.68	2.36
			0.74	2.51			0.93	2.55

The second was FBET, but close to F-P. The worst one was the classic BET equation due to its aforementioned problems at high relative vapor pressures. The *MSE* values from F-P equation were consistently smaller than the ones from FBET

5.8 Physical implications of the FBET and F-P equations

The good-fitness of F-P equations showed that the assumption of the stepwise manner of the state of the sorbed water molecules was correct.

Basically, these two equations are physically similar from a fractal point of view even though they have totally different formats. The FBET quantifies the geometry of the internal surfaces of the cell walls which are considered to be shaped by the geometry of the sorbed water molecules. If the former is considered to be the same as the latter, both equations can be considered to quantify the geometry of the same complex object from different angles, namely, either from the network of the sorbed water molecules or from the internal surfaces of the cell walls. From all twenty four figures (Figs. 5.15 to 5.38), the calculated curves from the FBET and F-P were close to each other. This can be further demonstrated by their corresponding residue pattern diagrams. They all pointed towards the fact of physical similarity in a sense of sorbed water structures, and geometry of the internal cell wall surfaces.

From Table 11, it seems that the h_c values were temperature-dependent (addressed in **section 5.9.3**). The D values increased with an increase in h with a D limit of 2.7. This increasing trend indicated that the geometry of the internal cell wall surfaces became increasingly complicated at higher moisture contents.

In terms of the values at different stages, the spatial distribution of the sorbed water molecules may have changed from the scattering points to linear, to something between a line and a plane, and transition near to a plane, and then toward a spatial distribution (far from a plane with a limit of 2.7 of D).

Table 12: Fractal-Polynomial coefficient (k_i) estimations

		UE-WRC		E-WRC		DFS		DFH	
		D_i	k_i	D_i	k_i	D_i	k_i	D_i	k_i
30d		2.33	7581.02	2.35	170.49	2.45	519.28	2.27	428.66
		2.22	-13170.32	2.10	-211.53	2.13	-1414.00	1.91	-737.62
		2.02	6414.12	1.75	64.64	1.81	915.61	1.58	332.02
		1.64	-812.67	M_{mono}	23.39	M_{mono}	39.50	M_{mono}	18.39
		M_{mono}	39.40	0.03		0.10		0.01	
	MSE	0.03		1.00		1.00		1.00	
	R^2	1.00							
30a		2.40	13230.00	2.24	3207.00	2.38	1396.00	2.26	889.19
		2.11	-19280.00	2.04	-6870.00	2.27	100.66	2.05	-1363.00
		1.72	7505.00	1.63	5111.00	1.95	-1799.00	1.71	494.29
		M_{mono}	47.88	M_{mono}	73.18	1.64	425.02	M_{mono}	36.66
						M_{mono}	26.64		
	MSE	0.05		0.02		0.04		0.04	
	R^2	1.00		1.00		1.00		1.00	
40d		2.52	228.79	2.39	82580.00	2.52	306.68	2.40	835.67
		2.39	-277.52	2.11	-135700.00	2.31	-436.88	2.28	-1889.00
		2.21	64.84	1.82	72200.00	2.06	150.29	2.00	1074.00
		1.67	1003	M_{mono}	595.05	1.67	689.12	M_{mono}	24.47
		M_{mono}	18.53			M_{mono}	21.20		
	MSE	0.05		0.02		0.15		0.27	
	R^2	1.00		1.00		1.00		0.99	
40a		2.36	16450.00	2.36	675.24	2.35	288.16	2.35	390.39
		2.27	-26920.00	2.06	-1087.00	2.05	-386.00	2.28	-0.23
		2.04	13040.00	1.77	431.02	1.53	118.64	2.05	-520.41
		1.71	58.02	M_{mono}	20.55	M_{mono}	9.36	1.53	151.32
		M_{mono}	25.33					M_{mono}	14.39
	MSE	0.12		0.07		0.06		0.13	
	R^2	1.00		1.00		1.00		1.00	
50d		2.44	500.69	2.54	897.78	2.59	2735.00	2.46	2054.00
		2.27	240.93	2.39	-1277.00	2.30	-5023.00	2.33	-2760.00
		2.04	-276.93	2.04	399.54	2.01	2594.00	1.76	1030.00
		1.61	53.28	M_{mono}	13.07	1.83	78.55	M_{mono}	26.62
		M_{mono}	8.98			M_{mono}	77.61		
	MSE	0.17		0.07		0.39		0.02	
	R^2	0.99		1.00		0.99		1.00	
50a		2.66	129.01	2.57	152.31	2.61	656.29	2.54	5324.00
		2.07	-184.19	2.45	1617.00	2.44	-907.34	2.39	-8994.00
		1.36	73.92	2.22	-2068.00	2.05	269.75	2.04	5599.00
		M_{mono}	-7.76	2.15	469.45	M_{mono}	5.95	1.80	-1915.00
				M_{mono}	7.99			M_{mono}	29.30
	MSE	0.14		0.08		0.18		0.02	
	R^2	0.99		1.00		0.99		1.00	

Note: 30d same as in Table 9

The corresponding moisture contents for these groups were about 0 - 5%, 5 – 10%, 10 - 15%, and 15 - 20% or above. Roughly, these ranges are considered in the classic BET theory to be formations of the monolayer, a transition of the monolayer to multilayer, and the multilayer, respectively.

The observations in this thesis were similar to the results from Hao and Avramidis (2001) by using the same method and analyzing Kelsey's (1957) sorption data (best data available). In that study, *D-M* plots were introduced and were at least two regions in the desorption and three regions in the adsorption which were situated at the similar locations as 5-10%, 10-15%, and 15-20%. Conclusively, the *D-M* plots were no longer distinctive beyond $M =$ 20% between sorption conditions at four the temperature levels. Also, the D values were no longer distinctive between two different temperature levels at $M >= 20\%$. At 10°C, the D values were all greater than 2. In desorption, two distinct regions ranging between moisture contents of 10-18% and 20-30% were identified. It was also evident that the D value in the adsorption was larger than that in the desorption at 25, 40, 55°C when M was less than 20%. At 10°C, the D value in the desorption was larger than that in the adsorption.

Hatzikiriakos and Avramidis (1994) used the same sorption data to characterize the wood surface by using fractal theory and three totally different equations were applied to determine D. Along the sorption isotherms, three regions were identified at the low, middle, and high sorption regions. From h of 0.2 to 0.85, the D value for all four temperatures was ranged between 2.5 to 2.8. The fractal region found at this range was based on the assumption that the wood-water system would just have one constant D value. On average, the D values are close to the calculated maximum ones in this study. This study showed that the D value did not remain

constant in the h range of 0.2 to 0.85. This pointed toward the fact that the wood-water system was not ideal and that its fractal property changed with moisture content and temperature.

Hartley and Avramidis (1993) also used the same sorption data to analyze the sorption isotherms by using the cluster formation theory. This theory considers the interactions between adsorbed molecules for a non-idealistic system. In the case of wood-water system, the interaction between adsorbed water molecules could result in cluster formation. A cluster may contain one, two, three, or n number of molecules. Cluster isotherms (a plot of average cluster size against M) can be divided into three regions for describing the adsorption process and at least two regions for describing the desorption process from low M up to M_{fsp}. In the first region, the dominant mechanism is chemical sorption between the sorption sites and water molecules. The second region is considered as an organizational region and the third region has physiosorption dominant mechanism according to Hartley and Avramidis (1993) and Hartley *et al.* (1992). The water cluster theory is considered as the more proper to explain the sigmoid curve of the wood sorption isotherms. They also pointed out that the geometry of surfaces should be taken into account with the states of the sorbed water molecules together when developing a sorption model for wood. If the geometry of the underlying surfaces are considered to be caused by the sorbed water, then these two things, namely, the geometry of the surfaces and the states of sorbed water molecules can be placed together and can be commonly explained by using a fractal approach.

The cluster isotherms were not developed in this research because they are also dependent on the value of dm/dh according to Eq. (2.11) in the hygroscopic range. In the cluster sorption isotherms, the cluster sizes changed with h in such a way that was similar way to the plot of dm/dh vs. h with three distinctive regions.

Both phenomena, clustering formation and fractality, are quite similar (Deutscher *et al.* 1983; Stauffer and Aharony 1992). A cluster's profile and its structure can be expressed by a D value. At certain points (thresholds), the cluster size will change dramatically and thus, lead to a distinct fractal dimension. The cluster profile of the adsorbed water molecules will determine the wood surface structure. Therefore, thresholds in the wood-water system within the hygroscopic range may appear at moisture contents near to 10 and 20%. These two points are close to the completion of the monolayer and the beginning of the full multilayer sorption points that have been reported in the past (Stamm 1964; Skaar 1972, 1988; Siau 1984). As a matter of fact, these two points physically imply much more than just the monolayer and multilayer levels in terms of past and present studies.

Based on the layering theory in the classic BET equation, three moisture content ranges (0 - 10%, 10 - 15%, and 15 - M_{fsp}) are corresponding to monolayer, a mix of monolayer and multilayer, and multilayer formations, respectively. From this study, the assumption in the first stage seems to be correct, but it is erroneous in the last stage because the clustering of water molecules is neglected. The middle stage is somehow correct because the clustering phenomenon in this stage would not be severe (cluster size is not large) (Hartley and Avramidis 1993; Hartley 1994). The layering formation theory can still be approximately applied at this stage as an average on the small cluster group. This observation was made from the fact that the BET equation can more or less fit the sorption data from low to high h if the D value is below 2.30.This can be seen from Figs. 5.37, and 5.38. The corresponding D values were 2.27 and 2.26, respectively. Such D values indicate that the underlying surface was no longer the flat surface, but something close to it. Namely, the surface was not very rough. The classic BET obviously failed to fit the sorption data in the high humidities in all the sixteen of the twenty

four cases in which the D values were all greater than 2.40. Such high D values indicate that the underlying surfaces became very rough and therefore the classic BET was no longer applicable. The greater the D values, the more the classic BET model resulted in erroneous estimations. This is reflected in Figs. 5.15 to 5.38 by the fact that the more inflectional the sorption curve at high humidities (the greater the dM/dh value), the greater the D value. In the following several subsections, the D relations to species, temperature, extractives content, location, and sorption condition are addressed.

5.9.1 Species and sapwood vs. heartwood

In terms of the calculated sorption data for the four types of wood as listed in Tables 1 to 4, the values of M at fixed relative vapor pressure and temperature did not differ greatly except in the case of UE-WRC. Generally, the difference in M was about 3%, 2%, and 1% between UE-WRC and the other three wood types (E-WRC, DFS, and DFH) at low, middle, and high humidities, respectively. This is believed to have resulted from deposition of extractives within the cell walls, allowing less space for water sorption. Stamm (1964) compiled a large set of sorption data taken from a number of different investigations for wood, wood components, hydrolysis, oxidation products of cellulose, and wood pulps. The results showed that the values of M for wood have a small variation with species and that the wood with high extractive content had a relatively low value of equilibrium moisture content.

In this study, the values of M were not evidently greater for DFS compared to DFH except in the case of 50°C and the very high humidities where the difference was about 2%. It is presumed that the difference in M between sapwood and heartwood exists because there is a difference in extractives content between them.

There was no conclusive correlation between the h_c values and species or locations. The h_c values from Table 12 showed positive relevance to temperature and are discussed in Section 5.3.4.

5.9.2 Sorption history (adsorption and desorption)

A difference existed in relation to the sorption history and with respect to the D value at the same temperature level. At 50°C, the D values for adsorption were greater than those for desorption for the four wood types in this study. At 40°C, the D values for desorption were greater than those for the adsorption for E-WRC, DFS, and DFH and had no apparent difference for UE-WRC in the same sense. At 30°C, no conclusive correlation as to which condition had a greater D value existed. It indicated that the D value was related to the value of dM/dh in addition to that of M. The greater the value of dM/dh, the greater the D value and thus, the rougher the underlying surfaces.

5.9.3 Temperature

Hartley (1994) pointed out that the bound water can exist in different states. These states can be described in two manners: one is by water cluster formation and the other is by formation of molecular water layers. This conclusion was based on NMR wood-water system studies. In this study, these results can be explained geometrically in terms of their D values. One was tightly bound to the sorption sites with the D value of less than 2 or about 2 (scattering sorption sites or monolayer, respectively). The other was towards clustering formation over the previously formed parts and cumulatively resulted in a greater D value of about 2.4 (being far from a plane). If the first part is dominant (either at the low sorption region or stronger sorption sites

involved or both), then the geometry of the surface would not be very rough. The locations of all sorbed water molecules are forced by the sorption sites or the underlying surfaces. Otherwise, they will have more chance to cluster together, and thus make the underlying surfaces rougher with a higher D value at high humidities. Clustering mechanism is the better way to explain the higher D value.

From Table 11, there was no sufficient evidence to show the relationship between the wood type and its h_c values. However, the lower h_c values at 50°C seemed to be lower than those at 30°C and 40°C in most cases. This could imply that the second part (cluster part with greater D value) was more important in controlling the geometry of the underlying internal surfaces of the cell walls at 50°C. For example, in the case of unextracted western red cedar, the lower h_c value for desorption at 30°C is 0.50 and it is 0.30 at 50°C.

The classic BET model cannot fit the sorption data at high humidities and the degree of fit is worse when temperature increase. This can be attributed to the greater D values and it can thus, be inferred that bigger cluster sizes are involved. For example, all types of wood tested in this study at 50°C had the highest D value (more than 2.4) at high humiditites which is far from being described as two dimensional. Stamm (1964) attributed the sudden change of M in sorption isotherms at high sorption regions and at higher temperatures to cellulose plasticization by heat and moisture occurring to such a degree that the internal stresses resulting from the original drying are suddenly relieved and the hydroxyl groups of the cellulose that have mutually satisfied each other are broken and thus, made available for water vapor sorption. If this is the case, the classic BET model should have fitted the experimental data well with a greater n value. Therefore, a totally different sorption mechanism must be used to account for the sudden increase in M. Otherwise, the lack of fitness of the classic BET model cannot be

explained with the same mechanism for both low and high humidities. Instead, water molecular clustering can more adequately explain the steady increase in M at high sorption regions. The cluster information can be obtained from its D value, namely, the greater D value implies the existence of a bigger cluster.

5.9.4 Extractives

Wood species with a high content of extractives show significantly lower hygroscopicity. This could result from the deposition of extractives within the cell walls thus allowing less space in wood for water adsorption. The bulking treatment for improving wood dimensional stability is based on this mechanism (Stamm 1964; Spalt 1957, 1958; Wangaard and Granados 1967). Compared to DF, the unextracted cedar is known to have a high level of extractives content. In this study, it was experimentally found to be 9.5% and most probably responsible for the lower hygroscopicity compared to the other three types of wood. Non-water soluble extractives and ash deposited in the lumens of wood add to the total weight without affecting the amount of water take-up to equilibrium, thus reducing the sorption per unit of dry weight at all relative vapor pressures. This further validates the fact that extractives are bulking chemicals for the cell walls (Stamm 1964, 1971). The removal of extractives raised the values of M to the values obtained with the other two types of wood (DFH and DFS) with lower extractives content. This result is similar to that reported by Wangaard and Ganados (1967). The reduced heat of wetting in cedar was considered to be a result of the high level of extractives content (Avramidis and Dubois 1992) and therefore, the lower number of accessible sorption sites available (Spalt 1979).

From the fractal point of view, at 50°C and adsorption, highest h_c for UE-WRC was 0.525, while it was 0.855 in E-WRC for the D value of about 2.60. This shows that at 50°C adsorption for UE-WRC, the second part formation of the sorbed water happened at the lower h than it did in E-WRC. It can further be concluded that fewer sorption sites may have resulted in an easier formation of the second state or second part of the sorbed water, namely, cluster formation might have happened at the lower h value.

In short, from the fractal point of view and stepwise assumption which was validated in Polynomial-Fractal sorption theory, the sorption properties of the wood can be divided into several different stages. These refer to scattering sorption sites along the polymer chains with D value of more than one, surface sorption sites with D at about 2, and spatially accumulative sorption sites within the microvoids of the cell walls with D more than 2 and an upper limit of 3. As M increases to about 12%, D increased over 1 by approaching 2. This phenomenon can be explained by the fact that each accessible sorption site adsorbs at least one water molecule. Therefore, the total adsorbed water molecules might have initially formed a continuous curve ($1 < D < 2$) and then begun to form a surface ($D = 2$) or something more than a surface ($D > 2$) afterwards. The value of D kept increasing with an increase in M and at about 18%, D was greater than 2.3 or 2.4 or 2.5 which is temperature related. Beyond that point D tends to become constant.

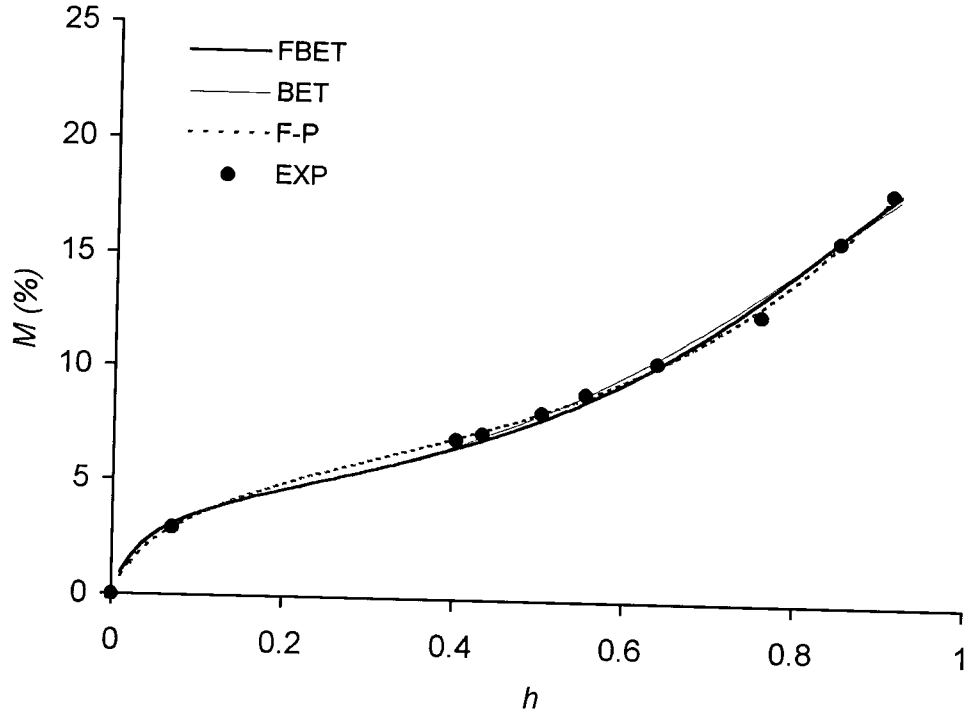

(a)

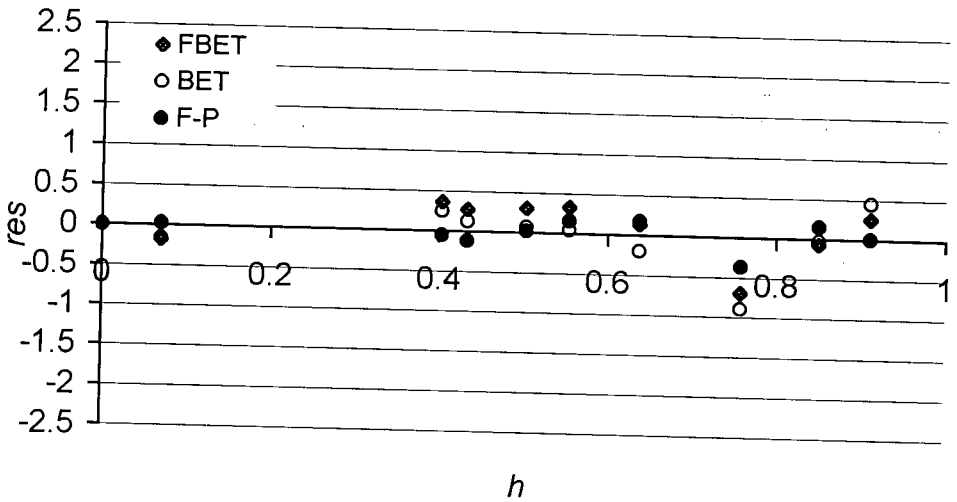

(b)

Fig. 5.15: The calculated desorption isotherms (a) and their residue patterns (b) for UE-WRC at 30°C

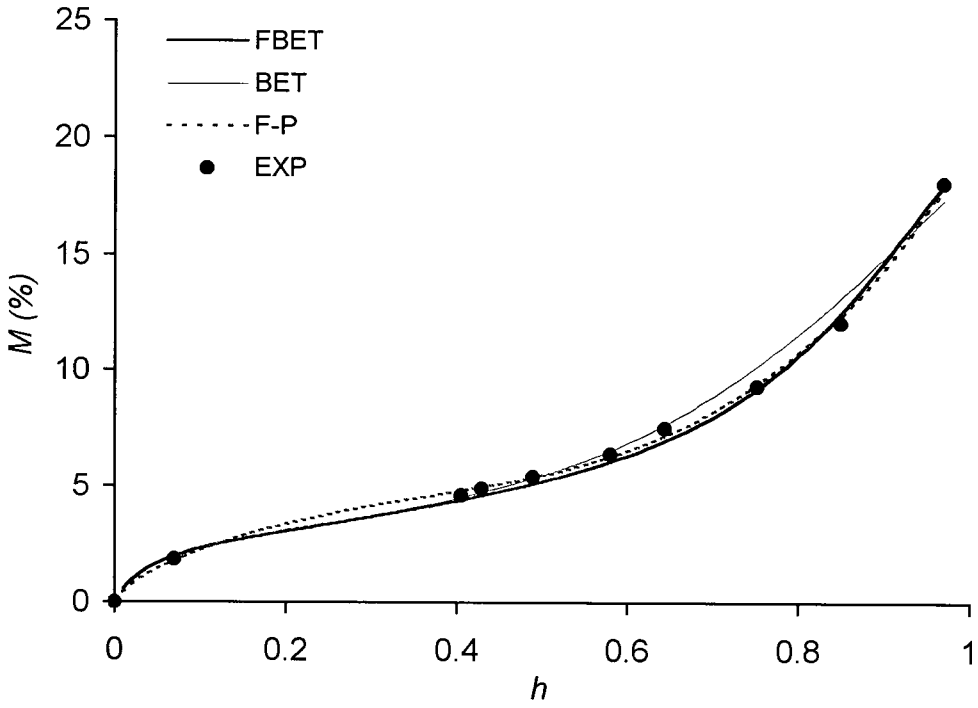

(a)

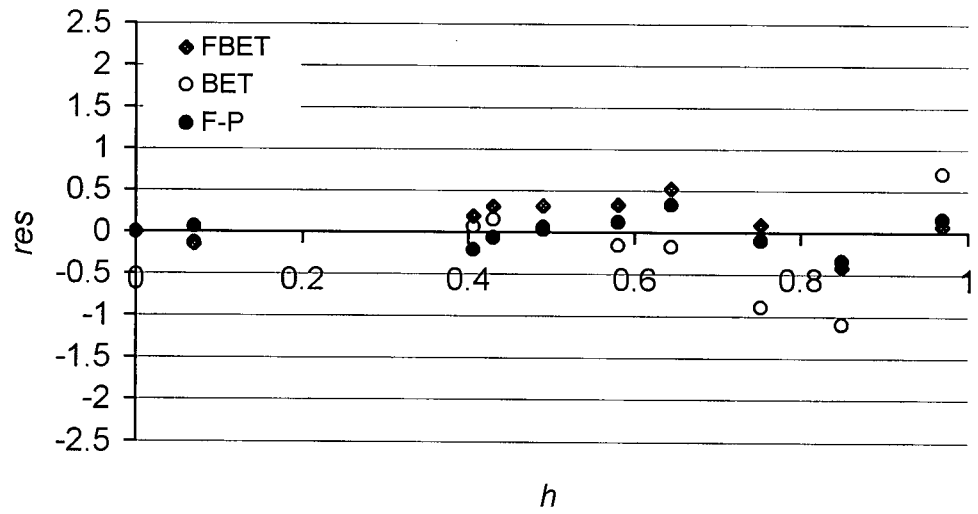

(b)

Fig. 5.16: The calculated adsorption isotherms (a) and their residue patterns (b) for UE-WRC at 30°C

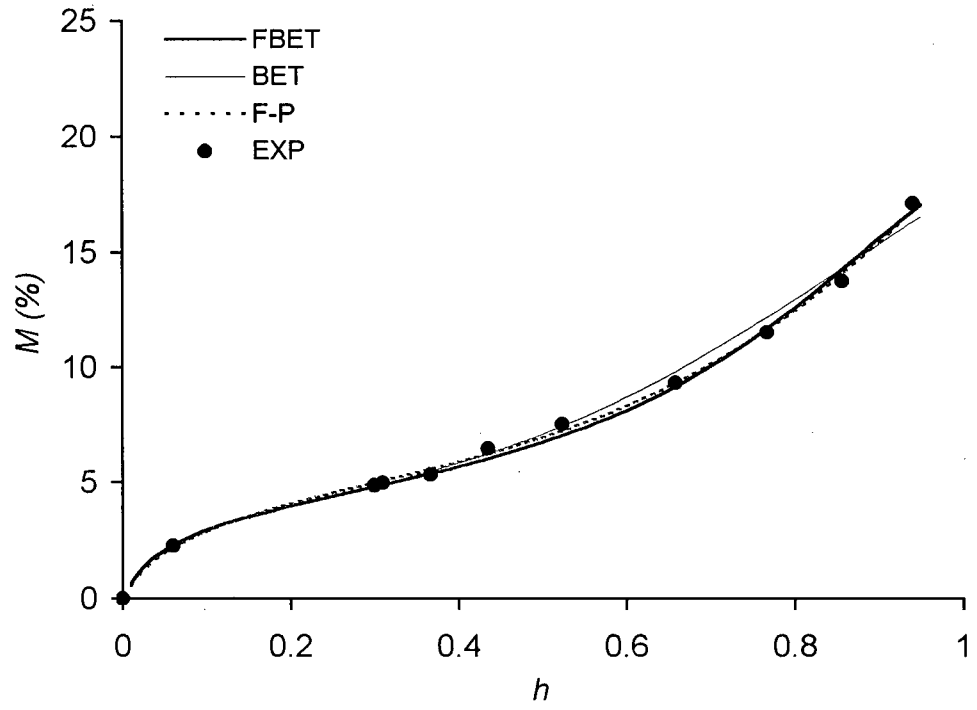

(a)

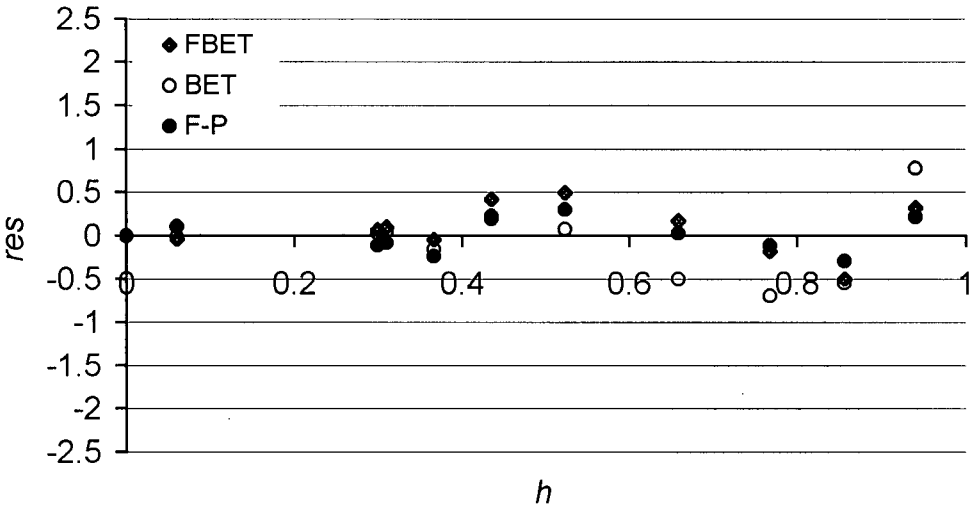

(b)

Fig. 5.17: The calculated desorption isotherms (a) and their residue patterns (b) for UE-WRC at 40°C

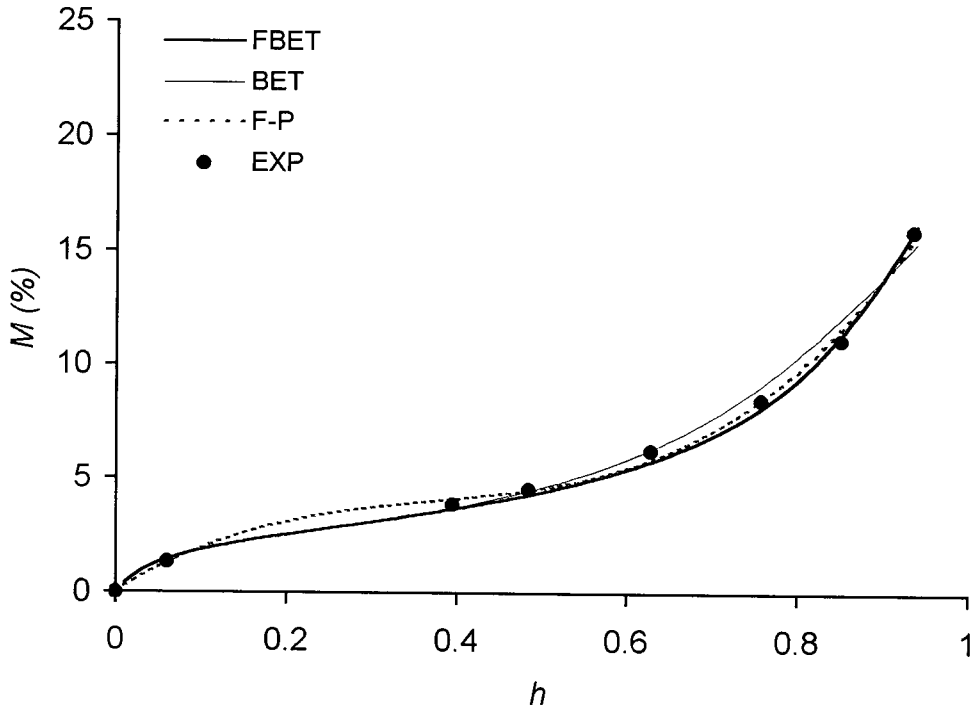

(a)

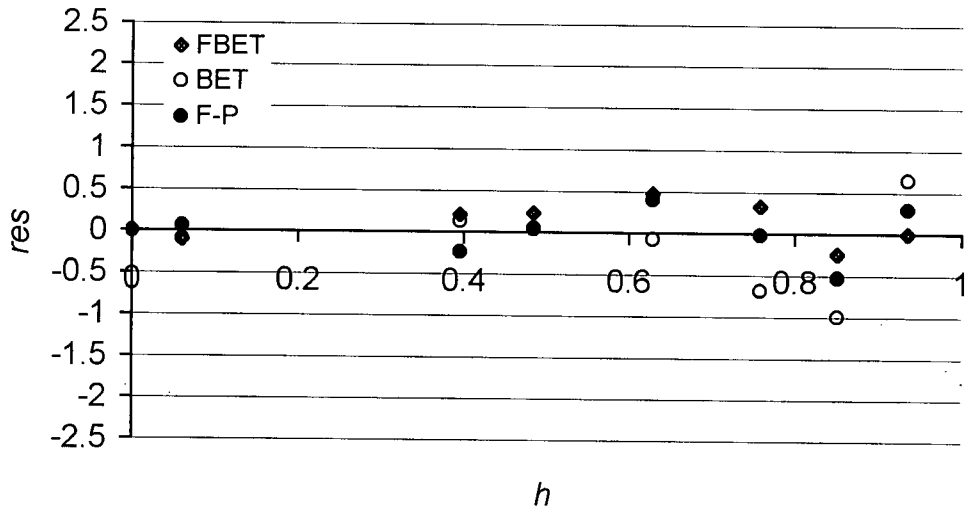

(b)

Fig. 5.18: The calculated adsorption isotherms (a) and their residue patterns (b) for UE-WRC at 40°C

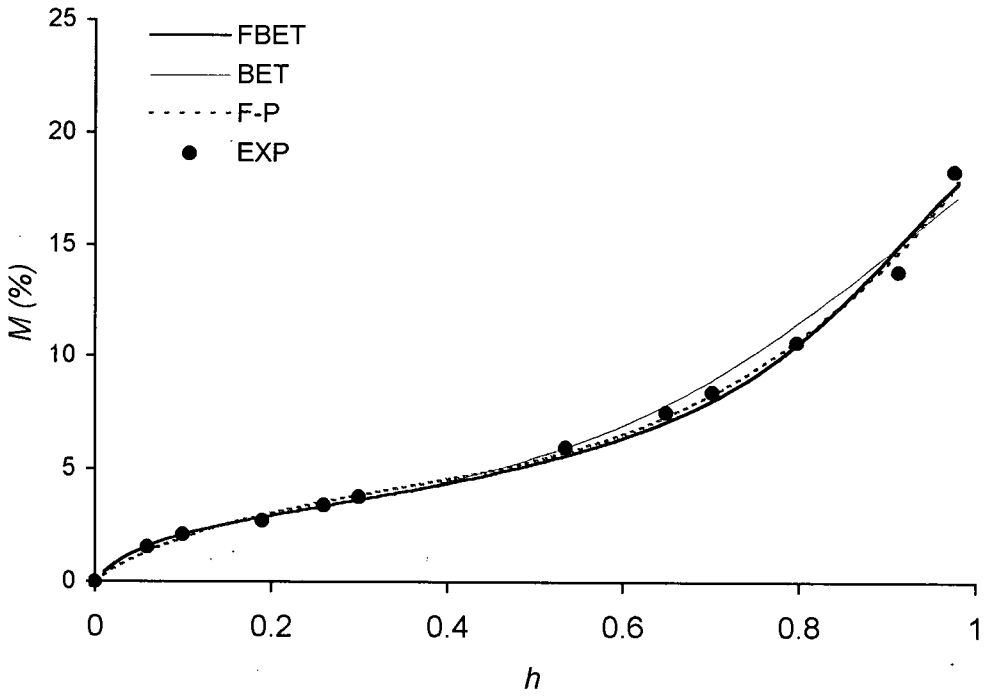

(a)

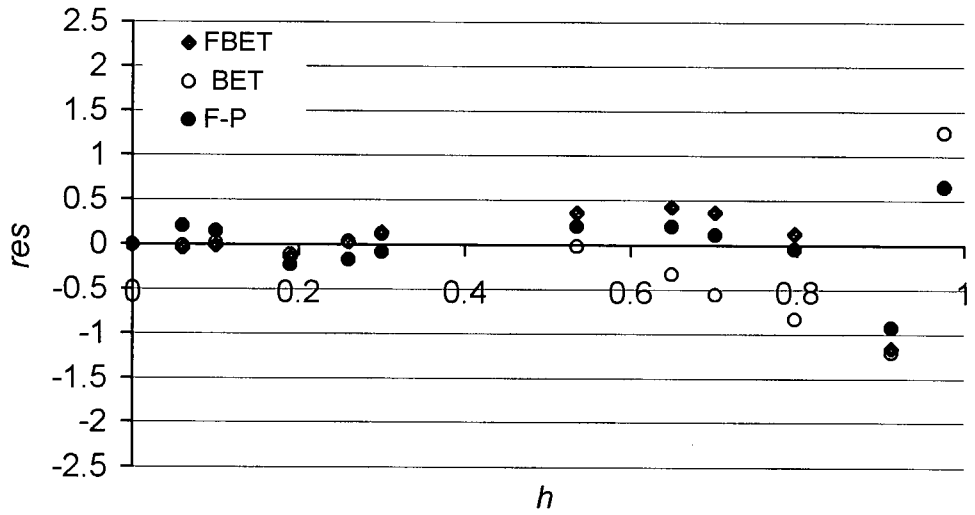

(b)

Fig. 5.19: The calculated desorption isotherms (a) and their residue patterns (b) for UE-WRC at 50°C

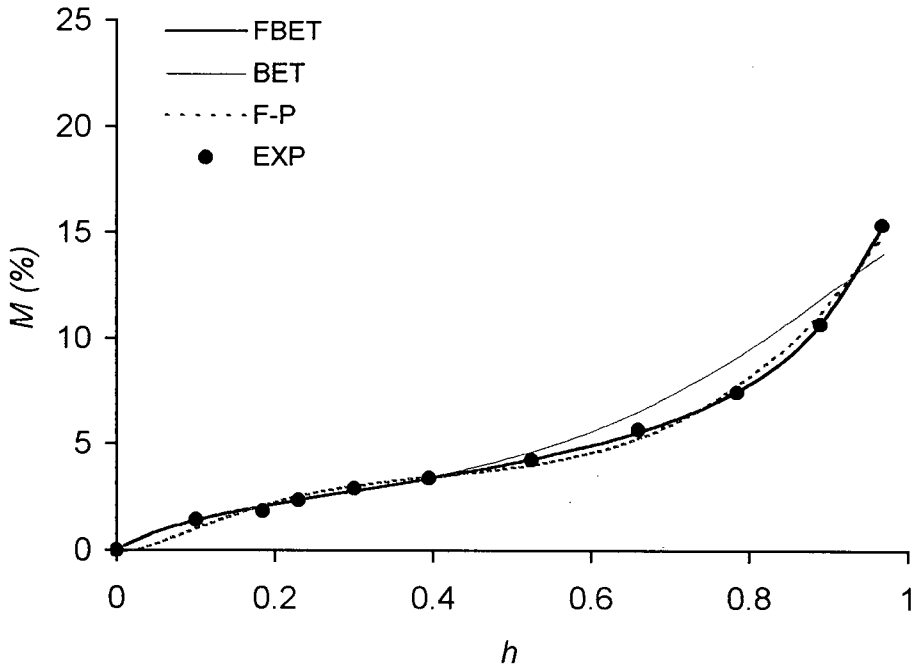

(a)

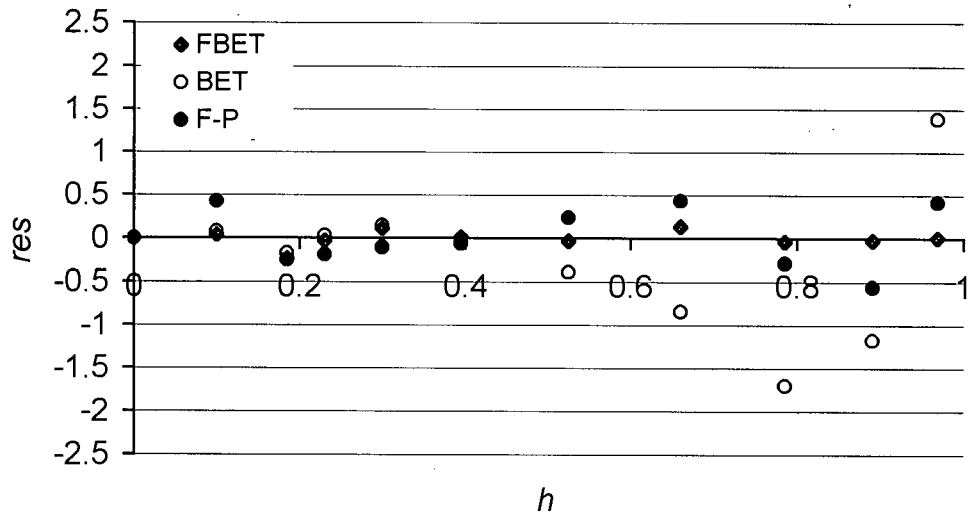

(b)

Fig. 5.20: The calculated adsorption isotherms (a) and their residue patterns (b) for UE-WRC at 50°C

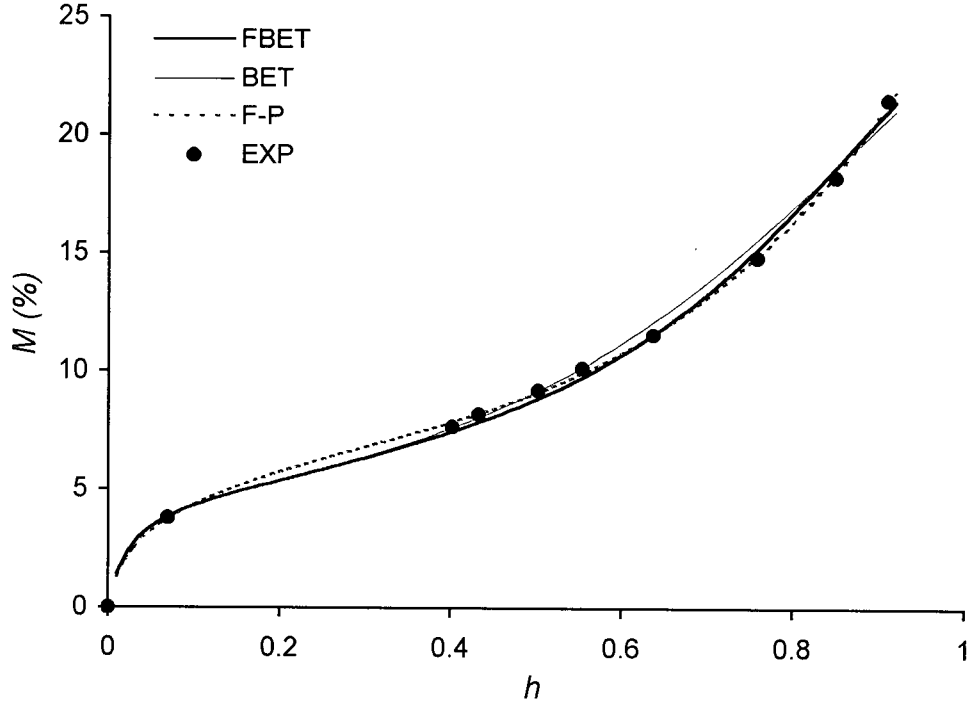

(a)

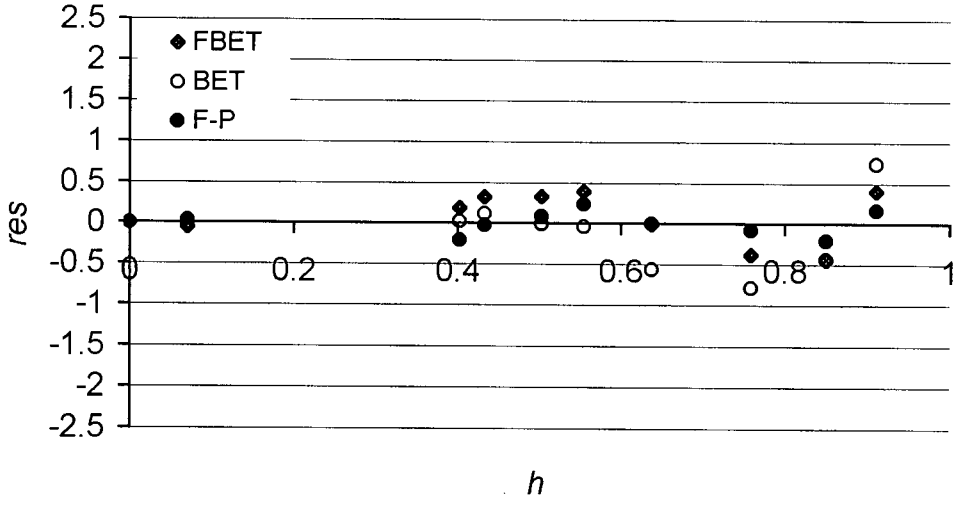

(b)

Fig. 5.21: The calculated desorption isotherms (a) and their residue patterns (b) for E-WRC at 30°C

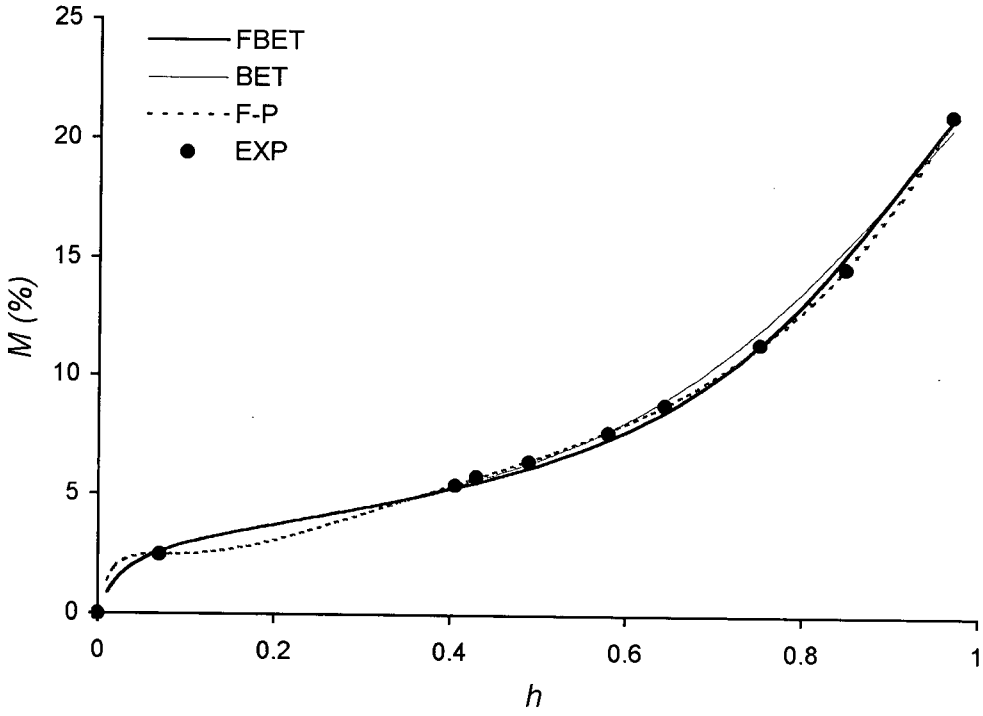

(a)

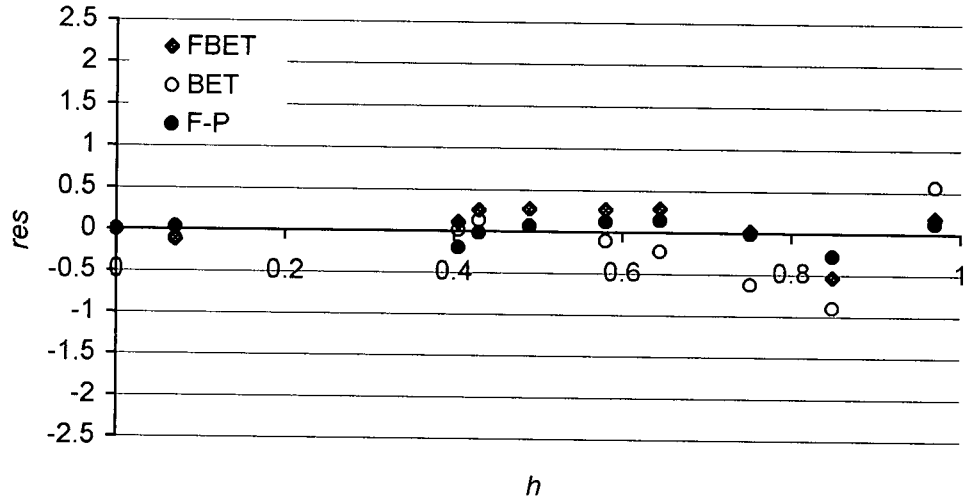

(b)

Fig. 5.22: The calculated adsorption isotherms (a) and their residue patterns (b) for E-WRC at 30°C

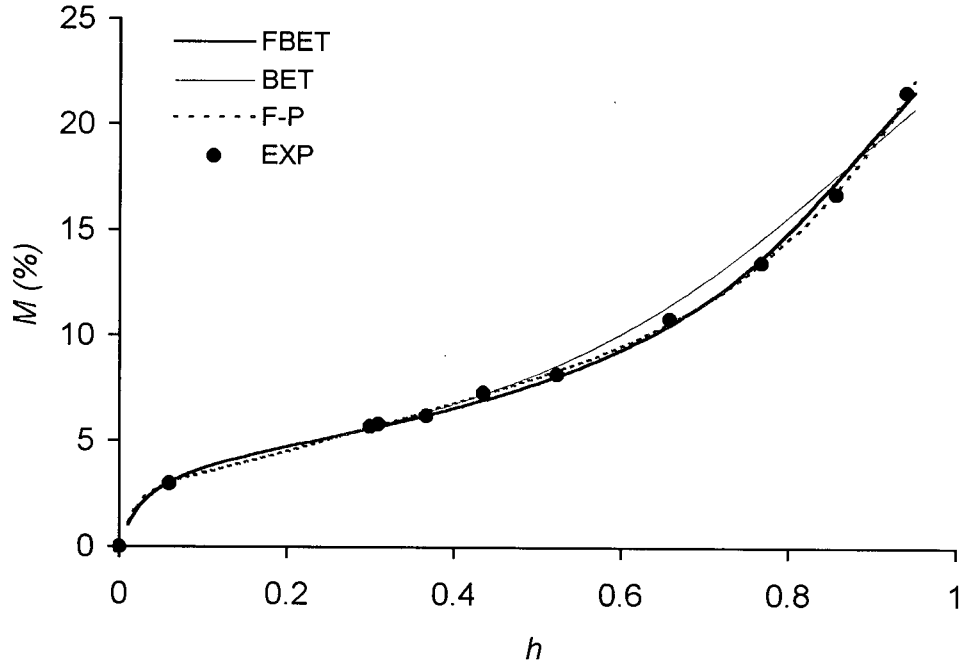

(a)

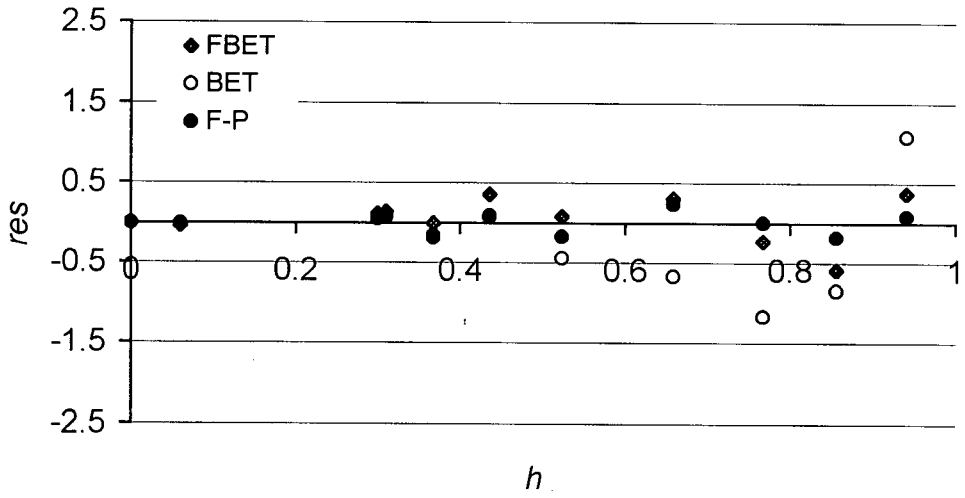

(b)

Fig. 5.23: The calculated desorption isotherms (a) and their residue patterns (b) for E-WRC at 40°C

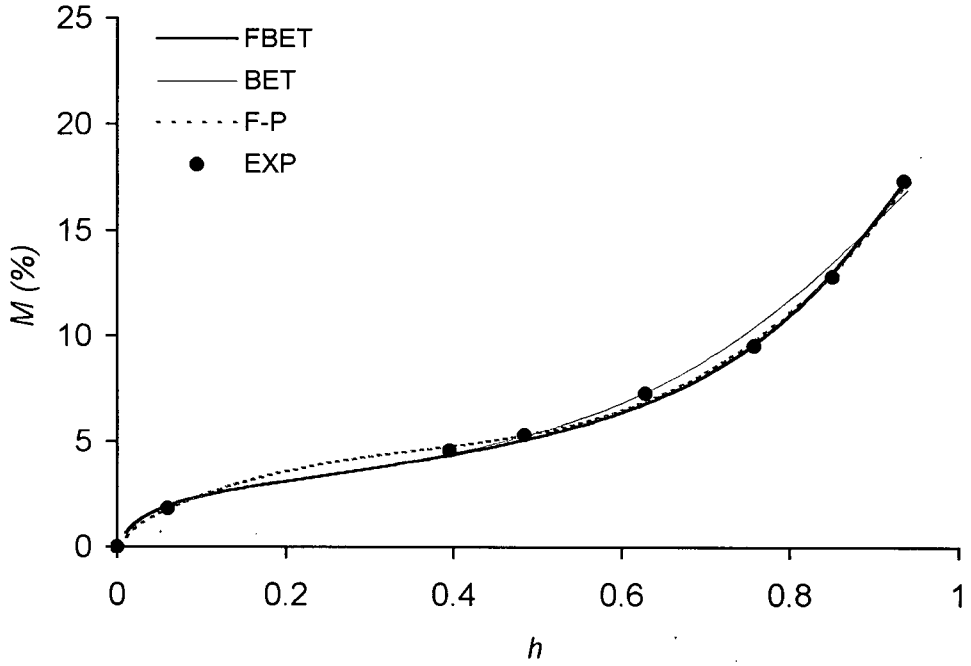

(a)

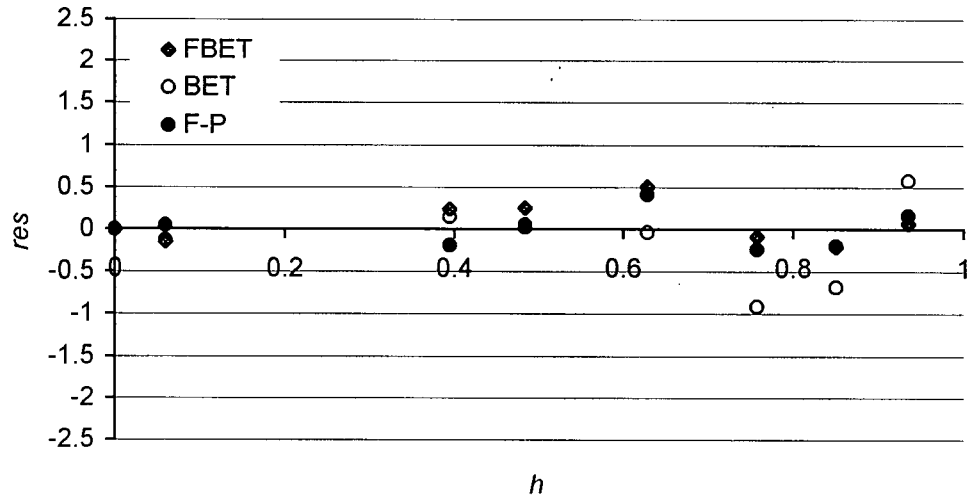

(b)

Fig. 5.24: The calculated adsorption isotherms (a) and their residue patterns (b) for E-WRC at 40°C

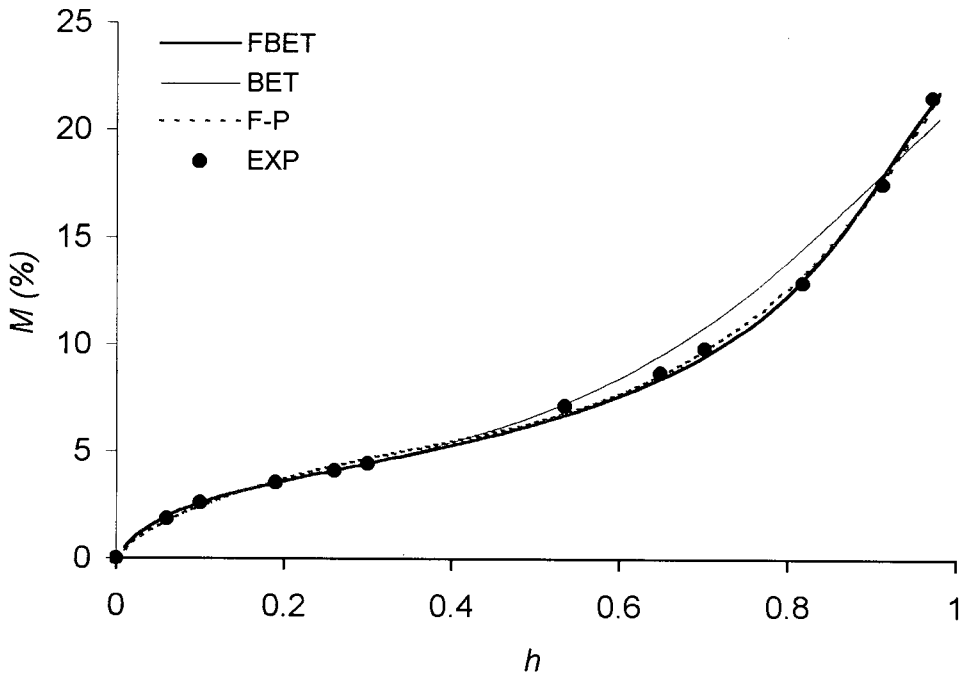

(a)

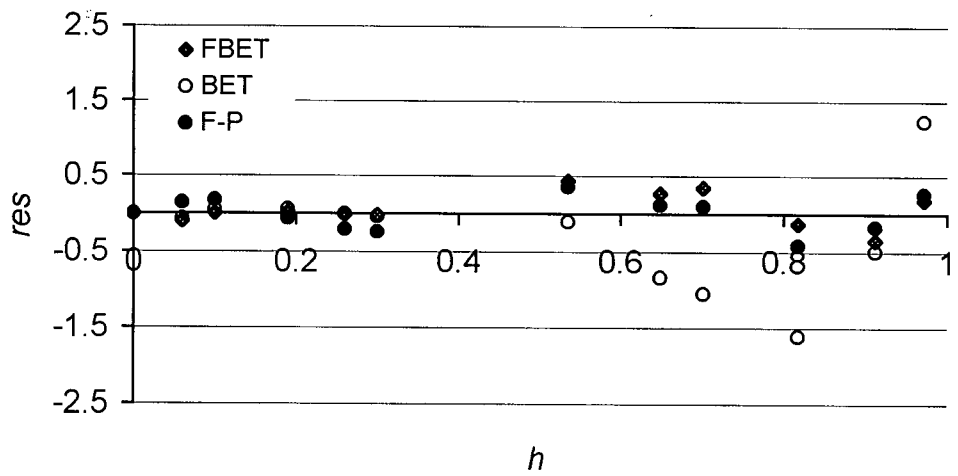

(b)

Fig. 5.25: The calculated desorption isotherms (a) and their residue patterns (b) for E-WRC at 50°C

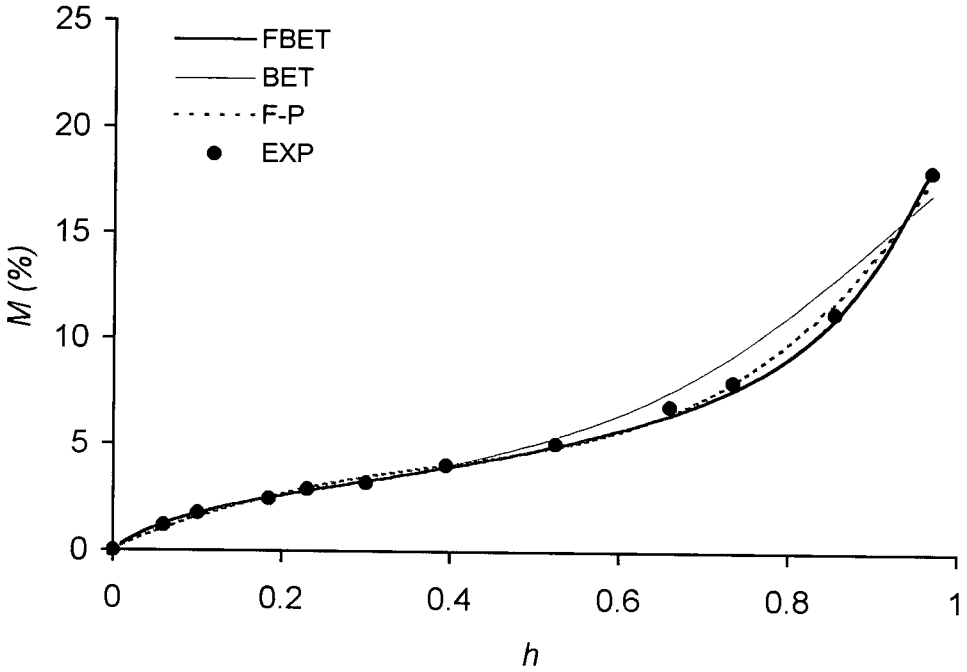

(a)

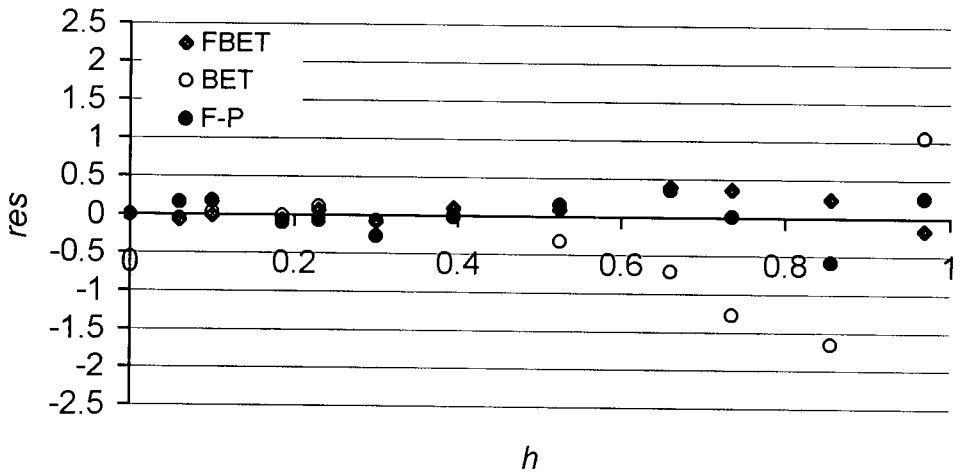

(b)

Fig. 5.26: The calculated adsorption isotherms (a) and their residue patterns (b) for E-WRC at 50°C

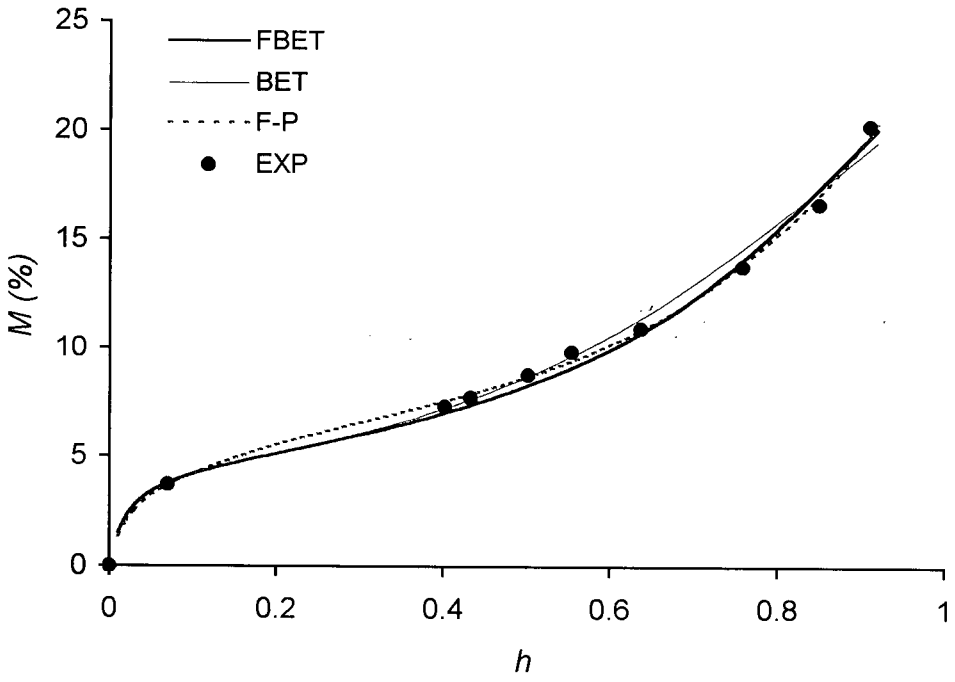

(a)

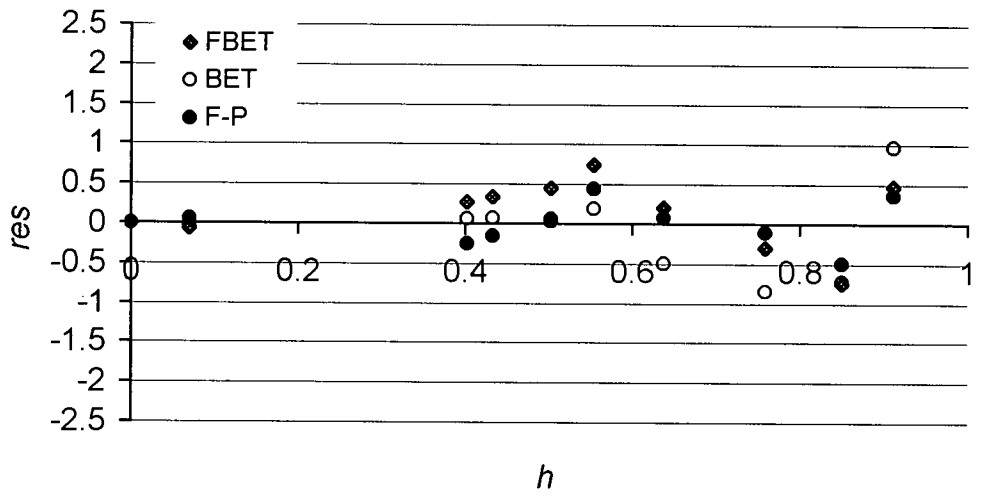

(b)

Fig. 5.27: The calculated desorption isotherms (a) and their residue patterns (b) for DFS at 30°C

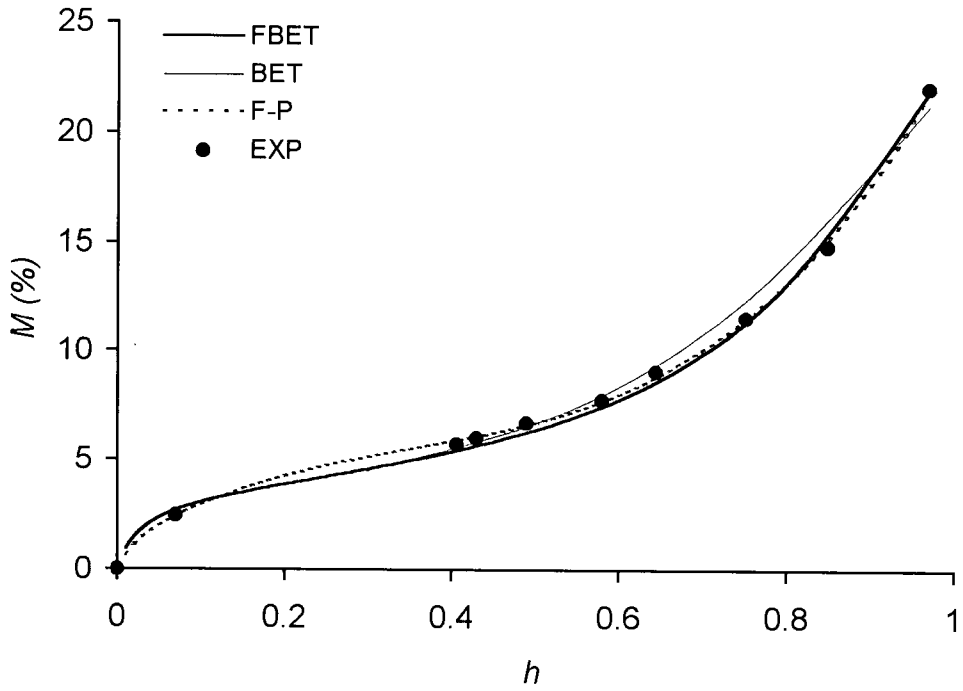

(a)

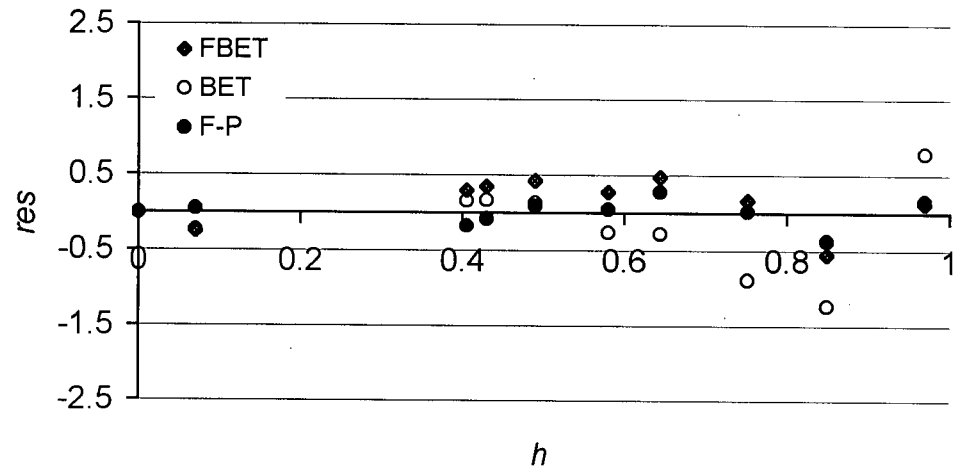

(b)

Fig. 5.28: The calculated adsorption isotherms (a) and their residue patterns (b) for DFS at 30°C

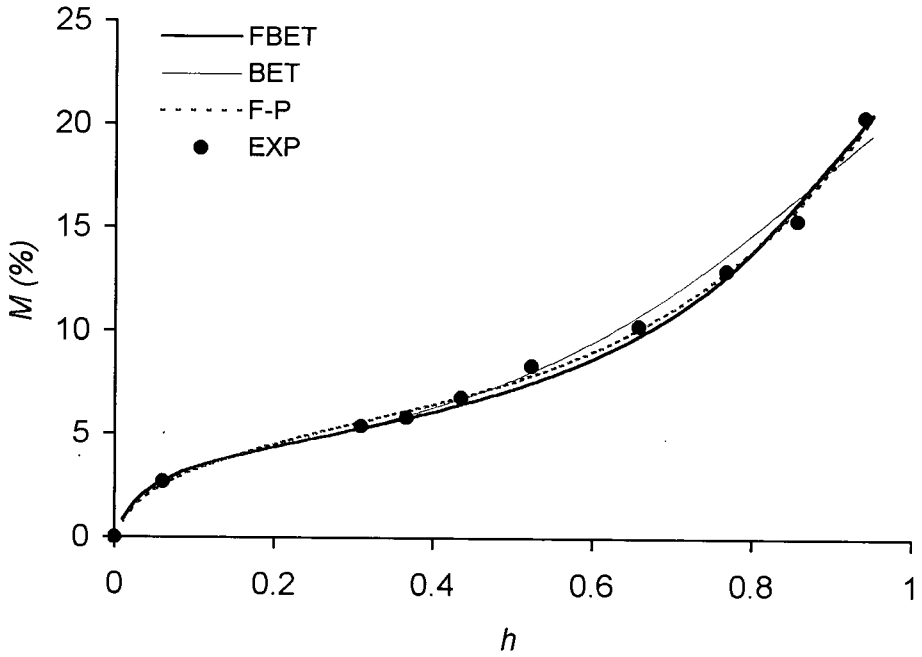

(a)

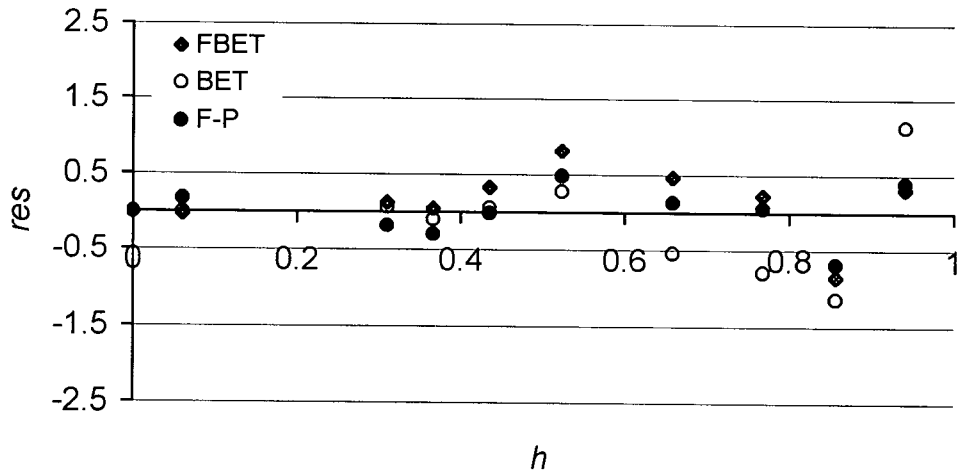

(b)

Fig. 5.29: The calculated desorption isotherms (a) and their residue patterns (b) for DFS at 40°C

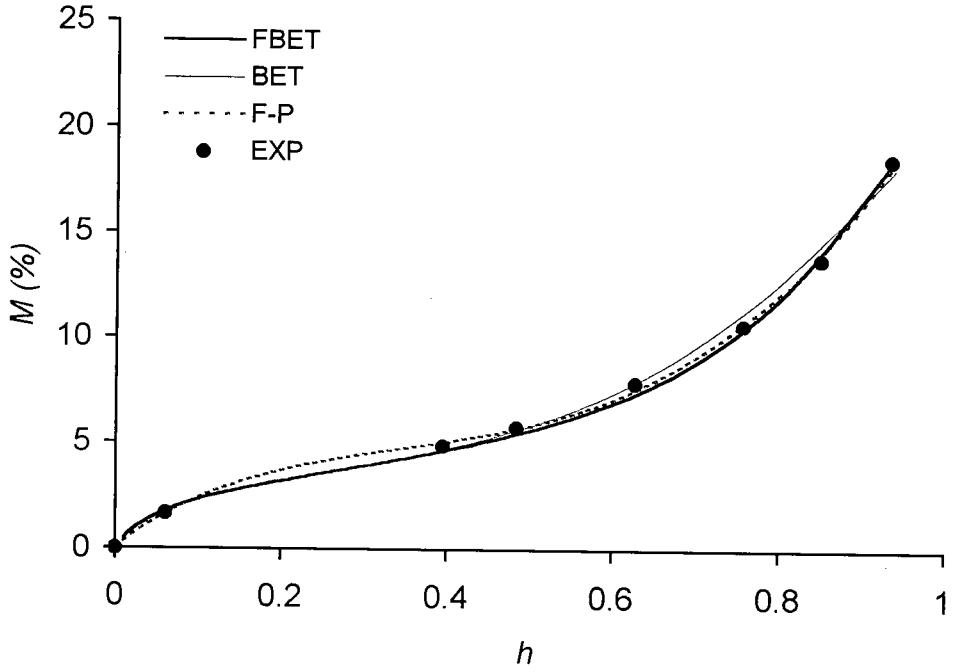

(a)

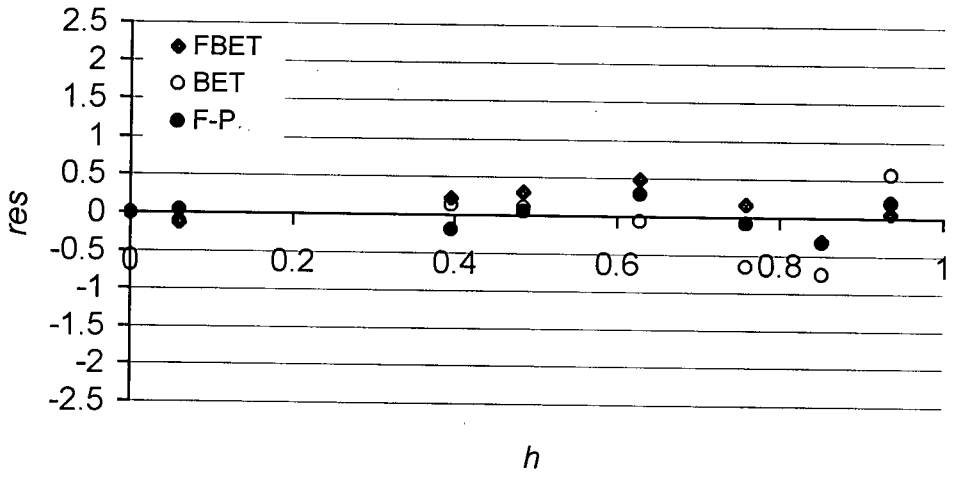

(b)

Fig. 5.30: The calculated adsorption isotherms (a) and their residue patterns (b) for DFS WRC at 40°C

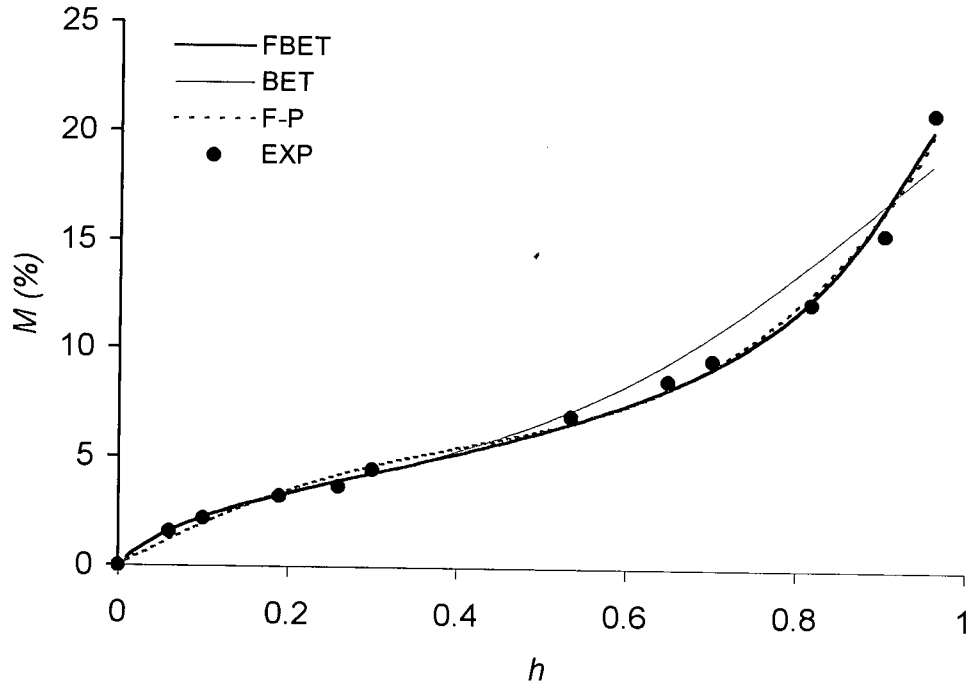

(a)

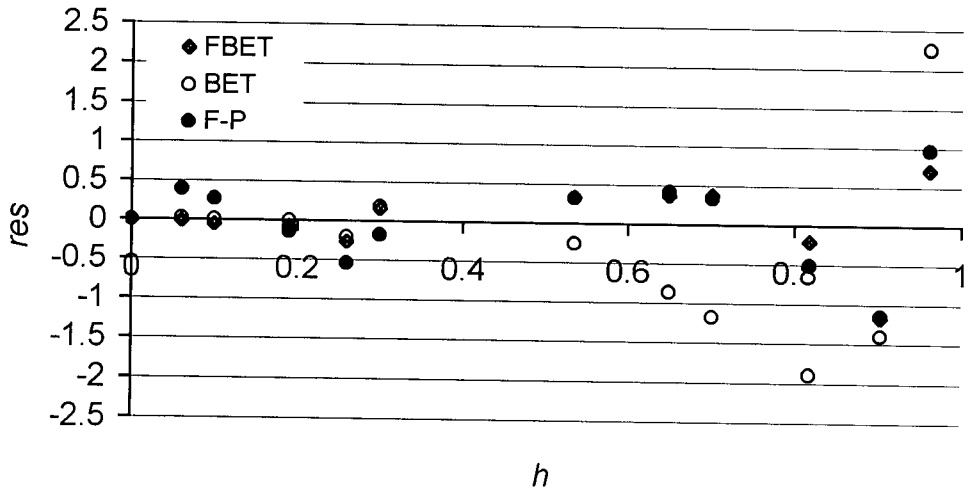

(b)

Fig. 5.31: The calculated desorption isotherms (a) and their residue patterns (b) for DFS at 50°C

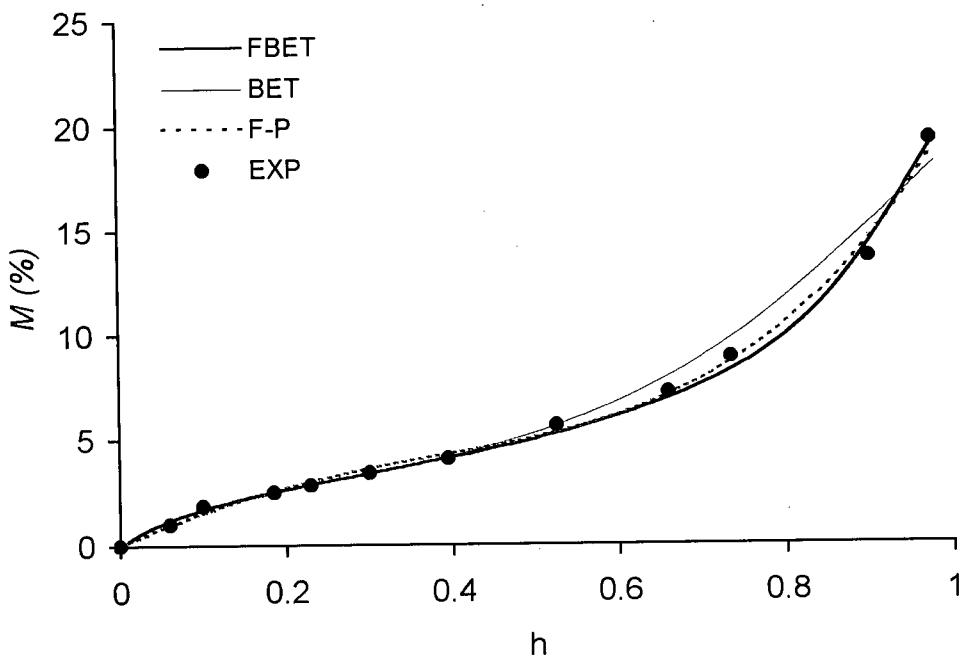

(a)

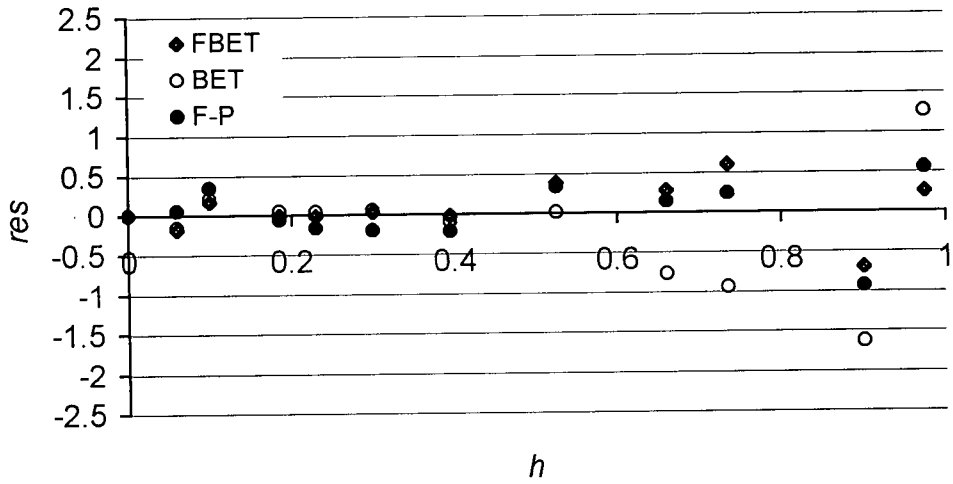

(b)

Fig. 5.32: The calculated adsorption isotherms (a) and their residue patterns (b) for DFS at 50°C

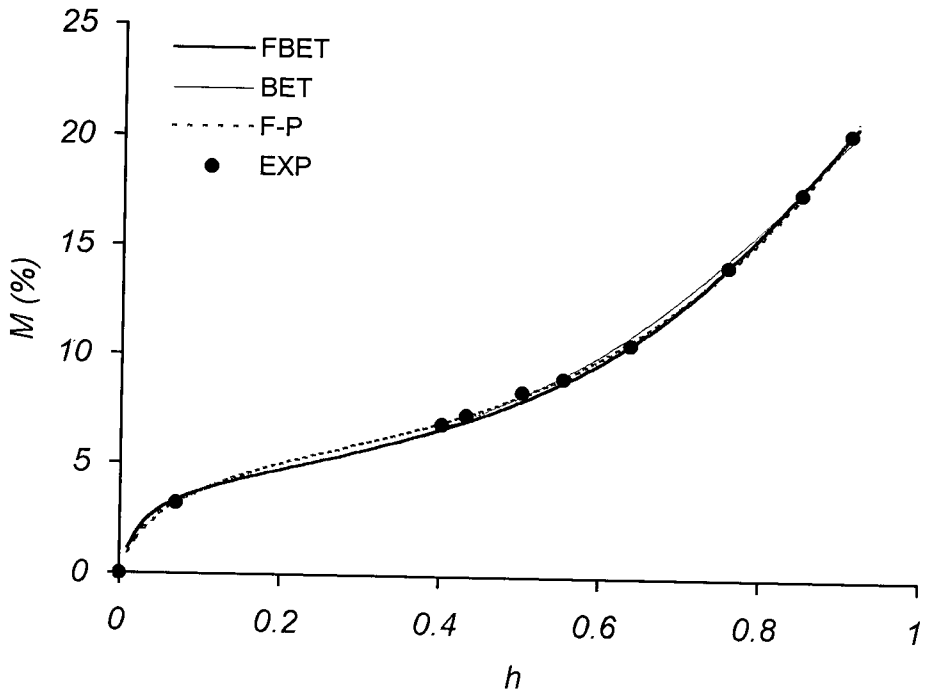

(a)

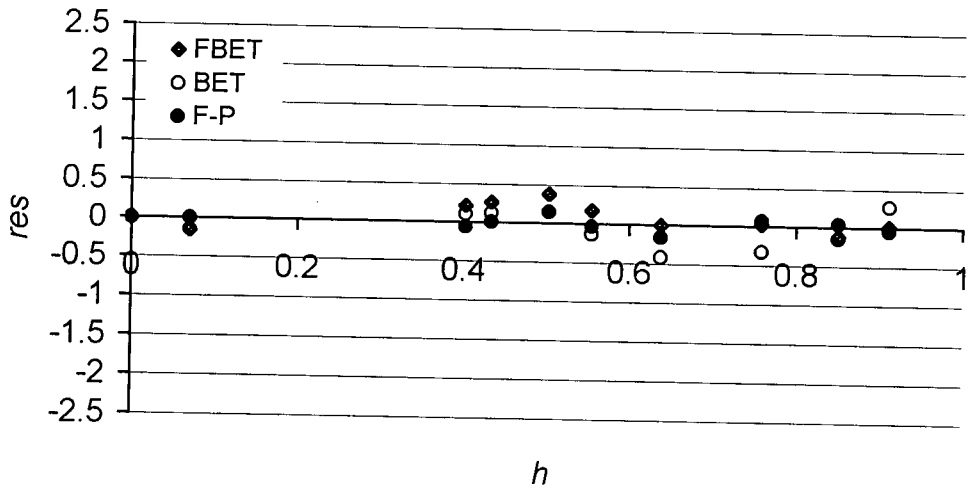

(b)

Fig. 5.33: The calculated desorption isotherms (a) and their residue patterns (b) for DFH at 30°C

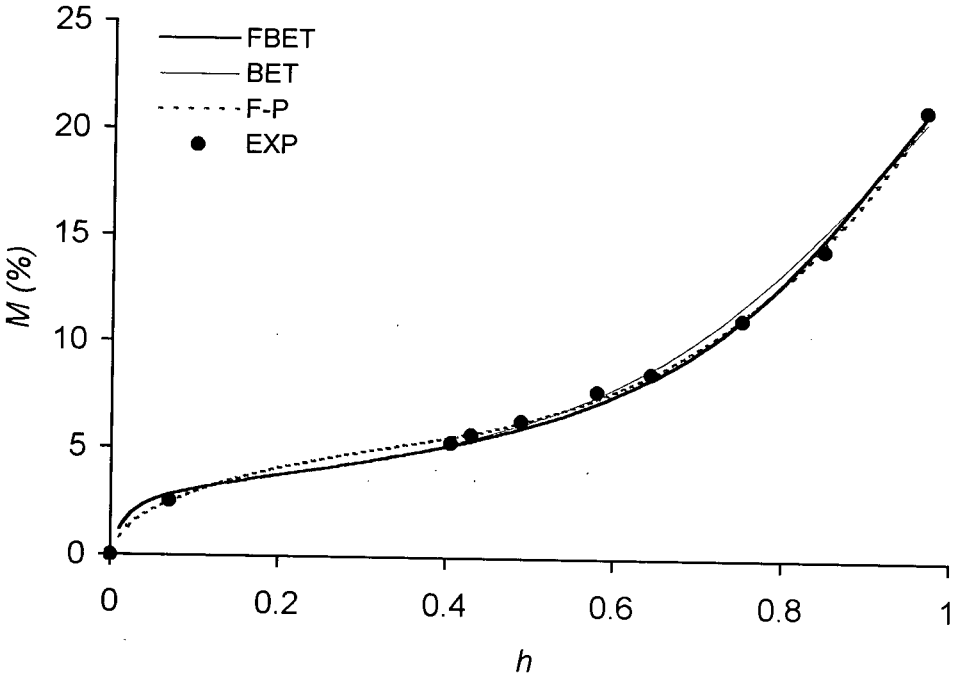

(a)

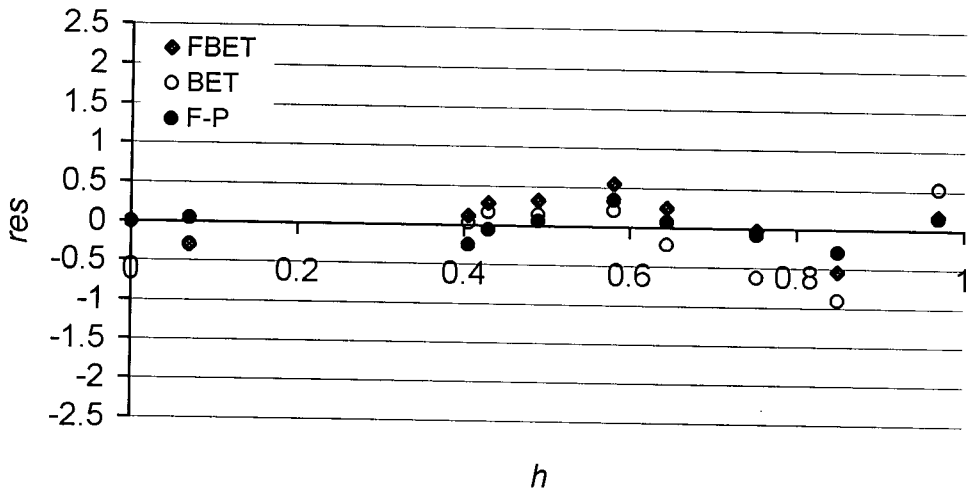

(b)

Fig. 5.34 The calculated adsorption isotherms (a) and their residue patterns (b) for DFH at 30°C

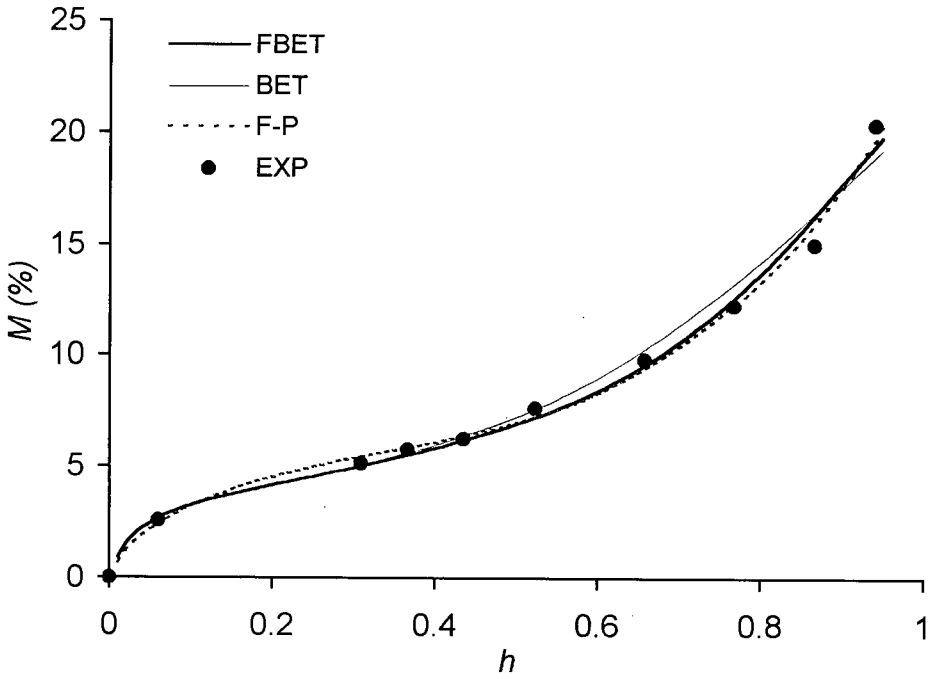

(a)

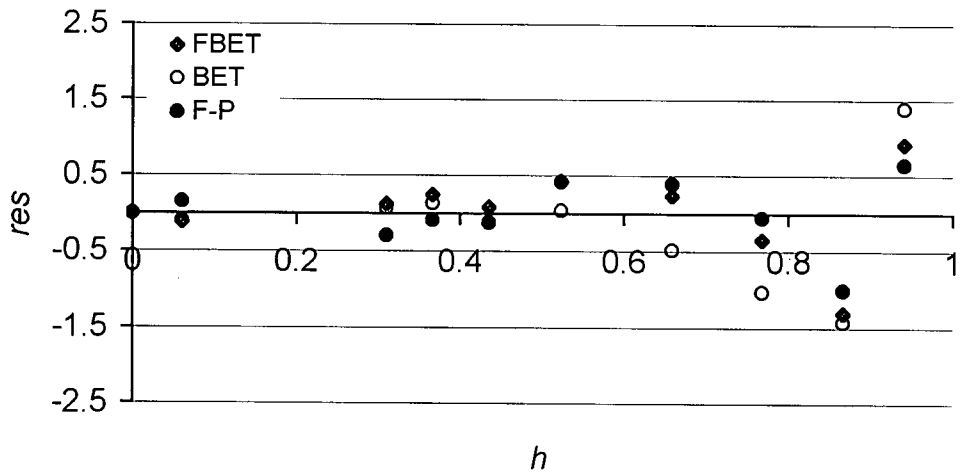

(b)

Fig. 5.35: The calculated desorption isotherms (a) and their residue patterns (b) for DFH at 40°C

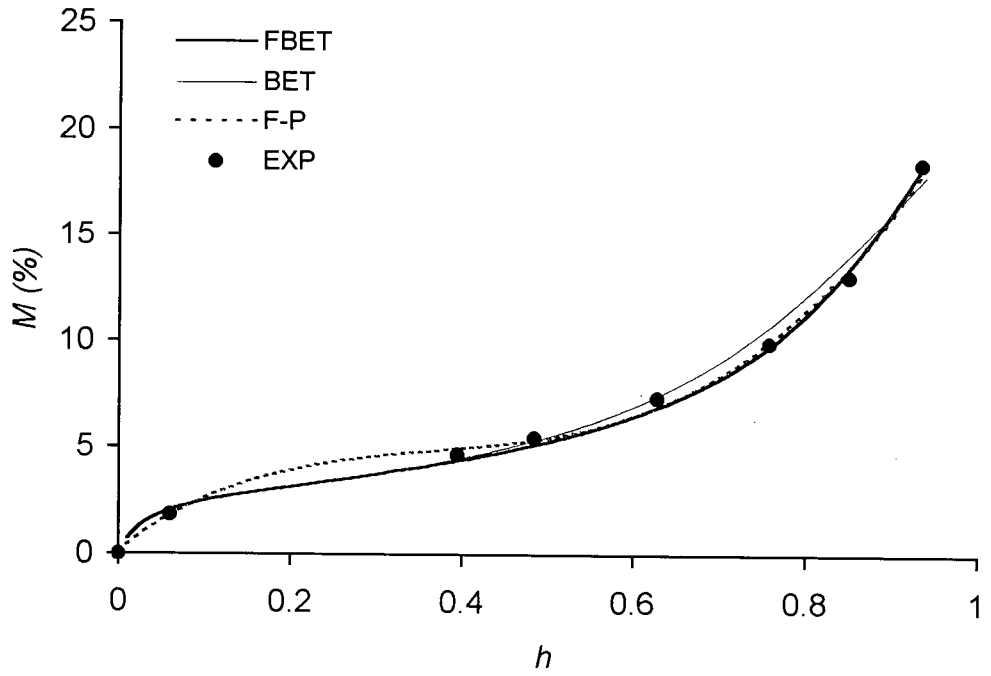

(a)

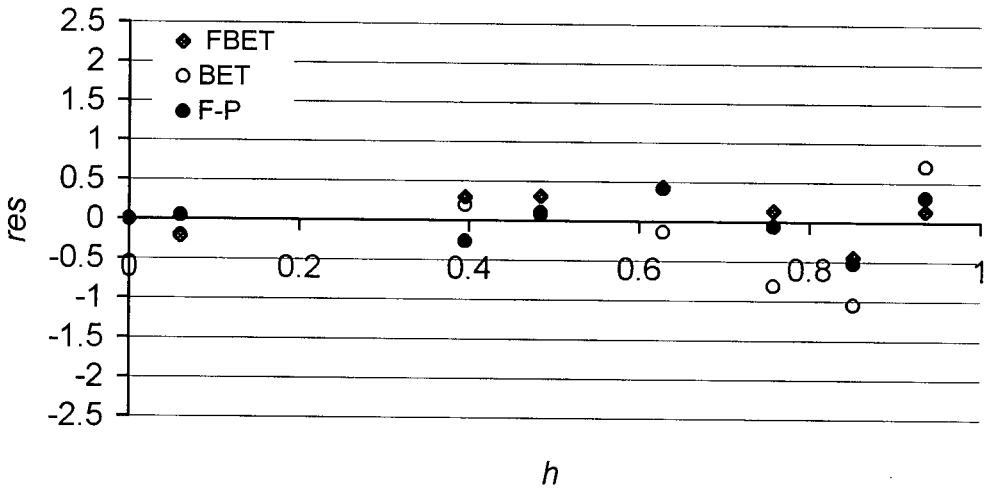

(b)

Fig. 5.36: The calculated adsorption isotherms (a) and their residue patterns (b) for DFH at 40°C

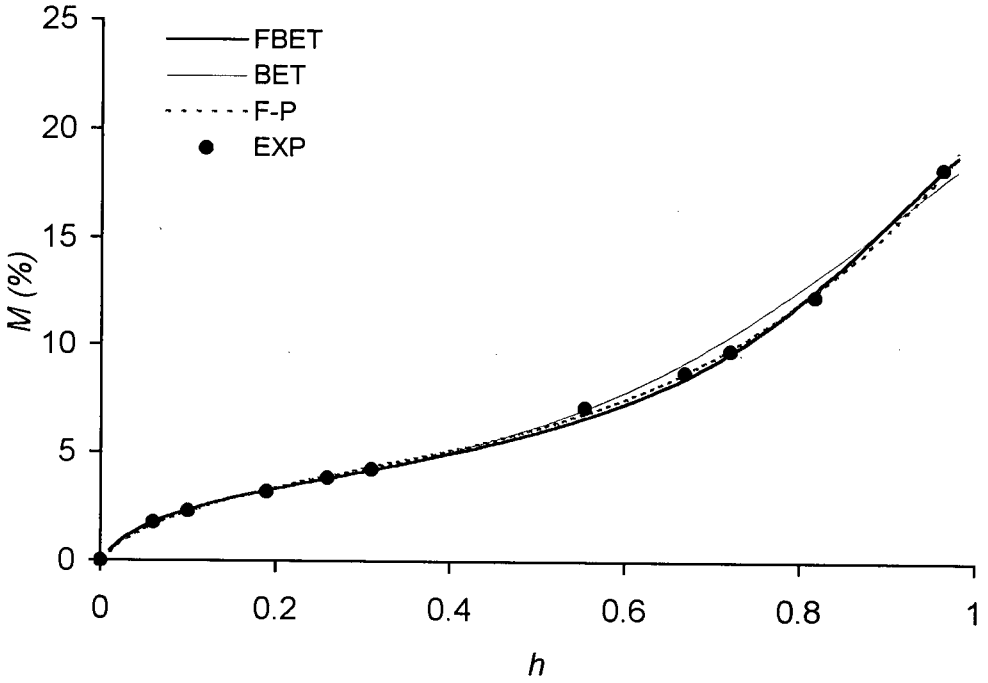

(a)

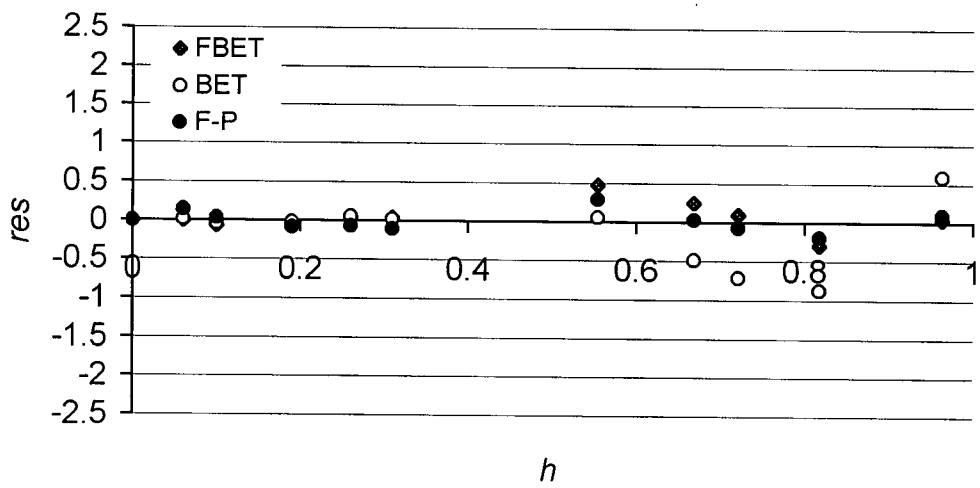

(b)

Fig. 5.37: The calculated desorption isotherms (a) and their residue patterns (b) for DFH at 50°C

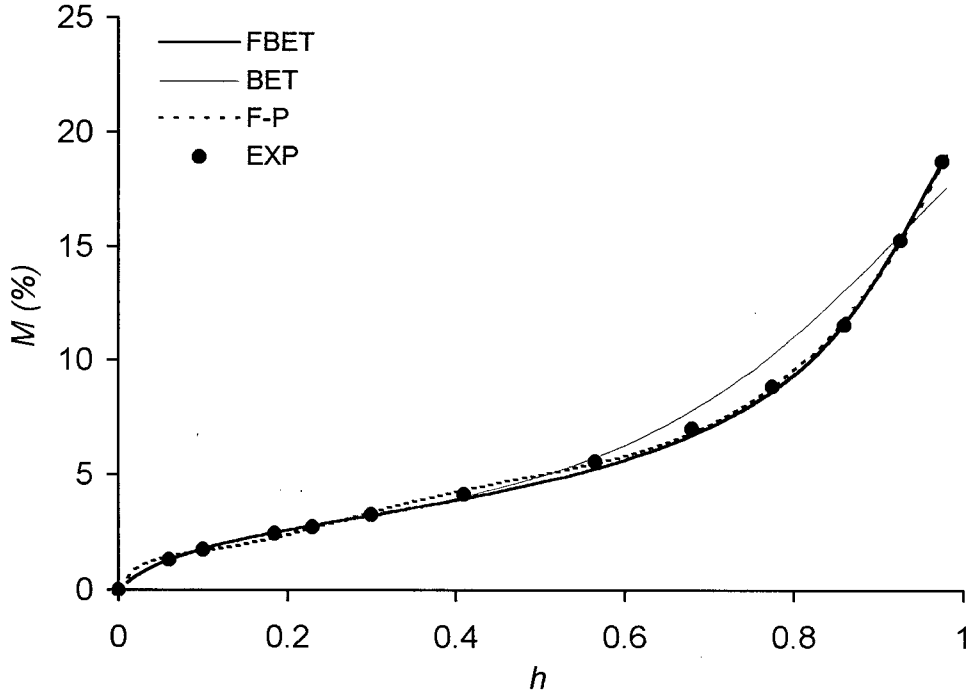

(a)

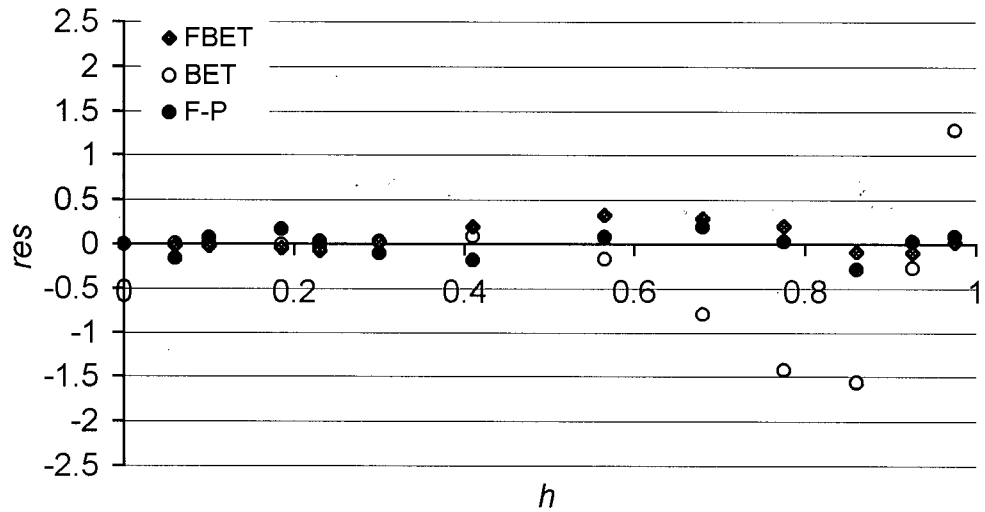

(b)

Fig. 5.38: The calculated adsorption isotherms (a) and their residue patterns (b) for DFH at 50°C

5.10 Examination of mass fractal phenomenon within the cell walls

To examine the existence of the mass fractal phenomenon for the bound water, the key issue is to measure the amount of sorbed water under different scales of dimension and examine the relationship between the amount of water and its corresponding scale. Therefore, it was assumed that the entire bound water within the cell walls was considered as a large spatial network of sorbed water molecules and that the network was distributed with a certain geometric pattern throughout the entire specimen. To discover the pattern, a simple way which was used in this study was to determine the amount of the bound water for the altered size of specimens.

5.10.1 Moisture content of the different volume of the cube specimens

The moisture content data of the cubic-shaped specimens with different volumes are listed in Tables 5 and 6. These data include the edge length of the cubic specimens, the amount of water sorbed, moisture content, the number of specimens and the standard deviation of moisture content for each size class are listed. From Figs. 5.5 and 5.6, it can be seen that the size or thickness of the specimens did not affect the moisture content in all relative vapor pressures and temperatures. The different behavior was reported by Christensen (1960) (mountain ash specimens of 20 microns, 180 microns, 1 mm and 3 mm), Schniewind (1956) (aspen, 0.05, 0.10, 0.20, 0.40, and 0.80 inches). They reported that the equilibrium moisture content was lower for the thicker specimens. Christensen (1960) indicated that water vapor sorption by wood is considered to be a dual process involving both diffusion and stress relaxation and the sorption rate is controlled primarily by the slower process of the two. At the lower moisture content, sorption is controlled by diffusion. Sorption will be controlled by the relaxation of swelling stresses at the higher moisture content regardless of the specimen size. Therefore, it was not a

coincidence that the study using the variable specimen sizes at high h values did not show a consistently decreasing trend of moisture content with an increase in the specimen size. Another factor to cause the different behavior in this study from the past investigations might result from the long equilibration times (about three months for the largest volumes of specimens) in addition to high relative humidity. In past researches, equilibrium state was normally attained in about two weeks. It should be pointed out that equilibration times increase substantially with specimen volume in this study.

5.10.2 D_m calculation

The calculation of D_m from the slope of the linear plot of log (mass of bound water in the cube) vs. log (edge length of the corresponding cube) was carried out. The linear model fitted the data very well with the R^2 being greater than 0.99. The high R^2 value resulted mainly from the scale-down effect (log scale). The high R^2 value might reflect fractal properties of the bound water at high h values, namely, its geometric pattern showed no significant changes under different scales (specimen sizes). A forced linear regression with slope 3 was added into each plot in order to examine if the calculated slope is different from slope 3 visually.

The calculated D_m values for unextracted western red cedar were 2.7845, 2.8976, and 2.9507 at 30, 40, and 50°C, respectively. The t-test results showed that the significant levels for those D_m values were p = 0.005, 0.10, and 0.15, for 30, 40, and 50°C, respectively (Appendix D). The calculated D_m values for Douglas-fir heartwood were 2.7677, 2.8406, 2.8872 at 30, 40, and 50°C, respectively. The t-test results showed that the significant levels for those D_m values were p = 0.025, 0.10, and 0.15, for 30, 40, and 50°C, respectively (Appendix D). The calculated D_m values for western red cedar seemed greater than those for Douglas-fir.

The only significant results were from the 30°C measurements on each sample of the studied species and slight measurement errors in water weight, equilibration, or very small fixed length measurement errors (i.e. 1mm) could shift the slope of the ln(water weight) against ln(length) curves to a slope of 3. Therefore, these experiments did not conclusively show evidence that water in these specimens at dimensions of 10 mm to 40 mm and of about 16% moisture content has fractal structure.

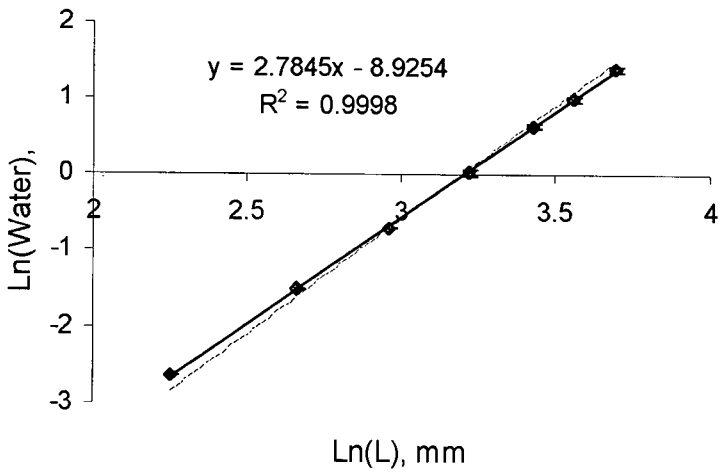

(a) 30°C

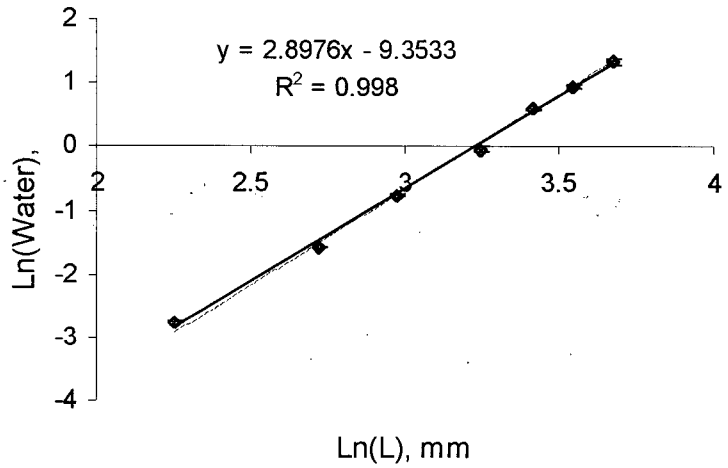

(b) 40°C

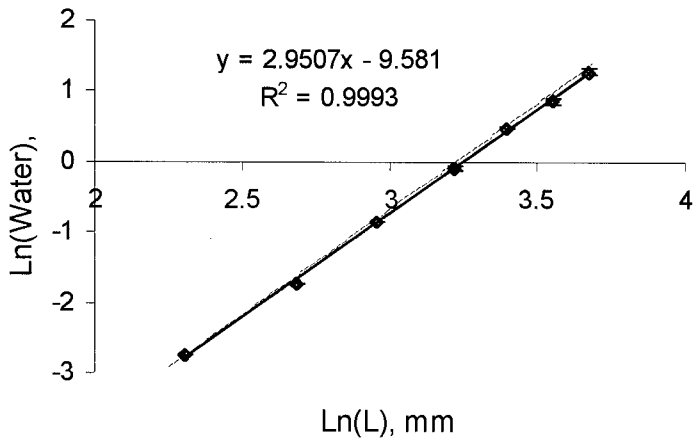

(c) 50°C

Figs.5.39: Relationship of the amount of sorbed water and its size scale for unextracted western red cedar (thick solid line: linear regression; thin dash line: linear regression with slope 3. Error bars are for mass of water in each specimen size)
a) 30°C; b) 40°C; c) 50°C

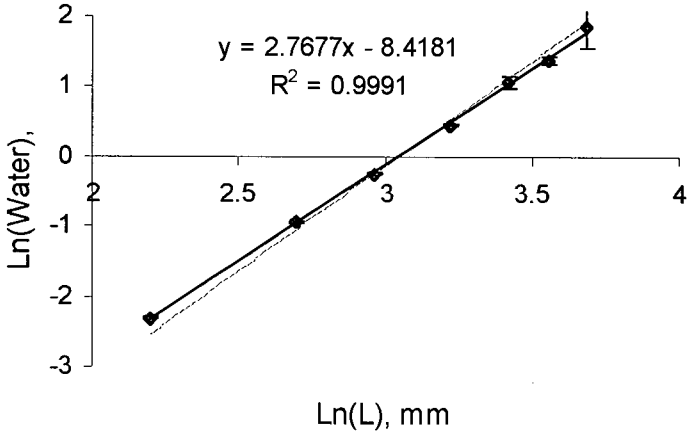
y = 2.7677x - 8.4181
R^2 = 0.9991
Ln(Water),
Ln(L), mm
2
1
0
-1
-2
-3
2
2.5
3
3.5
4

(a) 30°C

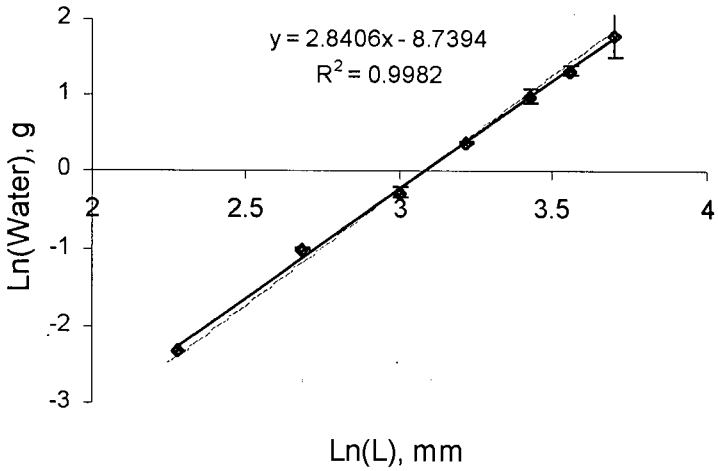
y = 2.8406x - 8.7394
R^2 = 0.9982
Ln(Water), g
Ln(L), mm
2
1
0
-1
-2
-3
2
2.5
3
3.5
4

(b) 40°C

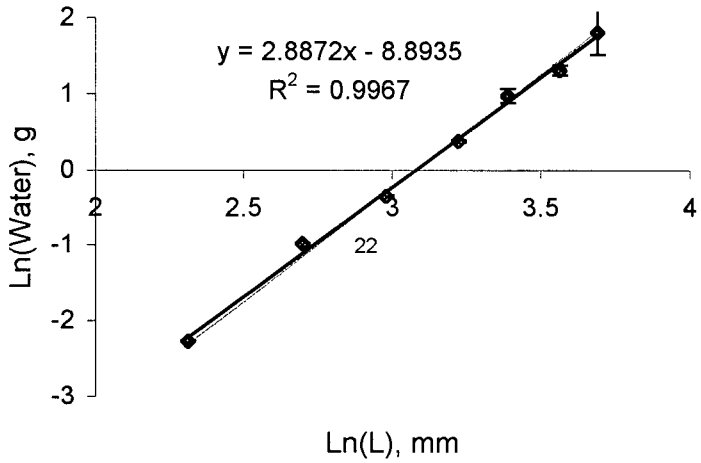

(c) 50°C

Figs.5.40: Relationship between the amount of sorbed water and its size scale for Douglas-fir heartwood (thick solid line: linear regression; thin dash line: linear regression with slope 3. Error bars are for mass of water in each specimen size).
a) 30°C; b) 40°C; c) 50°C

5.10.3 The difference between D and D_m in this study

The calculated D values in this study were based on the assumption of layering of sorbed water molecules. Hence, the resultant D values exhibited more spatial distribution of the sorbed water molecules. The calculated D_m values were based on weight of sorbed water and volume of specimen. The resultant D_m values showed a mass distribution of sorbed water.

Redinz and Guimaraes (1997) studied fractal properties of cell lumen systems of six Brazilian wood species by using water absorption at different pressures. It indicated that the cell lumens of those six species possessed fractal properties. Because the cell lumen system is a space separated from the cell wall system, the cell wall system could be fractal as well. This

study disagrees with the study of Redinz and Guimaraes (1997) on those six Brazilian wood species.

Because moisture content is equal to the ratio of weight of water and weight of oven-dry wood in percentage and because of the small variation in the moisture content between different specimen volumes in the study, the lack of fractal organization of the sorbed water between dimensions 10 mm to 40 mm is not surprising. If the adsorbed water were fractal, the solid wood structure would have to be fractal as well.

Chapter 6

Conclusions and future research recommendations

6.1 Conclusions

Under the light of this investigation, the following conclusions can be drawn:

1) Unextracted western red cedar showed the lowest hygroscopicity due to its high extractives content.
2) Hysteresis existed in all types of wood specimens used in this study.
3) Hygroscopicity decreased with an increase in temperature.
4) No significant difference in moisture content was found between the sapwood and heartwood in Douglas-fir.
5) Extracted cedar and Douglas-fir (both sapwood and heartwood) had no significantly different hygroscopicities.
6) Failure of the classic BET theory to predict the vapor sorption levels in wood at the high sorption regions ($h > 0.5$) can be attributed to the existence of a geometrically rough substrate surface with a D value from about 2.3 to 2.6. The geometry with D values of this range is far from being described as a flat surface ($D = 2$).
7) Modification of the classic BET theory based on fractal surface theory was successful for moisture sorption in wood. A rough surface sorption theory was suggested for vapor sorption in wood.
8) A new sorption theory with its equation was brought into the family of sorption theories. It considered both molecular layering and non-layering (clustering) sorption states. Its success

justified the assumption that the state dynamics of the sorbed water were stepwise or locative instead of continuously smooth and 3 or 4 steps were identified.

9) The existence of mass fractals for two wood types was examined. For unextracted cedar, the D value was 2.78 (significantly different from 3 at $p < 0.05$) at 30°C. For the Douglas-fir heartwood, the D values were 2.77 at 30°C in the same statistical sense.

6.2 Future research suggestions

Because of the heterogeneous properties of wood in both the macro- and micro-levels, wood research needs a simplified approach to deal with its complexity. The fractal approach has turned out to be the one with a single parameter to quantitatively describe spatial distribution of the concerned variables, such as sorption sites of wood within the cell walls and spatial distribution of pore space of the cell lumen system. With any of conventional approaches, such research mostly failed in the past. Therefore, future investigations are expected to help the quantitative understanding of the complexity of wood with a simple parameter (D) and use it as a predicting index to some wood physical properties, such as porosity, permeability, and diffusion. It is quite possible to use the fractal approach in other areas in wood science and technology to simplify research timing and costs. In short, this approach can deal with many complicated problems which elude the conventional methods.

The following should be addressed in future research efforts:

1) A reliable experimental study on small specimen sizes should be carried out to facilitate the development of sorption isotherms with an abundance of test points, namely, many humidities, especially, more values at high levels.

2) The two resulting sorption equations from this study should be applied to many wood species of different anatomical structure in order to investigate dynamics of sorbed water molecules.

3) An independent research study is needed to justify the results from the fractal approach. NMR could be used since it is capable of revealing states of the sorbed water within cell walls. The relationship between the tested states with NMR and the fractal approaches should be examined.

4) A wide temperature range should be used to examine its effect on the value of fractal dimension.

5) Examination of fractal properties within cell walls should be conducted using variable chemical probes with similar physical structures and properties, for example, alcohol derivatives.

6) Fractal distribution properties of wood cell wall needs to be investigated further by using oven-dry wood specimens.

7) The fractal dimension at the fiber saturation point should be evaluated.

8) The fractal dimension for cell lumens and its relationship to the porosity of wood should be examined.

9) Finally, the correlation level of the fractal dimension for the cell lumen system to its permeability should be investigated as well.

After a thorough research on wood using fractal approach, a better understanding in depth of the complex nature of water sorption, the geometry of cell lumens, relations between porosity/permeability and the geometry, and transport mechanisms in wood can be expected.

Literature Cited

Adamson, A. W. 1990. Physical chemistry of surfaces. 5th edition. New York: J. Wiley &Sons.

Aguerre, R. J., C. Suarez, and P. E. Viollaz. 1989a. New BET type multilayer sorption isotherms. Part I: Theoretical derivation of the model. J. Food. Sci., 22(4):

Aguerre, R. J., C. Suarez, and P. E. Viollaz. 1989b. New BET type multilayer sorption isotherms. Part II: Modeling water sorption in foods. J. Food. Sci., 22(4):

Atkins, P.W. 1970. Physical chemistry. 2nd edition. San Francisco: Freeman Publications. pp. 1012-1030.

Avramidis, S. 1989. Evaluation of "three variable" models for the prediction of equilibrium moisture content in wood. Wood Sci. Technol. 23: 251-258.

Avramidis, S. and J. Dubois. 1992. Sorption energies of some Canadian species. Holzforschung. 46(2): 177-179.

Avnir, D. and M. Jaroniec. 1989. An isotherm equation for adsorption in fractal surfaces of heterogeneous porous materials. Langmuir, 5: 1431-1433.

Avnir, D. and P. Pfeifer. 1983. Fractal dimension in chemistry: An intensive characteristic of surface irregularity. Nouveau J. DE Chime, 7(2): 71-72.

Avnir, D., D. Farin, and P. Pfeifer 1983. Chemistry in non-integer dimensions between two and three. II. Fractal surfaces of adsorbents. J. Chem. Phys., 79(7): 3566-3571.

Brunaner, S., P. H. Emmett, and E. Teller. 1938 Adsorption of gases in multilayer. J. Am. Chem. Soc., 60: 309-319.

Burrough, P. A. 1981. Fractal dimensions of landscapes and other environmental data. Nature, 294(19): 240-242.

Cahn, R. W. 1989. Fractal dimension and fracture. Nature, 338: 201.

Childs, T.F. 1972. Pulsed NMR study of molecular motion and environment of sorbed water on cellulose. Polymer 13:259-263.

Christensen, G. N. 1960. Kinetics of sorption of water vapor by wood. I. The effect of sample thickness. Aust. J. Applied Sci. 11: 295 – 304.

Cole, M. W. and N. S. Holter. 1986. Henry's law of adsorption on a fractal surface. Physical Review B. 33(12): 8806 – 8809.

Dent, R. W. 1977. A multilayer theory for gas sorption. Part I: Sorption of a single gas. Textile Res. J., : 145-152.

Deutscher, G., R. Zallen, and J. Adler. 1983. Percolation structures and processes. New York: Adam Hilger and Israel Physical Society, pp. 59-228.

Fan, K., S. G. Hatzikiriakos, and S. Avramidis. 1999. Determination of the surface fractal dimension from sorption isotherms of five species. Wood Sci. Technol., 33: 139-149.

Feder, J. 1988. Fractals. New York: Plenum.

Fripiat, J. J., L. Gatineau, and H. V. Damme. 1986. Multilayer physical adsorption on fractal surfaces. Langmuir, 2: 562-567.

Froix, M. F. and R. Nelson. 1975. The interaction of water with cellulose from NMR relaxation times. Macromolecules. 18(6): 726-730.

Goring, D.A.I. 1978. The effect of cellulose on the structure of water: view 1. In: Fiber water interactions in paper-making. Volume 2. London: The British Paper and Board Industry Federation.

Hailwood, A. J. and S. Horrobin. 1946. Adsorption of water by polymer: analysis in terms of a simple model. Trans. Faraday Soc. 426: 84 – 92.

Hao, B. 1997. Moisture sorption characteristics of five B.C. softwoods. Department of Wood Science. The University of British Columbia. (Directed Study Report).

Hao, B. and S. Avramidis. 2001. Wood sorption fractality in the hygroscopic range. Part I. Evaluation of a modified classic BET model. Wood and Fiber Sci., 33(1): 119 –125.

Hartley I. D. 1994. Characterization of water in wood below the fiber saturation point (Ph.D. thesis). The University of British Columbia, Department of Wood Science, Vancouver, BC, Canada

Hartley, I. D., F. A. Kamke, and H. Peemoeller 1992. Cluster theory for water sorption in wood. Wood Sci. Technol., 26(2): 83-99.

Hartley, I. D., F. A. Kamke, and H. Peemoeller 1994. Absolute moisture content determination of aspen wood below the fiber saturation point using pulsed NMR. Holzforschung 48(6): 474-479.

Hartley, I. D. and S. Avramidis 1993. Analysis of the wood sorption isotherm using clustering theory. Holzforschung, 47: 163-167.

Hartley, I.D., S. Avramidis, and A.L. MacKay 1996. H-NMR studies of water interactions in Sitka spruce and western hemlock: moisture content determination and second moments. Wood Sci. Technol. 30(2):141-148.

Hatzikiriakos, S. G. and S. Avramidis 1994. Fractal dimension of wood surfaces from sorption isostherms. Wood Sci. Technol., 28: 275-284.

Hernandez, R.E. and Bizon M. 1994: Changes in shrinkage and tangential compression strength of sugar maple below and above the fiber saturation point. Wood Fiber Sci. 26(3): 360-369.

Henderson, S.M. 1952. A basic concept of equilibrium moisture. Agr. Eng. 33:29-33.

Hsi, E., R. Hossfeld, and R. G. Bryant. 1977. Nuclear magnetic resonance study of water absorbed on milled northern white-cedar. J. Interface Sci. 62(3):389-395.

Jaroniec, M., R. K. Gilpin, and J. Choma 1993. Correlation between microporosity and fractal dimension of active carbons. Carbon, 31(2): 325-331.

Kutarov, V. V. and B. M. Kats. 1993. Determination of the fractal dimension of ion-exchange fibers from adsorption data. Russ. J. Phys. Chem., 67: 1854 – 1856.

Kelsey, K. 1957. The sorption of water vapor by wood. Aust. J. Appl. Sci. 8: 42-54.

Kolin, B. and T. S. Janezic. 1996. The effect of temperature, density, and chemical composition upon the limit of hygroscopicity of wood. Holzforschung. 50: 263-268

Langmuir 1918. J. Amer. Chem. Soc., 40: 1361 (Cited in Skaar 1972).

Le, C. V. and N. G. Ly. 1992. Multilayer adsorption fo moisture in wool and its application in fabric steaming. Textile Res. J., 62(11): 648-657.

Lefebvre, Y. 1992. Surface fractal dimension of some industrial minerals from gas-phase adsorption isotherms. J. Mater. Res., 7(7): 1888-1891.

Malmquist, L. 1958. Sorption as deformation in space. Kyteknisk Tidskrift, 4: 1-11 (Cited in Skaar 1972; 1988).

Malmquist, L. 1959. Sorption of water vapor by wood from the standpoint theory. Holz als Roh- und Werkstoff, 17(5): 171-178.

Malmquist, L. 1995. Sorption equilibrium in relation to the spatial distribution of molecules. Holzforschung, 49: 555-564.

Mandelbrot, B. B. 1977. Fractals. San Francisco: Freeman Publications.

Mandelbrot, B. B. 1982. The fractal geometry of nature. New York: Freeman.

Menon, R. S., A.L. Mackay, J.R. T. Hailey, M. Bloom, A. E. Burgess, and J.S. Swanson 1987. An NMR determination of the physiological water distribution in wood during drying. J. Appl. Polym. Sci. 33: 1141-1155.

Nagai, T. and T. Yano. 1990. Fractal structure of deformed potato starch and its sorption characteristics. J. Food Sci., 55(5): 1334-1337.

Neimark, A. V. 1990. Determination of the surface fractal dimensionality from the results of an adsorption experiment. Russ. J. Phys. Chem., 64: 2593-2605.

Pfeifer, P. 1986. Fractals in physics. Pro. 6th Int. Symp.

Pfeifer, P. and D. Avnir 1983. Chemistry in non-integer dimensions between two and three. I. Fractal theory of heterogeneous surfaces. J. Chem. Phys., 79(7): 3558 -3565.

Pfeifer, P., D. Avnir, and D. Farin 1984. Scaling behavior of surface irregularity in the molecular domain: From adsorption studies to fractal catalysts. J. Statistical Phys., 36: 699-715.

Pfeifer, P., M. Obert, and M. W. Cole 1989a. Fractal BET and FHH theories of adsorption: A comparative study. Proc. R. Soc. Lond. A. 423: 169-188.

Pfeifer, P., Y. J. Wu, M.W. Cole, and J. Krim 1989b. Multilayer adsorption of a fractally rough surface. Phys. Rev. Lett., 62: 1997-2000.

Pfeifer, P. and M. W. Cole. 1990. Fractals in surface science: Scattering and thermodynamics of adsorbed films. II. New J. Chem., 14: 221-232.

Redinz, J. A., and P. R. C. Guimaraes. 1997. The fractal nature of wood revealed by water absorption. Wood and Fiber Sci., 29(4): 333-339.

Russ, J. C. 1994. Fractal surfaces. New York and London: Plenum, pp. 1-19 and 227-259.

Sapoval, B. 1989. Fractal interfaces in diffusion, invasion, and corrosion. In fractal method to heterogeneous chemistry. New York: John Wiley & Sons. 227-246.

Schniewind, A. P. 1956. Sorption hysteresis in relation to wood thickness. For. Prod. J. June 1956: 225 – 229.

Siauw, H. N. and C. Fairbridge. 1987. Fractal description fo the surface structure of coke particles. Langmuir, 3: 340 - 345.

Simpson, W. 1973. Predicting equilibrium moisture content of wood by mathematical models. Wood Fiber, 5(1): 41-49.

Simpson, W. 1980. Sorption theories applied to wood. Wood Fiber, 12(3):183-195.

Siau. J. F. 1984. Transport Processes in Wood. Springer Series in Wood Science. Berlin, Heidelburg, New York.

Siau, J. F. 1995. Wood: influence of moisture content on wood properties. VPI: 245pp.

Skaar, C. 1988. Wood-water Relations. Heidelberg: Springer, 218pp.

Skaar, C. 1972. Water in wood. Syrause: Syrause Univ. Press, 30-70, 172-185.

Spalt, H.A. 1957. The sorption of water vapor by domestic and tropical woods. For. Prod. J., 7(10): 331-335.

Spalt, H.A. 1958. Water vapor sorption by wood. For. Prod. J. 8 (10): 288-295.

Spalt, A. H. 1979. Water-vapor sorption by woods of high extractive content. In: USDA Proceedings of the Symposium on wood moisture content – temperature and humidity relationship. VPI, Blacksburg, Virginia.

Stamm, A. J. 1964. Wood and Cellulose Science. New York: Ronald, 550pp.

Stamm, A. J., 1971. Review of nine methods for determining fiber saturation points of wood and wood products. Wood Sci. 4:114-128.

Stauffer, D. and A. Aharony. 1992. Introduction to percolaiton theory. 2nd edition. London: Taylor & Francis, pp. 1-88.

Steele, W. A. 1974. The interaction of gases with solid surfaces.Oxford: Pergamon, pp. 220-265.

Tait, M.J., A. Suggett, F. Franks, and S. Ablett, and P.A. Qickenden. 1972. Hydration of monosaccharides. Study by dielectric and nuclear magnetic relaxation. J. Solution. Chem. 1(2):131-151.

Vankateswaran, A. 1970. Sorption of aqueous and non-aqueous media by wood and cellulose. Chem. Rev., 70(60): 619-637.

Vanselow, R. and R. Howe. 1988. Chemistry and Physics of solid surfaces VII. London Paris Tokyo: Springer-Verlag, pp. 283-306.

Vorreiter, V. L. 1963. Fiber saturation moisture and maximum water adsorption of wood. Holzforschung. 17(5): 139.

Wangaard, F., and L.A. Granados. 1967. The effect of extractives on the water-vapor sorption by wood. Wood Sci. Technol., 1: 253-277.

Zhang, B. and S. Li. 1995. Determination of the surface fractal dimension for porous media by mercury porosimetry. Ind. Eng. Chem. Res., 34(4): 1383-1386.

Zimm, B. H. and J. L. Lundberg. 1959. Sorption of vapors by high polymers. J. Phys. Chem., 60: 425-428.

Zuritz, C., R. P. Singh, R.P., S. M. Moini, and S. M. Henderson. 1979. Desorption isotherm of rough rice from 10 to. 40 °C. Trans. ASAE. 22: 433-440.

Zar, J. H. 1999. Biostatistical analysis. 4th edition. Prentice Hall. pp: 324 –340.

Appendix A: derivations of the classic BET and the fractal BET (FBET)

The BET model is the generalization of Langmuir's theory to the multilayer adsorption. Therefore, the derivation of the BET model starts with Langmuir's derivation. The theoretical Langmuir sorption model is shown in Figure 2.1a (page 8).

1) Derivation of Langmuir's equation

The specific surface assumed to consist of a certain number of sorption sites S of which S1 are occupied and $S_0 = S - S_1$ are still free. The rate of evaporation is taken to be proportional to S_1, or equal to k_1S_1; The rate of condensation is proportional to the bare surface S_0 and the gas pressure p, or equal to k_2pS_0. At equilibrium, the rate of evaporation equals to that of condensation, namely,

$$k_1S_1 = k_2pS_0 = k_2p(S - S_1) \tag{1}$$

If θ denotes the fraction of the surface covered, then θ is equal to S_1/S. The Langmuir's equation is the following,

$$\theta = \frac{bp}{1+bp} \tag{2}$$

where $b = k_2/k_1$; k_1 and k_2 are constants, p is the vapor pressure, and θ is coverage in fraction.

Alternatively, θ can be replaced by M/M_m, where M_m is the total capacity of the monolayer adsorption, namely,

$$M = \frac{M_m bp}{1+bp} \tag{2.1}$$

2) **Derivation of the classic BET equation**

For most surfaces, the adsorption on them is multilayer rather than only monolayer. In this case, the BET model is used (Fig. 2.1b, c, page 8).

If s_0, s_1, s_2,... s_i,... represent the surface area that are covered by only 0, 1, 2, 3, ... i, ...layers of sorbed molecules, respectively. At equilibrium, these surface areas remain constant and the rate of condensation on the bare surface is equal to the rate of evaporation from the first layer,

$$a_1 p s_0 = b_1 s_1 e^{-E_1/RT} \tag{3}$$

where p is the vapor pressure, E_1 is the heat of adsorption of the first layer, and a_1 and b_1 are the constants.

Eq.(3) is essentially Langmuir's equation for monolayer molecular sorption, and implies the assumption that a_1, b_1, and E_1 are independent of the number of adsorbed molecules already present in the first layer. Similarly, the rate of the condensation on the top of the first layer is equal to the rate of evaporation from the second layer,

$$a_2 p s_1 = b_2 s_2 e^{-E_2/RT} \tag{4}$$

where the constants a_2, b_2, and E_2 are similarly defined to a_1, b_1, and E_1. Extending the same argument to the third and consecutive layers, the general form can be expressed as

$$a_i p s_{i-1} = b_i s_i e^{-E_i/RT} \tag{5}$$

The total internal surface area accessible to vapor molecules is given by

$$A = \sum_{i=0}^{\infty} s_i \tag{6}$$

The total volume adsorbed is

$$v = v_0 \sum_{i=0}^{\infty} i s_i \tag{7}$$

where v_o is the volume of adsorbed gas on one square centimeter of the adsorbent surface when it is covered with a complete monolayer of adsorbed gas. Therefore, the specific capacity of adsorption is expressed as

$$\frac{v}{Av_0} = \frac{v}{v_m} = \frac{\sum_{i=0}^{\infty} is_i}{\sum_{i=o}^{\infty} s_i} \tag{8}$$

where v_m is the volume of gas adsorbed when the entire adsorbent surface is covered with a complete monolayer.

Another important assumption for BET theory is that the evaporation-condensation properties of the molecules in the second and higher adsorbed layers are the same as those of the liquid state, namely,

$$E_2 = E_3 = \cdots = E_i = E_l \tag{9}$$

where E_l is the heat of liquefaction, and

$$\frac{b_2}{a_2} = \frac{b_3}{a_3} = \cdots = \frac{a_i}{b_i} = g \tag{10}$$

where g is an appropriate constant.

According to Eqs.(3, 4, 5, 9, and 10), s_1, s_2, s_3,... s_i can be expressed as the functions of s_0.

$$s_1 = ys_0 \tag{11}$$

where $y = (a_1/b_1)pe^{E_1/RT}$

$$s_2 = xs_1 \tag{12}$$

where $x = (p/g)e^{E_l/RT}$

$$s_3 = xs_2 = x^2 s_1 \tag{13}$$

$$s_i = xs_{i-1} = x^{i-1}s_1 = yx^{i-1}s_0 = cx^i s_0 \tag{14}$$

where $c = y/x = (a_1/b_1)e^{(E1-El)/RT}$

Therefore, Eq.(8) can be expressed as

$$\frac{v}{v_m} = \frac{cs_0 \sum_{i=1}^{\infty} ix^i}{s_0\left[1 + c\sum_{i=1}^{\infty} x^i\right]} \tag{15}$$

where c is a constant related to the heat of adsorption.

According to the infinite geometric progression, the summation in the denominator and numerator of Eq.(15) are equal to $x/(1-x)$ and $x/(1-x)^2$. Therefore, Eq.(15) can simply written as,

$$\frac{v}{v_m} = \frac{cx}{(1-x)(1-x+cx)} \tag{16}$$

To a planar surface at the saturation pressure of the gas, p_0, an infinite layers of molecules can be built up on the adsorbent, namely, v tends to infinity. In this case, x must tends to one in terms of Eq.(15). Hence, it is assumed that x is equal to p/p_0, namely, the relative vapor pressure. If replacing x with p/p_0 in Eq.(15) and rearranging it, the following form has been convenient to determine the internal surface contact area for porous or sorptive materials.

$$\frac{p}{v(p_0 - p)} = \frac{1}{v_m} + \frac{c-1}{v_m} \times \frac{p}{p_0} \tag{17}$$

The plot of $p/((v(p_0-p))$ against p/p_0 should give a straight line, with intercept $1/(cv_m)$ and slope $(c-1)/(v_m c)$. Then, the two important parameters in Eq.(17), v_m and c, can be calculated according to the intercept and slope. v_m is the volume of gas required to form a complete monolayer on the internal surface. c is the consatant related to the heat of adsorption. This way to calculate v_m and c values are justified in Chap 4 (page 51).

The linear relationship in Eq.(17) is just kept at low sorption region. Beyond this range, the experimental data and predicted values have deviations.

Wood is finite swelling material. This makes it impossible to adsorb infinite layers of water molecules. This means that the summations in Eq.(15) should be from zero to finite layer, n. The following form ($M = v$, $M_m = v_m$, $h = x$) is called the BET model with finite layers of sorbed molecules.

$$M = \frac{M_m ch}{1-h} \cdot \frac{1-(n+1)h^n + nh^{n+1}}{1+(c-1)h - ch^{n+1}} \tag{18}$$

where M and M_m are moisture content (%) at a given relative vapor pressure, h and at a full monolayer capacity, respectively, n is the number of molecular layers, and c is the constant related to heat of adsorption.

3) **Derivation of the fractal BET equation (FBET)**

In fractal surfaces, unlike the classic BET model, the number of water molecules on each layer of the stack is different because of the non-flat surface. In a stack, the difference of the number of the sorbed molecules between two consecutive layers, Fig. (4.2), page 45, over a rough/fractal surface is related to its D value and defined by coefficient f_i (Pfeifer *et al.* 1989a)

$$f_i = i^{2-D} = \frac{s_i}{s_1} \tag{19}$$

where i is the i-th layer from the bottom layer. The implication of Eq. (19) is that the number of sorbed water molecules become fewer and fewer as we move further away from the substrate because the available room for additional molecular sorption decreases.

The derivation of the fractal BET model has followed the framework of the classic BET (Brunaner *et al.* 1938; Skaar 1972), but has also taken the decreasing factor f_i into account on each layer of the stack. The total number of the water molecules (N_n) for a stack with n layers can be obtained by using Eq. (19) as,

$$N_n = p_n \sum_{i=1}^{n} i^{2-D} \tag{20}$$

$$V = \sum_{i=1}^{j} N_i = \sum_{i=1}^{j} p_i \sum_{m=1}^{i} m^{2-D} = \sum_{i=1}^{j} p_i \sum_{m=1}^{i} m^{2-D} \tag{21}$$

where p_n is the number of the water molecules of the first layer in the stack and n is the number of layers in the stack. The total number of the water molecules (V) for all j possible stacks is then obtained as in Eq. (21). According to Eq. (14), s_i is the area of the exposed surface over a planar surface, namely top layer area in the molecular stack which is same in the bottom layer. If over a rough surface, Eq. (14) still holds, but s_i is no longer same in the bottom layer; rather it is equal to $s_i' = p_i * i^{2-D}$ according to Eq. (19). Therefore,

$$cx^i s_0 = p_i i^{2-D} \tag{22}$$

thus,

$$p_i = cx^i s_0 i^{D-2} \tag{23}$$

The amount of the entire potential space for all water molecules on all first layers of the stacks can be expressed as:

$$V_m = \sum_{i=0}^{j} s_n = s_0 + \sum_{i=1}^{j} p_i \tag{24}$$

Therefore, the derived mathematical model has the following form when the right-hand side of Eq. (21) is divided by the right-hand side of Eq. (24) and *h*, n_{max}, *M*, M_m *are in place of x*, *j*, *V*, and V_m, respectively.

$$M = \frac{M_m c \sum_{n=1}^{n_{max}} \left(h^n n^{D-2} \sum_{i=1}^{n} i^{2-D} \right)}{1 + c \sum_{n=1}^{n_{max}} \left(h^n n^{D-2} \right)} \tag{23}$$

where M and M_m are moisture content (%) at a given relative vapor pressure h and at a full monolayer capacity, n is the number of layers, n_{max} is the maximum possible number of layers of the adsorbed water molecules in wood, and c is a constant related to the heat of adsorption.

Appendix B - calculation of confidence interval in C

```
#include <stdio.h>
#include <math.h>
#include <string.h>

void confidenceInterval(char []);

main() {

      char file[20]; // for input data file
      int kk  = 0;
      FILE* fpp;
      fpp = fopen("allFileName.txt", "r");

      do {
        printf("\n data file is being read......");
        fscanf(fpp, "%s", file);
        confidenceInterval(file);
        printf("\n %d", kk + 1);
        printf("-th has been done\n");
        kk++;
      } while ( kk < 24 );

      fclose(fpp);
      return 0;
}


void confidenceInterval(char *fileName) {

      FILE* fp1;
      char result[20];
      float data[10][2];
      double c_min, c_max, Mm_min, Mm_max;
      int sampleSize = 0;
      float a, b, a0, b0, amax, bmax, amin, bmin, sse1, sse2, sse1_max;
      float critical_value;
      float increment_a0, increment_b0;
      int i, j, flag;

      strcpy(result, fileName);
      strcat(result, "-oooo.txt"); // ooo no scale, oooo full scale
      fp1 = fopen(result, "w");

      FILE* fp; // for data file

      fp = fopen(fileName, "r");
      while (getc(fp) != EOF) {
            fscanf(fp, "%f%f", &data[sampleSize][0], &data[sampleSize][1]);
            sampleSize++;
      }

      sampleSize--; /* for last increment */
```

```
fclose(fp);

fprintf(fp1, "\nfile name: %s\n\n", result);

for (i = 0; i < sampleSize; i++ ) {
      fprintf(fp1, "%.4f  %.4f\n", data[i][0], data[i][1]);
}

float averX, sumX, averY, sumY, sumXY, sumXSq, sumYSq;
averX = sumX = averY = sumY = sumXY =
sumXSq = sumYSq = sse1 = sse2 = 0.0;

for ( i = 0; i < sampleSize; i++) {
      sumX = sumX + data[i][0];
      sumY = sumY + data[i][1];
      sumXY = sumXY + data[i][0]*data[i][1];
      sumXSq += data[i][0]*data[i][0];
      sumYSq += data[i][1]*data[i][1];
}

//printf("sumYSq = %f\n", sumYSq);
averX = sumX / sampleSize;
averY = sumY / sampleSize;

b = (sampleSize*sumXY - sumX * sumY)/(sampleSize*sumXSq
     - sumX*sumX);
a = averY - b*averX;

fprintf(fp1,"a = %.4f\tb = %.4f\n", a, b);


for (i = 0; i < sampleSize; i++ ) {
      sse2 = sse2 + pow((data[i][1] - a - b * data[i][0]), 2);
      sse1 = sse1 + pow(data[i][1], 2);
}

fprintf(fp1, "sse2 = %f\n", sse2);
fprintf(fp1, "sse1 = %f\n", sse1);

increment_a0 = a/50;
increment_b0 = b/50;

enum {four = 4, five = 5, six = 6};

switch(sampleSize) {
case four:
      critical_value = 6.94;
      break;
case five:
      critical_value = 5.79;
      break;
case six:
      critical_value = 5.14;
      break;
default:
      printf("acceptable sample size \n");
      break;
```

```
}

a0 = a/10.0;

/* max allowable sse1 value */
sse1_max = (2*critical_value/(sampleSize - 2) + 1)* sse2;

fprintf(fp1, "sse1_max = %f\n", sse1_max);

/* find amin, and bmax*/
for (j = 0; sse1 > sse1_max && a0 < 0.1; a0 += increment_a0,j++ )    {
    for (i = 0, b0 = 1.0; sse1 > sse1_max && b0 > 0;
                              b0 -= increment_b0, i++) {
         sse1 = 0.0;
         for (int n = 0; n < sampleSize; n++ ) {
            sse1 = sse1 + pow((data[n][1] - a0 - b0 *  data[n][0]), 2);
         }
    }
}


bmax = b0 + increment_b0;
a0 -= increment_a0;
if (a0 < a/8.0) a0 = a0*3.5;
amin = a0;


/* find amax and bmin */
sse1 = 0.5;
for (j = 0, a0 = 0.3; sse1 > sse1_max && a0 > amin;
                        a0 -= increment_a0,j++ ) {
    for (i = 0, b0 = 1.0; sse1 > sse1_max && b0 > 0;
                  b0 -= increment_b0, i++) {
      sse1 = 0.0;
      for (int n = 0; n < sampleSize; n++ ) {
      sse1 = sse1 + pow((data[n][1] - a0 - b0 * data[n][0]), 2);
      }
    }
}


bmin = b0 + increment_b0;
a0 +=increment_a0;
if (a0 > 8*a) a0 = a0/3;
amax = a0;

fprintf(fp1,"amin =%.4f amax =%.4f bmin =%.4f bmax = %.4f\n", amin,
amax, bmin, bmax);
c_max = 1.0 + bmax/amin;
c_min = 1.0 + bmin/amax;

Mm_min = 1.0/(bmax + amin);
Mm_max = 1.0/(bmin + amax);

fprintf(fp1, "\nConfidence Interval of c: %.4f%s%.4f\n", c_min," - ",
c_max);
```

```
        fprintf(fp1,"Confidence Interval of Mm: %.4f%s%.4f\n", Mm_min, " - ",
        Mm_max);

        fclose(fp1);
}
```

Appendix C - results of confidence intervals of c and M_m

file name: dfh30des.txt-oo.txt

```
0.5542  0.1378
0.5027  0.1207
0.4330  0.1045
0.4025  0.0977
0.0700  0.0236
a = 0.0064      b = 0.2304
sse2 = 0.000022
sse1 = 0.054594
sse1_max = 0.000105

amin =0.0023 amax =0.0166 bmin =0.2074 bmax = 0.2488

Confidence Interval of c: 13.4997 - 111.3783
Confidence Interval of Mm: 3.9827 - 4.4653
```

file name: dfh30ads.txt-oo.txt

```
0.0700  0.0299
0.4058  0.1282
0.4299  0.1322
0.4898  0.1510
0.5802  0.1780
0.6443  0.2102
a = 0.0055      b = 0.3040
sse2 = 0.000131
sse1 = 0.133451
sse1_max = 0.000468

amin =0.0019 amax =0.0245 bmin =0.2644 bmax = 0.3252

Confidence Interval of c: 11.7685 - 169.9689
Confidence Interval of Mm: 3.0574 - 3.4614
```

file name: dfh40des.txt-oo.txt

```
0.5237  0.1436
0.4353  0.1232
0.3667  0.1006
0.3098  0.0871
0.0600  0.0248
a = 0.0085      b = 0.2578
sse2 = 0.000014
```

```
sse1 = 0.054121
sse1_max = 0.000070

amin =0.0030 amax =0.0162 bmin =0.2371 bmax = 0.2783

Confidence Interval of c: 15.6138 - 94.9759
Confidence Interval of Mm: 3.5555 - 3.9483
```

file name: dfh40ads.txt-oo.txt

```
0.0600  0.0345
0.3954  0.1392
0.4843  0.1722
0.6280  0.2308
a = 0.0106      b = 0.3407
sse2 = 0.000099
sse1 = 0.103491
sse1_max = 0.000788

amin =0.0037 amax =0.0384 bmin =0.2845 bmax = 0.3867

Confidence Interval of c: 8.4101 - 104.9027
Confidence Interval of Mm: 2.5612 - 3.0969
```

file name: dfh50des.txt-oo.txt

```
0.5548  0.1753
0.3100  0.1056
0.2600  0.0909
0.1900  0.0731
0.1000  0.0482
0.0600  0.0358
a = 0.0193      b = 0.2803
sse2 = 0.000003
sse1 = 0.059114
sse1_max = 0.000012
amin =0.0177 amax =0.0212 bmin =0.2768 bmax = 0.2824

Confidence Interval of c: 14.0825 - 16.9376
Confidence Interval of Mm: 3.3325 - 3.3567
```

file name: dfh50ads.txt-oo.txt

```
0.0600  0.0493
0.1000  0.0631
0.1850  0.0931
0.2300  0.1102
0.3000  0.1316
a = 0.0288      b = 0.3467
sse2 = 0.000005
sse1 = 0.044558
sse1_max = 0.000022

amin =0.0254 amax =0.0326 bmin =0.3275 bmax = 0.3622

Confidence Interval of c: 11.0534 - 15.2810
Confidence Interval of Mm: 2.5805 - 2.7773
```

file name: dfs30des.txt-oo.txt

```
0.5542  0.1265
0.5027  0.1158
0.4330  0.0991
0.4025  0.0924
0.0700  0.0203
a = 0.0047      b = 0.2195
sse2 = 0.000001
sse1 = 0.048195
sse1_max = 0.000007
amin =0.0025 amax =0.0072 bmin =0.2140 bmax = 0.2228

Confidence Interval of c: 30.6395 - 89.4530
Confidence Interval of Mm: 4.4377 - 4.5195
```

file name: dfs30ads.txt-oo.txt

```
0.0700  0.0306
0.4058  0.1191
0.4299  0.1256
0.4898  0.1433
0.5802  0.1785
a = 0.0082      b = 0.2814
sse2 = 0.000088
sse1 = 0.083280
sse1_max = 0.000427
amin =0.0029 amax =0.0285 bmin =0.2403 bmax = 0.3135

Confidence Interval of c: 9.4425 - 109.7770
Confidence Interval of Mm: 3.1611 - 3.7207
```

file name: dfs40des.txt-oo.txt

```
0.4353  0.1135
0.3667  0.0993
0.3098  0.0830
0.0600  0.0239
a = 0.0095     b = 0.2405
sse2 = 0.000004
sse1 = 0.030213
sse1_max = 0.000033
amin =0.0036 amax =0.0153 bmin =0.2255 bmax = 0.2592

Confidence Interval of c: 15.6956 - 72.8846
Confidence Interval of Mm: 3.8053 - 4.1518
```

file name: dfs40ads.txt-oo.txt

```
0.0600  0.0386
0.3954  0.1347
0.4843  0.1627
0.6280  0.2145
a = 0.0178     b = 0.3057
sse2 = 0.000054
sse1 = 0.092135
sse1_max = 0.000432
amin =0.0062 amax =0.0383 bmin =0.2663 bmax = 0.3458

Confidence Interval of c: 7.9496 - 56.4285
Confidence Interval of Mm: 2.8405 - 3.2824
```

file name: dfs50des.txt-oo.txt

```
0.3000  0.0959
0.2600  0.0952
0.1900  0.0729
0.1000  0.0506
0.0600  0.0404
a = 0.0263     b = 0.2457
sse2 = 0.000043
sse1 = 0.027763
sse1_max = 0.000207
amin =0.0137 amax =0.0388 bmin =0.1940 bmax = 0.3021

Confidence Interval of c: 5.9961 - 23.1125
Confidence Interval of Mm: 3.1667 - 4.2950
```

file name: dfs50ads.txt-oo.txt

```
0.0600  0.0635
0.1000  0.0597
0.1850  0.0911
0.2300  0.1054
0.3000  0.1261
0.3950  0.1606
a = 0.0365     b = 0.3053
sse2 = 0.000151
sse1 = 0.068712
sse1_max = 0.000538
amin =0.0197 amax =0.0528 bmin =0.2490 bmax = 0.3711

Confidence Interval of c: 5.7164 - 19.8504
Confidence Interval of Mm: 2.5587 - 3.3132

file name: ewrc30des.txt-oo.txt

0.5027  0.1102
0.4330  0.0937
0.4025  0.0883
0.0700  0.0198
a = 0.0052     b = 0.2070
sse2 = 0.000002
sse1 = 0.029119
sse1_max = 0.000018
amin =0.0018 amax =0.0097 bmin =0.1969 bmax = 0.2176

Confidence Interval of c: 21.2637 - 121.6821
Confidence Interval of Mm: 4.5573 - 4.8392

file name: ewrc30ads.txt-oo.txt

0.0700  0.0304
0.4058  0.1261
0.4299  0.1304
0.4898  0.1493
0.5802  0.1805
a = 0.0089     b = 0.2897
sse2 = 0.000026
sse1 = 0.088687
sse1_max = 0.000126
amin =0.0031 amax =0.0194 bmin =0.2699 bmax = 0.3105

Confidence Interval of c: 14.8825 - 101.1756
Confidence Interval of Mm: 3.1887 - 3.4555
```

file name: ewrc40des.txt-oo.txt

```
0.4353  0.1057
0.3667  0.0933
0.3098  0.0772
0.2995  0.0750
0.0600  0.0214
a = 0.0076      b = 0.2275
sse2 = 0.000007
sse1 = 0.031937
sse1_max = 0.000036
amin =0.0017 amax =0.0133 bmin =0.2128 bmax = 0.2447

Confidence Interval of c: 17.0427 - 147.6015
Confidence Interval of Mm: 4.0597 - 4.4235
```

file name: ewrc40ads.txt-oo.txt

```
0.0600  0.0351
0.3954  0.1425
0.4843  0.1758
0.6280  0.2307
a = 0.0123      b = 0.3413
sse2 = 0.000047
sse1 = 0.105665
sse1_max = 0.000375
amin =0.0043 amax =0.0314 bmin =0.3038 bmax = 0.3789

Confidence Interval of c: 10.6654 - 89.2652
Confidence Interval of Mm: 2.6100 - 2.9833
```

file name: ewrc50des.txt-oo.txt

```
0.3000  0.0968
0.2600  0.0855
0.1900  0.0659
0.1000  0.0426
0.0600  0.0342
a = 0.0172      b = 0.2629
sse2 = 0.000004
sse1 = 0.024013
sse1_max = 0.000020
amin =0.0134 amax =0.0209 bmin =0.2482 bmax = 0.2797

Confidence Interval of c: 12.8505 - 21.8953
Confidence Interval of Mm: 3.4118 - 3.7159
```

file name: ewrc50ads.txt-oo.txt

```
0.0600  0.0531
0.1000  0.0632
0.1850  0.0930
0.2300  0.1035
0.3000  0.1336
a = 0.0312     b = 0.3318
sse2 = 0.000030
sse1 = 0.044029
sse1_max = 0.000146
amin =0.0206 amax =0.0415 bmin =0.2899 bmax = 0.3828

Confidence Interval of c: 7.9802 - 19.5807
Confidence Interval of Mm: 2.4788 - 3.0172
```

file name: uewrc30des.txt-oo.txt

```
0.5542  0.1374
0.5027  0.1233
0.4330  0.1055
0.4025  0.0967
0.0700  0.0258
a = 0.0085     b = 0.2273
sse2 = 0.000024
sse1 = 0.055228
sse1_max = 0.000116
amin =0.0030 amax =0.0192 bmin =0.2044 bmax = 0.2499

Confidence Interval of c: 11.6244 - 84.7699
Confidence Interval of Mm: 3.9545 - 4.4708
```

file name: uewrc30ads.txt-oo.txt

```
0.0700  0.0403
0.4058  0.1480
0.4299  0.1534
0.4898  0.1766
0.5802  0.2153
a = 0.0143     b = 0.3351
sse2 = 0.000084
sse1 = 0.124570
sse1_max = 0.000407
amin =0.0050 amax =0.0339 bmin =0.2963 bmax = 0.3767

Confidence Interval of c: 9.7375 - 76.3123
Confidence Interval of Mm: 2.6199 - 3.0287
```

file name: uewrc40des.txt-oo.txt

```
0.5237  0.1462
0.4353  0.1196
0.3667  0.1087
0.3098  0.0901
0.2995  0.0879
0.0600  0.0280
a = 0.0127     b = 0.2528
sse2 = 0.000023
sse1 = 0.064118
sse1_max = 0.000081
amin =0.0051 amax =0.0200 bmin =0.2364 bmax = 0.2718

Confidence Interval of c: 12.7969 - 54.5919
Confidence Interval of Mm: 3.6117 - 3.8995
```

file name: uewrc40ads.txt-oo.txt

```
0.0600  0.0480
0.3954  0.1693
0.4843  0.2073
0.6280  0.2711
a = 0.0216     b = 0.3886
sse2 = 0.000082
sse1 = 0.147444
sse1_max = 0.000647
amin =0.0076 amax =0.0465 bmin =0.3394 bmax = 0.4404

Confidence Interval of c: 8.2960 - 59.1789
Confidence Interval of Mm: 2.2322 - 2.5914
```

file name: uewrc50des.txt-oo.txt

```
0.5349  0.1929
0.3000  0.1130
0.2600  0.1030
0.1900  0.0851
0.1000  0.0527
0.0600  0.0409
a = 0.0214     b = 0.3180
sse2 = 0.000029
sse1 = 0.072280
sse1_max = 0.000103
amin =0.0154 amax =0.0278 bmin =0.3005 bmax = 0.3386
```

```
Confidence Interval of c: 11.8182 - 23.0116
Confidence Interval of Mm: 2.8247 - 3.0463
```

file name: uewrc50ads.txt-oo.txt

```
0.1000  0.0787
0.1850  0.1249
0.2300  0.1288
0.3000  0.1479
0.3950  0.1930
a = 0.0468      b = 0.3631
sse2 = 0.000210
sse1 = 0.097498
sse1_max = 0.001020
amin =0.0140 amax =0.0792 bmin =0.2519 bmax = 0.4843

Confidence Interval of c: 4.1790 - 35.5201
Confidence Interval of Mm: 2.0065 - 3.0195
```

Appendix D - *t*-test results of the calculated D values from cubic specimens

Notation used:
linear regression equation: y = a + b * x, where y = ln(Water), x = ln(Length), a = intercept, and b = slope

aver = average

aver x = average of x = x bar; same in y;

y head = estimated y for an individual x

std. Dev = standard deviation

total ss = total sums of squares = sum of $(y - \text{average of } y)^2$

reg ss = linear regression sums of squares = sum of $(y \text{ head} - y \text{ bar})^2$

res ss = linear residue sums of squares = sum of $(y - y \text{ bar})^2$ = total ss - reg ss

Sy,x = standard error of estimate = square root of (res ss/ (n - 2)); n - 2 = degree of freedom;

n = the number of experimental points

Sb = standard error of estimated slope = square root of $[Sy,x^2 / \text{sum of } (x - x \text{ bar})^2]$

t = calculated t value = (3 - slope estimate) / standard error of slope estimate; 3 is null hypothesis.

t values at different p	
t0.1(1)	1.47
t0.05(1)	2.01
t0.025(1)	2.57
t0.01(1)	3.365
t0.005(1)	4.03

Results of calculations:

Unextracted western red cedar at 30°C

	x	y	x^2	y^2	x*y	x - aver x	$(x - aver\ x)^2$
	2.252344	-2.6352645	5.073053	6.944619	-5.93552	-0.85942	0.738596
	2.663053	-1.508236	7.09185	2.274776	-4.01651	-0.44871	0.201338
	2.961141	-0.7029955	8.768355	0.494203	-2.08167	-0.15062	0.022686
	3.222469	0.0181346	10.38431	0.000329	0.058438	0.110709	0.012257
	3.430109	0.6307929	11.76565	0.3979	2.163688	0.318349	0.101346
	3.55934	0.9908786	12.6689	0.98184	3.526874	0.44758	0.200328
	3.693867	1.3817591	13.64465	1.909258	5.104034	0.582107	0.338849
sum	**21.78232**	**-1.8249309**	**69.39677**	**13.00292**	**-1.18067**		**1.615399**
Aver	**3.11176**	**-0.2607044**					
std. Dev		**1.4449428**					

total ss	**12.52716**
reg ss	**12.5249**
res ss	**0.002255**
Sy.x =	**0.021237**
Sb	**0.016709**
T	**6.128361** * p < 0.005

Unextracted western red cedar at 40°C

	x	y	x^2	y^2	x*y	x - aver x	$(x - aver\ x)^2$
	2.254445	-2.7410901	5.082521	7.513575	-6.17964	-0.86436	0.747119
	2.71866	-1.5611241	7.391114	2.437108	-4.24417	-0.40014	0.160116
	2.973998	-0.7535343	8.844663	0.567814	-2.24101	-0.14481	0.020969
	3.243764	-0.0363528	10.522	0.001322	-0.11792	0.124959	0.015615
	3.414772	0.5964711	11.66066	0.355778	2.036812	0.295967	0.087596
	3.54818	0.9463543	12.58958	0.895586	3.357835	0.429375	0.184363
	3.677819	1.3362371	13.52635	1.78553	4.914438	0.559014	0.312496
sum	**21.83164**	**-2.2130388**	**69.61689**	**13.55671**	**-2.47365**		**1.528273**
Aver	**3.118805**	**-0.3161484**					
std. Dev		**1.4638456**					

total ss	**12.85706**
reg ss	**12.8319**
res ss	**0.025168**
Sy.x =	**0.070947**
Sb	**0.05739**
t	**1.784285** * p < 0.1

unextracted western red cedar at 50°C

	x	y	x^2	y^2	x*y	x - aver x	$(x - \text{aver } x)^2$
	2.304583	-2.7410901	5.311103	7.513575	-6.31707	-0.8074	0.651888
	2.681706	-1.733868	7.191548	3.006298	-4.64972	-0.43027	0.185135
	2.95491	-0.8500349	8.731495	0.722559	-2.51178	-0.15707	0.024671
	3.221273	-0.0893778	10.3766	0.007988	-0.28791	0.109294	0.011945
	3.397524	0.4878435	11.54317	0.237991	1.65746	0.285545	0.081536
	3.54933	0.8619613	12.59774	0.742977	3.059385	0.437351	0.191276
	3.674527	1.275279	13.50215	1.626337	4.686047	0.562548	0.31646
sum	**21.78385**	**-2.789287**	**69.25381**	**13.85773**	**-4.36359**		**1.462911**
aver	**3.111979**	**-0.3984696**					
std. Dev		**1.4575253**					

total ss	**12.74628**
reg ss	**12.73704**
res ss	**0.009241**
Sy.x =	**0.04299**
Sb	**0.035543**
t	**1.378607** * $p < 0.15$

Douglas-fir heartwood at 30°C

	x	y	x^2	y^2	x*y	x - aver x	$(x - \text{aver } x)^2$
	2.198335	-2.3096097	4.832677	5.334297	-5.0773	-0.90787	0.82423
	2.695978	-0.9454621	7.268295	0.893899	-2.54894	-0.41023	0.168287
	2.962692	-0.2492309	8.777546	0.062116	-0.73839	-0.14351	0.020596
	3.221273	0.4518397	10.3766	0.204159	1.455499	0.115067	0.01324
	3.42198	1.0616025	11.70995	1.127	3.632782	0.315774	0.099713
	3.557061	1.3812316	12.65268	1.907801	4.913125	0.450855	0.20327
	3.686126	1.8615809	13.58752	3.465483	6.862021	0.57992	0.336307
sum	**21.74344**	**1.2519519**	**69.20527**	**12.99475**	**8.498792**		**1.665644**
aver	**3.106206**	**0.1788503**					
std. Dev		**1.458929**					

total ss	**12.77084**
reg ss	**12.75893**
res ss	**0.011911**
Sy.x =	**0.048808**
Sb	**0.037818**
t	**2.707694** * $p < 0.025$

Douglas-fir heartwood at 40°C

	x	y	x^2	y^2	x*y	x - aver x	$(x - \text{aver } x)^2$
	2.277267	-2.323196	5.185946	5.39724	-5.29054	-0.84516	0.714293
	2.683074	-0.9983146	7.198887	0.996632	-2.67855	-0.43935	0.19303
	3.000222	-0.2665731	9.001333	0.071061	-0.79978	-0.1222	0.014934
	3.218076	0.3856025	10.35601	0.148689	1.240898	0.09565	0.009149
	3.423937	0.989504	11.72334	0.979118	3.387999	0.301511	0.090909
	3.557061	1.327075	12.65268	1.761128	4.720487	0.434635	0.188907
	3.697344	1.7963655	13.67035	3.226929	6.64178	0.574918	0.33053
sum	**21.85698**	**0.9104633**	**69.78855**	**12.5808**	**7.222295**		**1.541752**
aver	**3.122426**	**0.1300662**					
std. Dev		**1.4412019**					

total ss	**12.46238**
reg ss	**12.44007**
res ss	**0.022308**
Sy.x =	**0.066796**
Sb	**0.053795**
t	**1.903525** * $p < 0.1$

Douglas-fir heartwood at 50°C

	x	y	x^2	y^2	x*y	x - aver x	$(x - \text{aver } x)^2$
	2.311545	-2.2701179	5.34324	5.153435	-5.24748	-0.81177	0.658966
	2.698673	-0.9800296	7.282836	0.960458	-2.64478	-0.42464	0.180318
	2.981633	-0.3514032	8.890137	0.123484	-1.04776	-0.14168	0.020073
	3.224062	0.3798738	10.39458	0.144304	1.224737	0.10075	0.010151
	3.39081	0.9755026	11.49759	0.951605	3.307744	0.267498	0.071555
	3.565581	1.3066016	12.71337	1.707208	4.658794	0.442269	0.195602
	3.690877	1.8076328	13.62258	3.267536	6.671751	0.567565	0.322131
sum	**21.86318**	**0.8680601**	**69.74433**	**12.30803**	**6.923012**		**1.458796**
aver	**3.123312**	**0.1240086**					
std. Dev		**1.4259724**					

total ss	**12.20038**
reg ss	**12.16015**
res ss	**0.040234**
Sy.x =	**0.089704**
Sb	**0.074271**
t	**1.378742** * $p < 0.15$